National Institute for Public Health
and the Environment
Ministry of Health, Welfare and Sport

Uncertainty in the determined **nitrogen deposition** in the Netherlands

Status report 2023

Uncertainty in the determined nitrogen deposition in the Netherlands
Status report 2023

RIVM report 2022-0085

Colophon

R. Hoogerbrugge (author), RIVM
M. Braam (author), RIVM
K. Siteur (author), RIVM
C. Jacobs (author), RIVM
S. Hazelhorst (author), RIVM
G. Stefess (author), RIVM
E. van der Swaluw (author), RIVM
R. Wichink Kruit (author), RIVM
J. Wesseling (author), RIVM
A. van Pul (author), RIVM

Contact:
Ronald Hoogerbrugge
Centre MIL
ronald.hoogerbrugge@rivm.nl

Synopsis

Uncertainty estimates of the nitrogen deposition in the Netherlands

Status report 2023

Every year, RIVM produces maps that show how much nitrogen is deposited in the Netherlands. We refer to this as nitrogen deposition. RIVM determines the nitrogen deposition by combining model calculations with measurements. These model calculations are necessary because measurements cannot be performed everywhere in the Netherlands. The deposition is influenced by the weather, the roughness of the terrain and characteristics of the vegetation. These factors give rise to a degree of uncertainty.

In this technical report, RIVM describes how the uncertainties in terms of deposition levels are derived. In terms of degree, the uncertainties are similar to earlier estimates in 2004 and 2010, but they are now better underpinned.

The uncertainty in a calculated deposition level is expressed as the probability of the calculated level deviating from the actual level. On the national scale, the probability that the calculated level deviates by between less than 20% and up to 30% from the actual level is considerable (95%). For specific areas in the Netherlands, there is a considerable probability (95%) that the calculated level deviates by between less than 60% and up to 70% from the actual level. This latter uncertainty applies when the deposition is calculated for a very small area, such as a hectare or a square kilometre. The degree of uncertainty of to the national nitrogen deposition is lower because uncertainties in the processes affecting deposition average out on the national scale.

The results also show the largest contributors to the uncertainties in the overall nitrogen deposition. The most important factor in this regard is the uncertainty in the dry deposition, which entails nitrogen depositing on soil or vegetation directly from the air. There can be considerable variation from area to area and there is insufficient information to quantify this process.

Keywords: nitrogen deposition, uncertainty, dry deposition, OPS, DN, measuring and modelling, COTAG

Publiekssamenvatting

Onzekerheid in de bepaalde stikstofdepositie in Nederland
Status report 2023

Elk jaar maakt het RIVM kaarten die aangeven hoeveel stikstof in Nederland op de bodem neerslaat. Dit noemen we stikstofdepositie. Het RIVM bepaalt de stikstofdepositie door modelberekeningen met metingen te combineren. Modelberekeningen zijn nodig omdat niet overal in Nederland kan worden gemeten. Het weer, de ruwheid van het land en eigenschappen van de begroeiing beïnvloeden de depositie en zorgen voor een bepaalde onzekerheid.

In dit technische rapport beschrijft het RIVM hoe de onzekerheden in de depositiewaarden worden bepaald. De grootte van de onzekerheden zijn vergelijkbaar met de eerdere schattingen uit 2004 en 2010, maar zijn nu beter onderbouwd.

De onzekerheid in de berekende depositiewaarde drukken we uit in de kans dat de berekende waarde een bepaalde afwijking heeft van de werkelijke waarde. Landelijk gezien is de kans groot (95 procent betrouwbaarheidsinterval) dat de berekende waarde minder dan 30 procent afwijkt van de werkelijke waarde. Op een specifieke locatie in Nederland is de kans groot (95 procent betrouwbaarheidsinterval) dat de berekende waarde minder dan 70 procent afwijkt van de werkelijke waarde. Deze onzekerheid geldt wanneer de depositie wordt berekend voor een heel klein gebied, zoals een hectare of een vierkante kilometer. De kleinere onzekerheid in de landelijke stikstofdepositie komt omdat onzekerheden in processen die invloed hebben op de depositie, op landelijke schaal uitmiddelen.

De onzekerheden hebben geen betrekking op berekeningen voor specifieke projecten maar uitsluitend voor de totale depositie. De resultaten laten ook zien waar de grootste onzekerheden in de totale stikstofdepositie door komen. De onzekerheid in de droge depositie is daar het belangrijkste onderdeel van. Bij droge depositie komt stikstof direct via de lucht op de bodem of in de vegetatie terecht. De hoeveelheid kan van plek tot plek sterk verschillen en er is weinig informatie beschikbaar om dit proces te kwantificeren.

Kernwoorden: stikstofdepositie, onzekerheid, droge depositie, OPS, DN, meten en modelleren, COTAG

Contents

1 Nederlandse samenvatting
Onzekerheid in de stikstofdepositie

1.1 Inleiding

1.1.1 *Systeem van emissies en deposities*
Het RIVM brengt elk jaar kaarten uit van de stikstofdepositie in Nederland. De doelen van deze kaarten zijn beleidsmonitoring en het monitoren van de stikstofdepositie. Voorbeelden zijn de Grootschalige Depositiekaarten Nederland, GDN (Hoogerbrugge et al., 2022) en de Depositiekaarten stikstof Natura 2000-gebieden, DN. De resultaten van de DN-kaarten worden gebruikt in de stikstofmonitoring voor de Wet stikstofreductie en natuurverbetering, Wsn (Marra et al., 2022).
De kaarten worden gemaakt op basis van een combinatie van metingen en modelberekeningen van stikstof.

De modelberekeningen beschrijven de keten van emissie via transport naar depositie (Figuur 1). Door emissie komen er stikstofverbindingen in de lucht. Verkeer en industrie stoten voornamelijk stikstofoxiden (geoxideerd stikstof) uit, en de landbouw voornamelijk ammoniak (gereduceerd stikstof). De hoeveelheid van een stof per volume-eenheid heet de concentratie. In de lucht worden de stoffen verder met de wind mee getransporteerd en vinden er chemische omzettingen plaats.
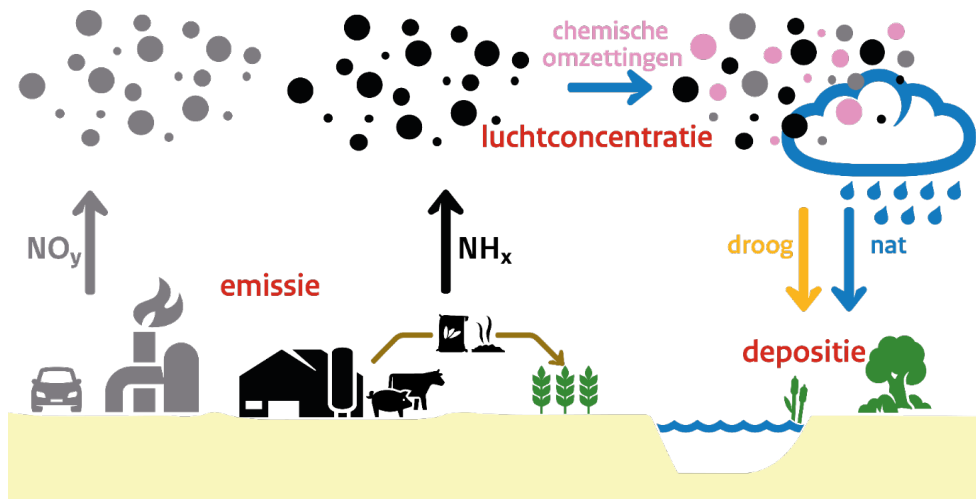
Figuur 1 Overzicht van de stikstofroutes door de lucht

De stoffen verdwijnen vervolgens uit de lucht als gevolg depositie. Er zijn twee manieren van depositie (zie de rechterkant in Figuur 1).
Ten eerste kunnen de componenten met het regenwater mee neerslaan (**natte depositie**) in de vorm van nitraat (geoxideerd stikstof in oplossing) en ammonium (ammoniak in oplossing).
Ten tweede kunnen planten, bodem en de waterlaag daarop ze direct uit de lucht opnemen (**droge depositie**). Hierbij onderscheiden we primaire componenten en secundaire componenten. De primaire componenten zijn direct uitgestoten: ammoniak (NH_3) en stikstofoxiden ($NO_x = NO + NO_2$). De secundaire componenten ontstaan door

chemische reacties in de atmosfeer (bijvoorbeeld ammoniumsulfaat, ammoniumnitraat).
Dit rapport gaat dan ook over zes componenten waaruit de totale stikstofdepositie bestaat:

$$D_{\text{N tot}} = D_{\text{NO}_3 \text{ nat}} + D_{\text{NO}_x \text{ primair droog}} + D_{\text{NO}_x \text{ secundair droog}} + \\ D_{\text{NH}_4 \text{ nat}} + D_{\text{NH}_3 \text{ primair droog}} + D_{\text{NH}_4 \text{ secundair droog}}$$

Vgl. 1
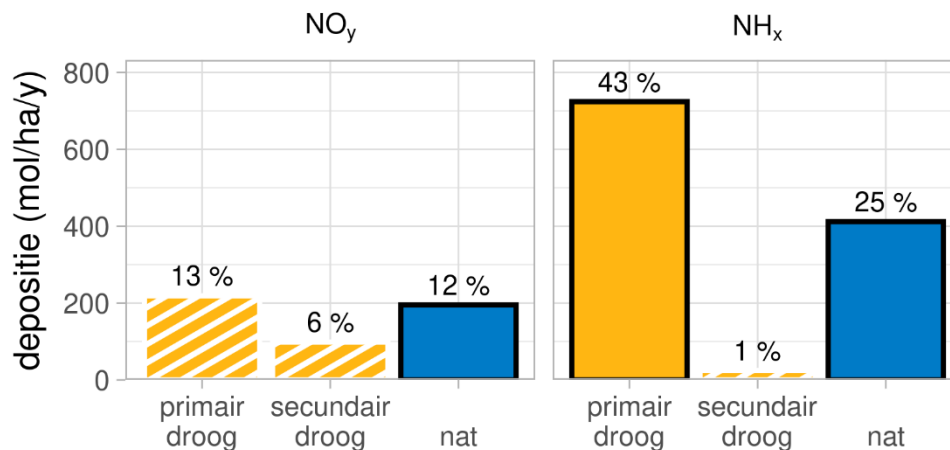
Figuur 2 Gemiddelde berekende Nederlandse depositiebijdrage per component over de periode 2005-2021 voor geoxideerd (links) en gereduceerd stikstof (rechts). Voor $D_{\text{NO}_x \text{ primair droog}}$, $D_{\text{NO}_3 \text{ secundair droog}}$, $D_{\text{NH}_4 \text{ secundair droog}}$ (gestreept) zijn alleen concentratiemetingen beschikbaar. Voor $D_{\text{NO}_3 \text{ nat}}$, $D_{\text{NH}_3 \text{ primair droog}}$, $D_{\text{NH}_4 \text{ nat}}$ (gevuld en zwart omkaderd) zijn concentratie- én depositiemetingen beschikbaar.

In Figuur 2 staat hoeveel iedere component bijdraagt aan de totale Nederlandse depositie. Verder is aangegeven of van een component alléén concentratiemetingen beschikbaar zijn, of zowel concentratie- als depositiemetingen.

1.1.2 *Beschikbare metingen*
Een overzicht van alle relevante stikstofmetingen staat in het rapport over de meetstrategie stikstof (Wichink Kruit et al., 2021). Van alle stikstofcomponenten zijn jaarlijkse concentratiemetingen beschikbaar. Het meten van natte depositie is relatief eenvoudig. Natte depositie meten we door eerst het regenwater op te vangen, en dan te meten hoeveel er van de stikstofcomponent in het regenwater zit.
Het meten van droge depositie van gasvormige componenten en fijnstofdeeltjes is moeilijker. Figuur 2 laat zien dat de droge depositie van ammoniak de grootste bijdrage heeft in Nederland.
Het RIVM monitort op zes plekken droge depositie van ammoniak met een meetsysteem dat we het COTAG-systeem noemen (Rutledge-Jonker et al., 2023). In Bargerveen (2012), de Oostelijke Vechtplassen (2014), de Hoge Veluwe (2017), het Noordhollands Duinreservaat (2021), Veenkampen (2022) en Haaksbergerveen (2023). Er waren tijdens de analyse van dit onderzoek alleen van de eerste drie COTAG-systemen jaarcijfers beschikbaar (Rutledge-Jonker et al., 2023). In de analyses van dit rapport gebruiken we alleen die metingen. Van ammoniak hebben we dus concentratie- én enkele depositiemetingen.

De droge depositie van stikstofoxides en fijnstofdeeltjes wordt nu (nog) niet gemeten. Voor deze componenten zijn dus alleen de concentratiemetingen beschikbaar.

1.1.3 *Modelberekeningen en onzekerheid*
1.1.3.1 Onzekerheden
Het is niet mogelijk om overal in Nederland te meten. Om toch de situatie voor heel Nederland in kaart te brengen, gebruikt het RIVM rekenmodellen. Deze modellen worden ook gebruikt om te berekenen hoe de concentratie en depositie van stikstof zich in de toekomst kunnen ontwikkelen. Deze modelberekeningen hebben een bepaalde mate van onzekerheid.

Het bestuderen van de onzekerheid in de stikstofdepositie is lastiger dan van de concentraties in de lucht. Dit komt doordat depositie moeilijker te meten is. Maar ook het modelleren van het depositieproces van stikstof is complex. Het model moet alle zes de componenten en de bijhorende depositiepaden meenemen en berekenen.
De onzekerheid in de gemodelleerde totale stikstofdepositie op 1 x 1 km^2 is eerder geschat op 70% (Velders et al., 2010). Deze waarde was gebaseerd op een analyse uit 2004 (van Jaarsveld, 2004). In dit rapport geven we een update van deze waarde, gebaseerd op een uitbreiding van de eerder gevolgde methode. Schattingen van de onzekerheden in concentraties en de natte depositie zijn beschikbaar, bijvoorbeeld in de EMEP-statusrapporten (EMEP, 2022). Dit geldt niet voor schattingen van de onzekerheid in de totale stikstofdepositie. Walker et al. (2019) schrijven dat er geen generieke schattingen beschikbaar zijn van de onzekerheid in gemodelleerde stikstofdeposities.

1.1.3.2 Modelprocessen
Zoals we eerder schreven, hangt de depositie af van de concentratie. Voor de natte depositie neemt het model in de berekening ook de neerslagduur en -intensiteit mee.

De hoeveelheid droge depositie is een vermenigvuldiging van de luchtconcentratie van de stikstofcomponent met de depositiesnelheid van die component. De depositiesnelheid is een maat voor het gemak waarmee stoffen door de lucht naar het aardoppervlak bewegen en daarna door bodem en planten worden opgenomen. Dit is voor elke stikstofcomponent anders. Belangrijke factoren die depositiesnelheid bepalen, zijn het weer, landgebruik, ruwheid, de bodemsoort en vegetatiesoort.

Bij de droge depositie van ammoniak op vegetatie is ook de hoeveelheid ammoniak die in de vegetatie zit van belang. Modellen houden hier rekening mee door het zogenoemde compensatiepunt te bepalen. Deze waarde hangt af van de plantensoort en bijvoorbeeld de temperatuur. Als het compensatiepunt hoger is dan de concentratie in de lucht is er geen depositie maar emissie.

We gaven al aan hoe de hoeveelheid concentratie een effect heeft op de depositie, maar het omgekeerde geldt ook. De hoeveelheid depositie heeft invloed op de concentratie. Depositie draagt bij aan de verwijdering van een component uit de atmosfeer, waardoor de

concentratie daalt. Deze interactie tussen concentratie en depositie wordt ook wel een negatieve terugkoppeling genoemd. Dit bestuderen we in meer detail in paragraaf 1.4 en Hoofdstuk 5.

1.1.3.3   Het OPS-model, GCN/GDN en DN
Het RIVM berekent de stikstofdepositie met het Operationele Prioritaire Stoffen model (OPS-model; Sauter et al., 2023; van Jaarsveld, 2004). Dit model is een rekenprogramma om de verspreiding van verontreinigende stoffen in de lucht en de depositie te modelleren. OPS is de basis voor de GCN/GDN-kaarten (Hoogerbrugge et al., 2022) en voor de DN-kaarten (https://monitor.aerius.nl/).
Voor beide modelsystemen leggen we een rooster ('grid') van vakjes over Nederland en berekenen we voor elk vakje de concentratie en depositie van de verschillende componenten. De vorm en schaal (resolutie) van de vakjes verschilt tussen de modellen. GCN/GDN rekent op vierkanten van 1×1 km^2. DN rekent op hexagonen (zeshoeken) met een oppervlak van 1 ha. GCN/GDN rekent voor heel Nederland, en DN rekent specifiek voor de stikstofgevoelige natuur in Natura 2000-gebieden.

1.1.3.4   De modelkalibratie
In GCN/GDN en DN kalibreren we de modeluitkomsten met metingen. Dit wordt gedaan om een systematische afwijking tussen het model en de metingen te corrigeren. De aanpak van de kalibratie verschilt per component:

- De natte depositie kalibreren we aan de hand van de natte depositiemetingen.
- Voor de droge depositie van ammoniak kalibreren we aan de hand van alleen de concentratiemetingen (Hoogerbrugge et al., 2022; Velders et al., 2010). Dit komt doordat er onvoldoende droge depositiemetingen beschikbaar zijn en omdat de metingen een lokale weergave zijn en dus minder geschikt voor landelijke interpolatie..
  Met andere woorden: de kalibratie van de droge depositie is op één deel van het proces uitgevoerd, namelijk alleen de concentratie en niet de depositiesnelheid. Dit is niet optimaal, want een belangrijke processtap kan dus niet worden gekalibreerd.
- De droge depositie van NO$_2$ en secundaire componenten worden niet gekalibreerd in GCN/GDN en DN.

In deze Nederlandse samenvatting rapporteren we de gekalibreerde modelberekeningen. Daarom zijn de onzekerheden ook representatief voor de nauwkeurigheid van de gepubliceerde deposities in GCN/GDN en DN. De berekende onzekerheden betreffen de onzekerheden in de totale depositie en hebben geen betrekking op de onzekerheid van een projectberekening voor een individuele bron.
In het rapport tonen we ook de ongekalibreerde resultaten, omdat die informatie relevant is voor het mogelijke verbeteringen in het OPS-model.

1.1.4   *Nederlandse samenvatting en rapport*
We bespreken in dit rapport de volgende zaken:

1. De onzekerheden in de zes componenten en de totale depositie. Deze onzekerheden bepalen we door de modelwaarden te vergelijken met metingen (Paragraaf 1.2 en Hoofdstuk 3).
2. De totale onzekerheid van de zes componenten voor Nederland en voor de Nederlandse Natura 2000-gebieden (Paragraaf 1.3 en Hoofdstuk 4).
3. De negatieve terugkoppeling tussen de droge depositie en de concentratie (Paragraaf 1.4 en Hoofdstuk 5)
4. Een vergelijking tussen GCN/GDN en DN (Paragraaf 1.5 en Hoofdstuk 6)
5. Ten slotte de discussie, conclusie en aanbevelingen (Paragraaf 1.6 en Hoofdstuk 7). Dit rapport is een 'statusrapport'. Het geeft de huidige stand van zaken weer over de onzekerheden in de modellering van de stikstofdepositie. In dit laatste deel bespreken we de beperkingen en verbeterpunten.

1.2   Onzekerheden in de zes componenten van de stikstofdepositie

1.2.1   *Methode*
De eerste stap is het bepalen van de onzekerheid voor de zes stikstofcomponenten. We doen dit door jaarcijfers van de OPS-berekeningen te vergelijken met de beschikbare metingen. We nemen data van alle beschikbare jaren mee in de periode van 2005 tot 2021. Zoals we eerder aangaven, rapporteren we in de Nederlandse samenvatting alleen de gekalibreerde modelberekeningen. Voor de meeste componenten is de modelkalibratie ook gebaseerd op metingen (zie vorige paragraaf, Hoogerbrugge et al., 2022). Met andere woorden, we gebruiken de meting dus zowel voor de modelkalibratie als voor de modelvalidatie. Om ervoor te zorgen dat we de validatie onafhankelijk van de kalibratie uitvoeren, gebruiken we de 'leave one out'-methode. Dit betekent dat we tijdens de validatie voor elk meetpunt een kalibratiekaart maken waar dat specifieke meetpunt niet in zit. Na kalibratie is het gemiddelde verschil tussen modelberekening en meting weggenomen en liggen de punten rond de 1:1-lijn. De onzekerheid die wij hier beschouwen, is dus de afwijking ten opzichte van deze lijn.
De onzekerheden van de zes componenten hieronder rapporteren we in 2σ. Dit komt voor een normale verdeling ongeveer overeen met het 95% betrouwbaarheidsinterval. Stel, de 2σ-onzekerheidswaarde is 34% en de meting is 400 mol/ha/y (zie de resultaten voor natte depositie in de volgende paragraaf). Dan is er 2,5% kans dat de modelwaarde eigenlijk 34% lager is, dus 256 mol/ha/y. En er is ook 2,5% kans dat de modelwaarde 34% hoger is, dus 536 mol/ha/y. We bepalen de onzekerheden door de berekeningen te vergelijken met de metingen. In de modelonzekerheid is dus ook de meetonzekerheid meegenomen. De impact van de meetonzekerheid is in dit rapport ook geanalyseerd.

a
NH$_x$ natte depositie (mol/ha/y)

b
NO$_y$ natte depositie (mol/ha/y)
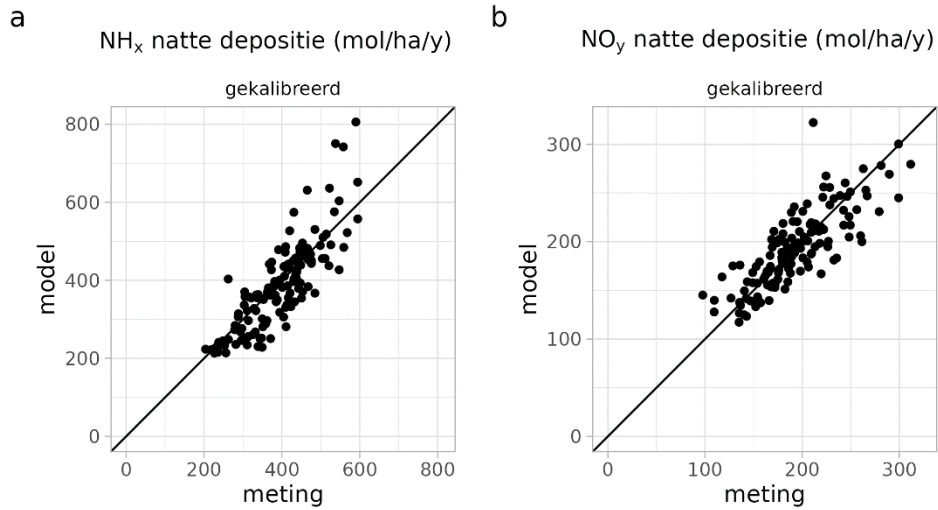
Figuur 3 Vergelijking tussen gemeten en berekende natte depositie van NH$_4^+$ (a) en NO$_3^-$ (b).

1.2.2 Onzekerheden in de natte depositie

Voor de natte depositie zijn metingen beschikbaar. Dus hier kunnen we metingen en modelberekeningen direct met elkaar vergelijken. In Figuur 3 staat deze relatie voor ammonium (NH$_4^+$) en geoxideerd stikstof (nitraat, NO$_3^-$).

Uit de spreiding rondom de 1:1-lijn volgt dat de relatieve modelonzekerheid (2σ) 34% is voor ammonium, en 26% voor nitraat.

1.2.3 Onzekerheden in de droge depositie van ammoniak

Van de zes componenten is voor Nederland de gasvormige droge depositie van ammoniak de grootste. Dit is ook de enige component waarvan momenteel droge depositiemetingen beschikbaar zijn. Daarnaast zijn er voor ammoniak concentratiemetingen beschikbaar. Hierdoor kunnen we ook een schatting maken van de onzekerheid in de depositiesnelheid van ammoniak.
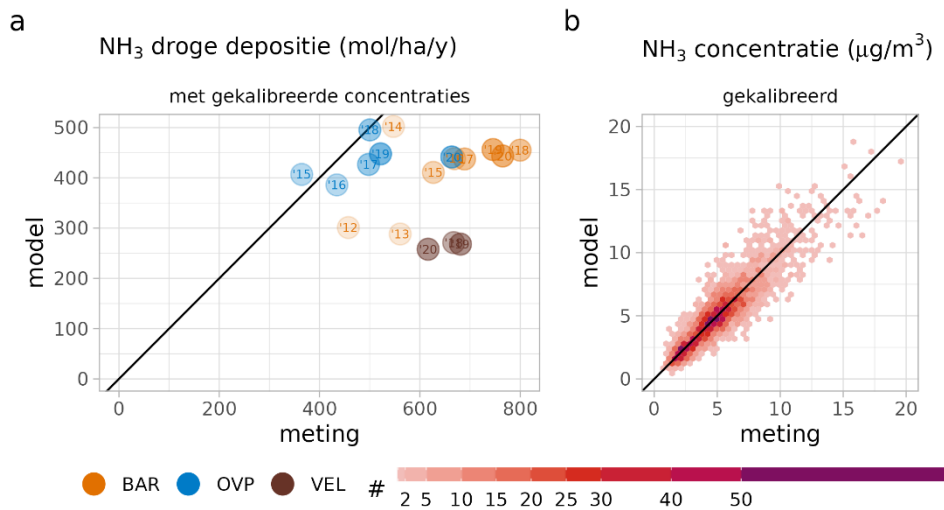
Figuur 4a Vergelijking tussen de gemeten en berekende droge depositie van NH₃. De kleuren geven de verschillende locaties aan: oranje is BAR, Bargerveen, blauw is OVP, Oostelijke Vechtplassen en bruin VEL, de Hoge Veluwe.
Figuur 4b Vergelijking tussen de gemeten en berekende NH₃-concentraties. De kleuren geven de aantal metingen in de hexagoon weer: hoe donkerder hoe meer metingen.

De vergelijkingen tussen de modelberekeningen en de metingen voor de droge depositie en concentratie van ammoniak staan in Figuur 4.
De vergelijking voor droge depositie van ammoniak tussen de COTAG-metingen en het OPS-model laat een grote spreiding zien (Figuur 4a). Hierdoor is de bijhorende onzekerheid ook groot: ongeveer 120% (2σ). In de meeste gevallen zijn de meetwaarden hoger dan de modelwaarde. Ze liggen onder de 1:1-lijn. Het is niet mogelijk om een modelkalibratie voor de droge depositie uit te voeren, aangezien het hier om maar drie locaties gaat.

Uit de concentratie- en depositiemetingen hebben we ook depositiesnelheid van ammoniak afgeleid. Deze waarden hebben we ook vergeleken met eerdere afgeleide depositiesnelheden (Appendix E). Dit zijn vaak buitenlandse metingen. Deze literatuurwaarden laten een grote spreiding zien, waar de recente Nederlandse metingen bij aansluiten. Deze grote spreiding is een tweede reden dat het niet verstandig is om op basis van een kleine set metingen generieke kalibraties toe te passen.
Van de ammoniakconcentratie zijn grote sets aan metingen beschikbaar. Deze vergelijking staat in Figuur 4b. Uit de vergelijking tussen de berekende en gemeten NH₃-concentraties volgt een onzekerheid van 45% (2σ).

OPS berekent de droge depositie door de depositiesnelheid met de concentratie te vermenigvuldigen. Door deze twee onzekerheden te combineren kunnen we indirect een onzekerheid afleiden van de effectieve depositiesnelheid voor ammoniak. Die is 113% (2σ).

1.2.4 *Onzekerheden in de droge depositie NO_2, NO_3^- en NH_4^+*
Voor stikstofdioxide en de fijnstofdeeltjes die stikstof bevatten (NO_3^- en NH_4^+) zijn geen recente Nederlandse droge depositiemetingen beschikbaar. Hier vergelijken we alleen de berekende en gemeten concentraties met elkaar (Figuur 5). De onzekerheid in de modelconcentratie is 21% voor NO_2, 45% voor NO_3^- en 72% voor NH_4^+ (2σ).
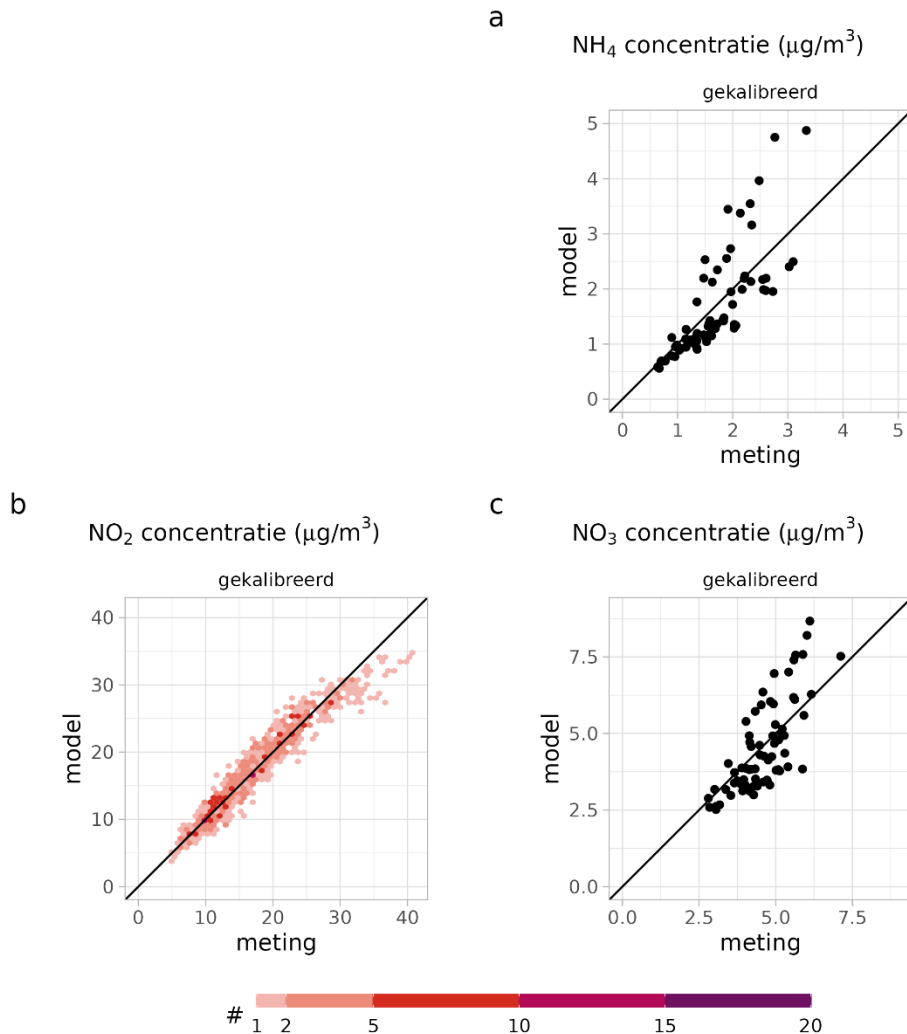
Figuur 5a Vergelijking tussen de gemeten en berekende NH_4^+-concentraties. Figuur 5b Vergelijking tussen de gemeten en berekende NO_2 -concentraties. De kleuren geven de aantal metingen in de hexagoon weer: hoe donkerder hoe meer metingen.c: Vergelijking tussen de gemeten en berekende NO_3^--concentraties.

Voor de schatting van de onzekerheid in de droge depositie is er ook een schatting in de onzekerheid van de depositiesnelheid nodig. We nemen de berekende onzekerheid in de depositiesnelheid van ammoniak, en trekken daar de onzekerheid door het compensatiepunt van af (zie §3.5.2). De reden hiervoor is dat NO_2 in tegenstelling tot NH_3 geen compensatiepunt heeft. Verder hangt de bepaling van de compensatiepunt van verschillende parameters af en is deze daardoor

onzeker. Uiteindelijk komt de onzekerheid van de depositiesnelheid van NO_2 uit op 91% (2σ). En de onzekerheid in de droge depositie van stikstofoxides op 94% (2σ).
Voor de onzekerheid in droge depositiesnelheden van fijnstofdeeltjes gebruiken we dezelfde waarde van 91% (2σ). Hierdoor wordt de onzekerheid in droge depositie van NH_4^+ 121% (2σ) en van NO_3^- 104% (2σ).

1.2.5 *Conclusies*
Deze analyse geeft aan dat de onzekerheid in de droge depositiesnelheid de grootste bijdrage levert aan de onzekerheid in de totale depositie.

1.3 Totale onzekerheid

Nu de onzekerheden van alle zes componenten bekend zijn, kunnen we ze combineren tot een totale onzekerheid.
In de onzekerheidsanalyse van de totale depositie kunnen we niet aannemen dat de onzekerheden in de zes componenten onafhankelijk van elkaar zijn. Sommige componenten correleren met elkaar. Zo wordt natte depositie beïnvloed door de regenduur en regenintensiteit, en daardoor zal de natte depositie van ammonium en nitraat voor een deel gecorreleerd zijn.

We maken daarom een correlatietabel (Table 5 in Paragraaf 4.1), waar voor alle componenten onderling een correlatie is weergegeven.
De onderlinge correlatie tussen de natte depositiecomponenten bepalen we uit de metingen, want dit zijn gecombineerde metingen. Voor de andere componenten schatten we de correlatie met behulp van modelberekeningen (zie voor meer detail Paragraaf 4.1).

Deze tabel gebruiken we bij het optellen van de onzekerheden, om zo tot een totale onzekerheid in de stikstofdepositie te komen. De totale onzekerheid is dan een combinatie van de onzekerheden per component en de onzekerheid door de correlatie tussen de componenten.

Dit resulteert in een gemiddelde onzekerheid in de totale stikstofdepositie van ongeveer 60-70% (2σ) voor een willekeurige locatie in Nederlands natuurgebied. Dit betekent 900-1100 mol/ha/j. Deze 60% à 70% komt goed overeen met de eerdere schatting (Velders et al., 2010). Het voordeel ten opzichte van de eerdere onzekerheidsschattingen is dat de definitie van de onzekerheidsmaat nu veel scherper is. Merk op dat dit de onzekerheid is van de waarde zelf, dus in absolute zin. Er is 5% kans dat de gerapporteerde modelwaarde 60-70% lager of hoger is. Maar in veel gevallen worden modelwaarden relatief met elkaar vergeleken. Voorbeelden hiervan zijn vergelijking van verschillende jaren in trendanalyses, of het vergelijken van het wel of niet meenemen van bepaalde bronnen. In deze situaties vallen veel van de bovenstaande onzekerheden tegen elkaar weg. Hierdoor zal de onzekerheid kleiner worden. Dit wordt in een volgende rapportage verder uitgewerkt.

1.4 Effecten van interacties tussen depositie en concentratie

1.4.1 De negatieve terugkoppeling

In de vorige paragrafen bleek dat de onzekerheid in de droge depositie wordt gedomineerd door de onzekerheid in de depositiesnelheid. In werkelijkheid is de relatie tussen de onzekerheid in de depositie en de depositiesnelheid complexer.

Laten we de vergelijking van de depositie erbij pakken. De droge depositie (D_droog) is de concentratie (C) vermenigvuldigd met de depositiesnelheid (V_d):

Vgl. 2

Een lokale verandering in de depositie zal de lokale concentratie in de atmosfeer nauwelijks beïnvloeden. Maar dit wordt anders op een grotere ruimtelijke schaal, vanaf enkele kilometers.

Stel, de depositiesnelheid is te hoog gemodelleerd. Volg de genummerde pijlen in Vgl. 2. Merk op dat het ook omgekeerd geldt.

1 → Dan is er daardoor ook een *hogere* depositie.

2 → Bij transport over langere afstanden zal deze hogere depositie leiden tot merkbaar *lagere* concentraties. Want bodem en vegetatie nemen meer stoffen uit de lucht op.

3 → Daardoor zal de depositie weer enigszins *afnemen*. Want er zitten minder stoffen in de lucht die opgenomen kunnen worden.

De interactie tussen depositie, depositiesnelheid en concentratie zorgt dus voor een negatieve terugkoppeling. De initiële toename van de depositie is uiteindelijk minder groot, dankzij de extra afname van de concentratie tijdens het transport. Dit betekent een demping van de fout of de onzekerheid in de depositie op grotere schaal.

1.4.2 Onderzoeksmethode

In Hoofdstuk 5 onderzoeken we in hoeverre dit effect de onzekerheden in de depositie beïnvloedt. Dat doen we door verschillende berekeningen ('runs') met OPS uit te voeren.

In elke run gebruiken we een andere depositiesnelheid voor alle graslanden in Nederland. We hebben de depositiesnelheid beïnvloed door de oppervlakteweerstand van de graslanden aan te passen.[1] In de Nederlandse samenvatting laten we alleen de resultaten zien van de run waar de oppervlakteweerstand 20% is van normaal en de run waar die 500% is van normaal. In Hoofdstuk 3 staan de resultaten van de overige runs.

Daarna berekenen we op ruim driehonderd verschillende locaties de lokale depositiesnelheid en de depositie ter plaatse. We onderzoeken dan per run wat de invloed is van de toename of afname van de oppervlakteweerstand van gras op de lokale depositiesnelheid en

---

[1] Zoals in 1.1.3 is beschreven, hangt de depositiesnelheid af van verschillende factoren, zoals het weer, het gewas en de bodem. OPS berekent de depositiesnelheid met het weerstandsmodel. Eén van de drie parameters van dit model is de zogenaamde oppervlakteweerstand. Als de oppervlakteweerstand laag is, nemen de bodem (of het water) en de vegetatie gemakkelijk de bepaalde componenten op, en is de depositiesnelheid hoog. Zie ook Hoofdstuk 5.

depositie. Ook kijken we naar het effect op de totale depositie in heel Nederland.

We verwachten dat het aanpassen van de depositiesnelheid via de oppervlakteweerstand van graslanden een effect heeft op de totale depositie in heel Nederland. Dit komt doordat bijna 40% van het Nederlandse oppervlak grasland is. De depositieverandering heeft door transport met de wind niet alleen boven grasland een effect op de concentratie in de lucht, maar ook boven ander landgebruik.
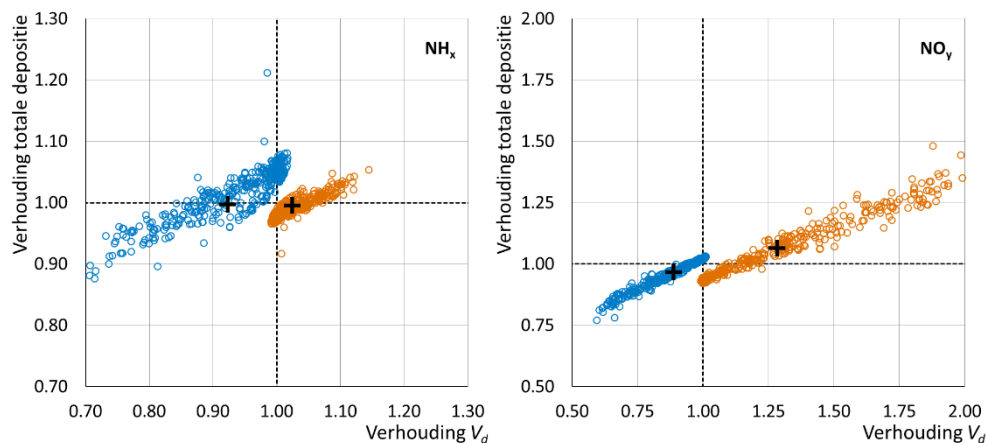
Figuur 6 Het relatieve effect van de verandering van de oppervlakteweerstand op de lokale depositiesnelheid (horizontale as) en op de berekende totale depositie (verticale as) van NH$_x$ (links) en NO$_y$ (rechts).
De totale depositie is de som van de droge en natte depositie van alle componenten, zoals berekend met OPS ($D_{NH_x\,tot} = D_{NH_4\,nat} + D_{NH_3\,primair\,droog} + D_{NH_4\,secundair\,droog}$, en $D_{NO_y\,tot} = D_{NO_3\,nat} + D_{NO_x\,primair\,droog} + D_{NO_3\,secundair\,droog}$).
Bij oranje run is de oppervlakteweerstand van gras 20% van de normale waarden, en bij de blauwe run 500%.
Veranderingen worden weergegeven als de verhouding met het resultaat van de normale run. De ✚ tekens geven een uit deze berekeningen geschat gemiddeld effect voor Nederland, na weging met landgebruik.

1.4.3 Resultaten

De OPS-resultaten laten diverse vormen van compensatie zien. Figuur 6 geeft weer hoe een verandering in depositiesnelheid de lokale en landelijk gemiddelde depositie beïnvloedt. De cirkels zijn de ruim driehonderd locaties waar we de lokale depositiesnelheid en depositie bepalen. Op de horizontale as staat de verhouding in de lokale depositiesnelheid van de nieuwe run ten opzichte van normaal. Dit geeft dus de lokale invloed van de aanpassing van de oppervlakteweerstand van gras op de depositiesnelheid weer. Deze verhouding zal afhangen van de hoeveelheid gras direct rondom een specifieke locatie. Op de verticale as staat de verhouding van de totale depositie ten opzichte van normaal, ofwel het effect op de depositie.

De figuur laat de resultaten zien van twee runs op alle locaties. Bij de oranje run is de oppervlakteweerstand van gras 20% van de normale waarden (een factor 5 lager). Hierdoor is de depositiesnelheid boven gras hoger dan normaal (in de meeste gevallen is de verhouding $V_d > 1.0$). De invloed op V_d verschilt per locatie omdat de hoeveelheid

grasland in de omgeving van elke locatie verschilt. Bij de blauwe run is de oppervlakteweerstand 500% (een factor 5) groter dan normaal. We zien nu het omgekeerde, de depositiesnelheid is lager dan normaal.

De invloed op de depositie is lager dan de verandering van de depositiesnelheid: de verticale bandbreedte is kleiner dan horizontale. Zie bijvoorbeeld de oranje 20%-run van NO_y: het effect op $V_{d\,NOy}$ ligt tussen 1.0 en 2.0 en voor $D_{tot\,NOy}$ tussen 0.9 en 1.5. Dit komt door de invloed van de verandering op de concentratie in de lucht. De hogere depositiesnelheid van grasland in heel Nederland gaat gepaard met lagere concentraties in de lucht en omgekeerd. De droge depositie op de individuele locaties wordt daardoor iets lager dan je zou verwachten op basis van de verandering in de depositiesnelheid ter plekke.
De concentratieverandering beïnvloedt ook de natte depositie. De lagere concentratie bij hogere depositiesnelheid leidt tot minder natte depositie, en omgekeerd. Dit draagt sterk bij aan het dempende effect op de berekende totale depositie (nat en droog).

In Figuur 6 is ook de invloed op het Nederlands gemiddelde te zien (+). We zien dat forse veranderingen in de depositiesnelheid nauwelijks effect hebben op de berekende gemiddelde depositie. Dit komt doordat er naast de dempende effecten ook concentratieveranderingen boven gebieden met andere landgebruik (niet-gras) optreden. De bijbehorende depositieveranderingen zijn in veel gevallen tegengesteld aan die boven gras. En dus zal dit bij middeling over grote gebieden het effect op de depositie door de aanpassingen van gras verder compenseren.
De interactie tussen depositie en concentratie op grote schaal zorgt ervoor dat ook lokaal de onzekerheid in de depositie minder is dan de onzekerheid in de depositiesnelheid. Voor de stikstofoxides is dit in deze berekeningen ongeveer een factor twee lager, en voor ammoniak een factor drie. Na het middelen naar landelijke schaal, heeft een forse verandering in de depositiesnelheid van gras zelfs nauwelijks effect op de depositie. De verhouding in de totale gemiddelde depositie blijft in deze berekeningen vrijwel 1 voor ammoniak. Voor NO_x is de relatieve afwijking in de totale depositie maar ongeveer een kwart van de gemiddelde relatieve afwijking in de depositiesnelheid.
Dit betekent dat de aangenomen één-op-één foutenvoortplanting in paragraaf 1.2 en 1.3 in feite schaalafhankelijk is. De onzekerheid neemt dus af bij het modelleren van grotere gebieden.

Het ligt dan ook voor de hand dat de onzekerheid in de totale stikstofdepositie op Nederlandse schaal aanzienlijk kleiner is dan de 60-70% op lokale schaal.

Volgens de bovenstaande berekeningen zou de fout op Nederlandse schaal wel eens een factor twee (tot drie) kleiner kunnen zijn. Voorlopig gebruiken we die factor en komen zo uit op een onzekerheid van 20-30% (2σ). Maar een meer definitieve kwantificering van het schaaleffect, waarbij we ook rekening houden met andere typen afwijkingen en met meer oppervlaktetypen, vereist nog veel meer verschillende berekeningen. Dit onderzoek is onderdeel van het Nationaal Kennisprogramma Stikstof (NKS).

1.5 Vergelijking GCN/GDN met DN

Ten slotte vergelijken we de resultaten van de GCN/GDN-kaarten met die van de DN-kaarten. Ook hier gebruiken we voor beide modellen de aan de metingen gekalibreerde modelwaarden. Zoals eerder beschreven, worden in DN de concentraties en deposities op een honderdmaal hogere resolutie dan GCN/GDN. Daarom worden in de DN sommige emissies ook op hogere resolutie gebruikt, zonder de som van de lokale emissies te veranderen.

N-depositie (mol/ha/yr)

$y = 1.003x$, $R^2 = 0.9996$,

RMSE $= 25$ mol/ha/yr
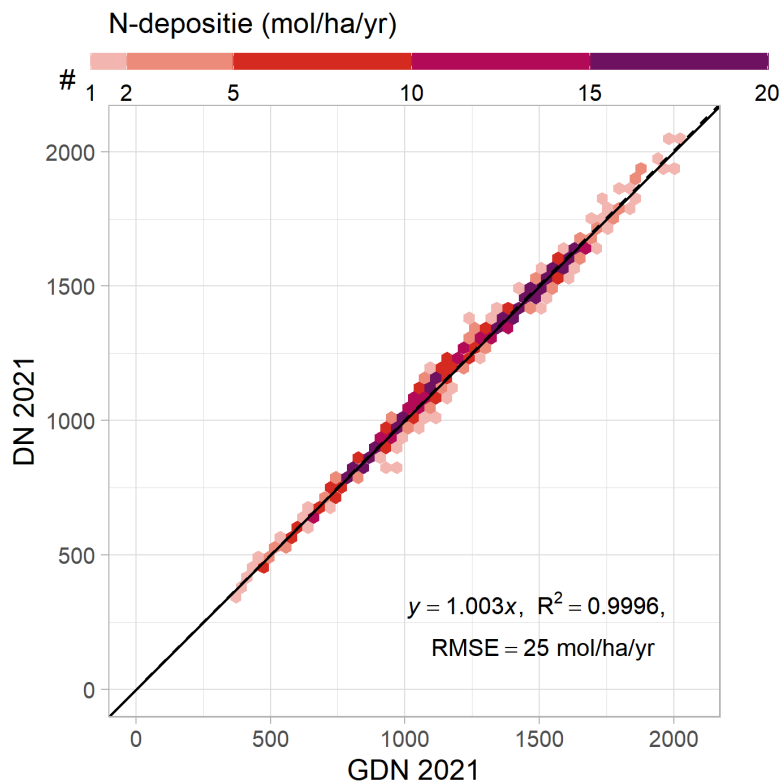
Figuur 7 Vergelijking tussen berekeningen van GDN op 1 × 1 km² en DN op 100m² hexagonen voor de totale stikstofdepositie (som van de zes componenten). De kleuren geven het aantal waarden binnen een hexagoon in de grafiek weer: hoe donkerder hoe meer waarden.

Figuur 7 geeft de vergelijking van de depositieberekeningen van DN met die van GCN/GDN weer. Hierbij hebben we alleen de 1 × 1 km² grid-cellen van GCN/GDN meegenomen, waarbij voor DN minimaal negentig van de honderd hexagonen beschikbaar zijn. Het gemiddelde van de DN-waarde is telkens vergeleken met de GDN-waarde. Het systematische verschil tussen de modellen voor depositie is minder dan 1%. Dit komt doordat hierbij van hetzelfde model, emissie en metingen uitgegaan is. De verschillen hebben een spreiding van 25 mol/ha (RMSE) en worden onder andere veroorzaakt door de hogere resolutie van de DN-emissies. De grootste verschillen treden vooral op als er bij de meetpunten lokale bronnen zijn.
De variabiliteit van de DN-hexagoondeposities binnen een 1 × 1 km² grid-cel is aanzienlijk (circa 30% (2σ)).

1.6 Discussie, conclusie en aanbevelingen

Dit statusrapport geeft een overzicht van de beschikbare kennis over onzekerheden in stikstofdepositieberekeningen van de monitoringskaarten (GCN/GDN en DN). De onzekerheidsberekening is gebaseerd op de vergelijking van modelberekeningen met de beschikbare metingen. De bepaling van de onzekerheid in de depositie is complexer dan de bepaling van die in concentraties. Dit komt doordat directe metingen van de droge depositie grotendeels ontbreken.
De stikstofdepositie is opgebouwd uit verschillende componenten. Deze zijn zowel nat als droog en betreffen zowel ammoniak als stikstofoxides en een aantal reactieproducten. Gezien de complexiteit is er nog geen volledige onzekerheidsanalyse bekend. Daarom is dit de eerste aanzet om tot zo'n schatting te komen. Deze onzekerheid is groter dan de onzekerheden in bijvoorbeeld de luchtkwaliteitsmodellering.

De belangrijkste conclusies zijn dat:
-de onzekerheid van de totale stikstofdepositie bedraagt ongeveer 60-70% (2σ) op een willekeurige locatie in Nederland. Deze schatting is ongeveer gelijk aan eerdere schattingen. Deze nieuwe schatting is dus consistent met de informatie die aanwezig was toen er beleidskeuzes gemaakt werden ten aanzien van toetsing en monitoring;
-de onzekerheid in het Nederlands gemiddelde van de stikstofdepositie bedraagt 20-30% (2σ).

De onzekerheidsschatting op lokale schaal is qua ruimtelijke resolutie representatief voor een willekeurig meetlocatie en de omgeving direct rondom dat meetpunt: de zogeheten 'footprint'. Dit is het gebied bovenwinds dat invloed heeft op de meting, ongeveer 100-1000 m. De ruimtelijke resolutie van DN (hexagoon van 1 ha) als de GDN (grid-cel van 1×1 km^2) liggen dus beide in de range van deze representativiteitsschatting. Op basis van dit onderzoek kunnen we niet onderscheiden of deze onzekerheid representatief is voor een ha of een km2. Maar de kleinere schaal van DN heeft wel als voordeel dat variaties in de depositie binnen 1×1 km^2 zichtbaar worden. Dit kan, omdat verschillen in de locatie van bronnen of lokale eigenschappen van het aardoppervlak per hexagoon een andere depositiewaarde kunnen opleveren.

Het effect van de resolutie op de onzekerheidsschatting kent een tegenstelling. Aan de ene kant laat de vergelijking tussen DN en de GDN zien dat er binnen een 1×1 km^2 grid-cel forse verschillen kunnen optreden. Met name als een bron en het meetpunt dicht bij elkaar zitten. Dat wijst erop dat berekeningen op de fijne schaal zinvol zijn, omdat dan variaties in de depositie tussen hexagonen zichtbaar zijn. Anderzijds wordt een sterk dempend effect op de onzekerheid waargenomen als de depositie over een groter gebied wordt bepaald. Om dat te kwantificeren, is er meer en andersoortig onderzoek nodig. Bij toetsing over grotere gebieden, zoals de Commissie Hordijk adviseert (Hordijk et al., 2020), zou het dempend effect inderdaad tot kleinere onzekerheden in de depositie kunnen leiden. Maar merk op dat dit dus alleen geldt voor de gemiddelde depositie over het gebied.

In dit statusrapport hebben we praktische keuzes over de uitvoering moeten maken:
- In de zes depositiecomponenten is een aantal componenten samengenomen. Zo zitten NO_y, HNO_3^- en nitraathoudende deeltjes in de droge depositie van secundaire componenten.
- In de schatting van de correlatie tussen de diverse onzekerheden hebben we de feedback tussen depositiesnelheid en concentratie niet meegenomen. Bij een analyse die daar meer op is toegespitst, zou dit tot lagere onzekerheidsschattingen kunnen leiden.
- De aanwezige informatie over depositiesnelheden van deeltjes en stikstofoxiden is erg beperkt.

De diverse verbeterpunten komen aan bod in een volgend statusrapport. Ook zullen we dan kijken naar de onzekerheden in de sectorbijdragen en naar de onzekerheid van een individuele bron of projectbijdrage.
De systematische afwijkingen tussen modelberekeningen en metingen worden gecorrigeerd door de modelberekeningen te kalibreren aan de metingen. Daarmee verbetert de (nauwkeurigheid van de) depositieberekening. Maar op locaties waar een sterke kalibratieslag nodig is, zullen interpretaties van modeluitkomsten minder nauwkeurig zijn.
Er zijn diverse onderzoeken geprogrammeerd binnen het NKS om de inzichten in processen en onzekerheden te verbeteren en deze systematische onzekerheden te verkleinen. Bijvoorbeeld door het doen van meer metingen, of door vergelijkingen met andere modellen en een gevoeligheidsanalyse van de diverse parameters in het OPS-model. Dit sluit aan bij de ambitie van het ministerie van LNV om een transparante en wetenschappelijk solide basis te hebben voor het nationale stikstofbeleid met gekwantificeerde onzekerheden.

2   Introduction

2.1   Aim of the study

The deposition of nitrogen compounds may result in a loss of biodiversity in nature areas. In the Netherlands, the deposition of nitrogen is exceeding the critical loads on a large scale.[2] Therefore, the current policy in the Netherlands focuses on reducing the nitrogen deposition.
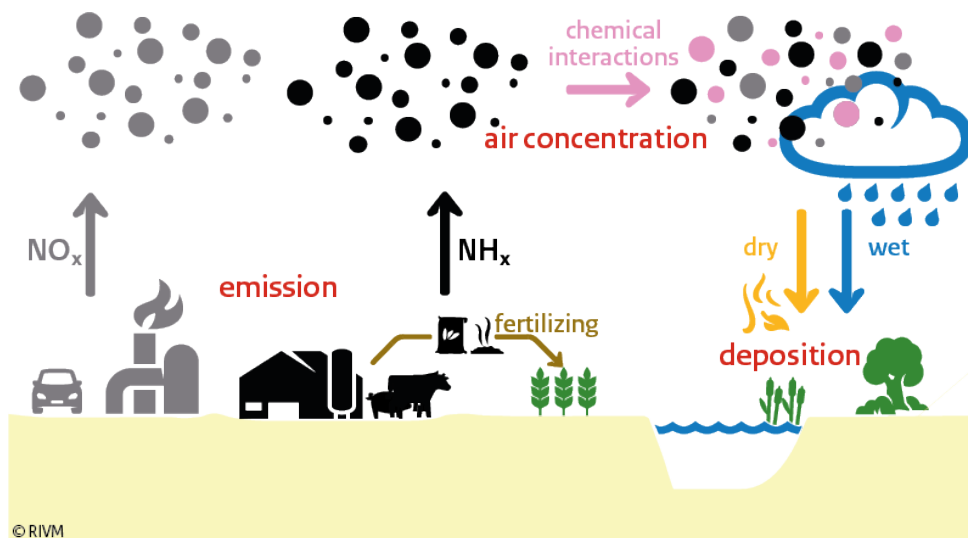
Figure 1 Reactive nitrogen in the air, left: the sources of reduced (NH_x, black) and oxidised (NO_x, grey), right: dry (yellow) and wet (blue) deposition.

The nitrogen deposition consists of various compounds: oxidised nitrogen (such as nitrogen oxides and nitrate) and reduced nitrogen (such as ammonia and ammonium). The oxidised nitrogen originates mainly from emissions from traffic and industrial activities by way of combustion processes. The reduced nitrogen largely originates from agricultural activities.

The nitrogen deposition in the Netherlands is determined by means of a combination of calculations based on the OPS model (Sauter et al., 2023; van Jaarsveld, 2004) and measurements. The OPS model is the basis for two sets of calculations. First, RIVM calculates the total (annual) nationwide nitrogen deposition at a 1×1 km^2 resolution for the GCN/GDN maps (Grootschalige Concentratiekaart Nederland/ Grootschalige Depositiekaart Nederland, Hoogerbrugge et al., 2022). Second, RIVM calculates at a hectare scale for a subset of Natura 2000 areas for the DN maps (Depositiekaarten stikstof Natura 2000-gebieden, https://monitor.aerius.nl/).
Uncertainty plays an important role in the debate on nitrogen deposition numbers and their policy implications. Uncertainties are present in many aspects of the current method by which the nitrogen deposition is

---

[2] Critical load is defined as "the highest deposition of nitrogen as NO_x and/or NH_y below which harmful effects in ecosystem structure and function do not occur according to present knowledge" (ICP, M&M, 2004).

determined: in the emissions, in the modelling of the atmospheric processes (dispersion, transport, chemistry, deposition) and in measurements. To identify areas for improvement, frequent scientific reviews have been carried out (Hordijk et al., 2020; Sutton et al., 2015). In these reviews the importance of uncertainty analysis is identified.

Analysis of the uncertainty in concentrations and wet deposition are available in, for example, the EMEP status report (EMEP, 2022). The EMEP does not report the uncertainty of the total nitrogen deposition. Walker et al. (2019) state that complete uncertainty analysis of the modelled total nitrogen deposition is not yet available.

The government aims at a transparent and scientifically robust basis for the national nitrogen policy that quantifies uncertainties. To achieve this, the Dutch Ministry of Agriculture, Nature and Food Quality (ministerie van Landbouw, Natuur en Voedselkwaliteit: LNV) has initiated a National Knowledge Programme on Nitrogen (Nationaal Kennisprogramma Stikstof: NKS). The NKS programme will propose and implement improvements in the measurement and modelling system that is used to evaluate the nitrogen deposition on nature areas. Thus, a thorough quantification of the uncertainties in determining the nitrogen deposition is important. This is not only important for policy support and communication purposes, but also for setting up a reference to quantify the uncertainty reduction by improving the model and measurement system. Moreover, the knowledge on the most important sources of uncertainties will be used to prioritise research activities.

Insight into and quantification of uncertainties is wanted in various types of (policy) indicators or calculations, including:
- uncertainty in the nitrogen deposition on the Netherlands and its nature areas;
- uncertainty in the nitrogen deposition on 1×1 km^2 and ha scales;
- uncertainty in the exceedance of the critical loads of nature areas and the area(s) where critical loads are exceeded;
- uncertainty in the trends in the nitrogen deposition in time;
- uncertainty in the emission contribution by sectors to the nitrogen deposition on the Netherlands;
- uncertainty in the contribution by a single source to the nitrogen deposition on a specific nature area on a local scale, i.e. within 25 km from the source;
- uncertainty in the contribution by a single source to the nitrogen deposition on a specific nature area on a large scale, i.e. up to a few hundred km.

In general, no detailed uncertainty analyses of the above indicators or calculations have been carried out yet. However, Van Jaarsveld (2004) did analyse the uncertainty in the deposition. On the basis of this analysis, a 70% uncertainty was estimated in the first publication of the GDN (Velders et al., 2010). A more precise estimation of the uncertainty on the regional and national scales is desirable, as is an uncertainty estimate on a local scale. In this report, we will estimate the uncertainties in the nitrogen deposition on national and local scales.

This report should be considered as a status report in which we give an outline the current knowledge on the various uncertainties and options to improve the uncertainty estimates.

On the basis of these options, along with new methods and measurements becoming available from the NKS programme and literature, we will update this report. Subsequently, we will also take uncertainty estimates for other indicators or calculations into account.

2.2 Detailed background

In this section, we will give a more detailed overview of the various N compounds, and of the processes and methods that are important in this study.

As stated before, nitrogen deposition consists of both oxidised and reduced nitrogen. Both groups contain primary compounds as well as compounds that are formed by chemical reactions in the atmosphere (secondary compounds). For instance, particles called secondary inorganic aerosols (SIAs).

Oxidised nitrogen contains one or more oxygen atoms. The main species in the gas phase are nitrogen oxides (NO, NO_2 and HNO_3), while in SIA, it is nitrate (NO_3^-).

Reduced nitrogen contains hydrogen atoms. The main species are ammonia (NH_3) in the gas phase and ammonium NH_4^+ as the secondary compound.

The amount of these compounds per unit volume of air is called the concentration. The amount of these compounds that get to the surface per surface area (e.g. m^2 or ha) per unit of time is called deposition. The concentration influences the deposition. In general, the larger the concentration, the larger the deposition on the Earth's surface.

Two mechanisms of deposition can be distinguished (see Figure 1, right-hand side). First, the compounds get to the surface in and with precipitation, which is called wet deposition. Second, plants and soils absorb nitrogen compounds from the air, which is called dry deposition. Apart from concentration, there are other processes and factors that influence deposition. These differ across the six compounds. For instance, wet deposition is influenced by the amount and intensity of the precipitation.

For dry deposition, the deposition velocity is important. The deposition velocity is a measure of how easily the compounds move through the air towards the Earth's surface and are subsequently absorbed by soil and plants. The deposition velocity differs for each N compound. And it also strongly depends on the weather, land use and roughness of the Earth's surface, soil type and vegetation type.

Since the deposition velocity is important to the calculation of the dry deposition, it is also important to have an estimate of uncertainty within the deposition velocity. Therefore, it is important to note that while the concentration influences the deposition, it also works the other way around: the amount of deposition has an effect on the concentration because mass is removed from the atmosphere by that deposition and thus reduces the concentration. We will analyse this effect in Chapter 5. Given the different species and mechanisms, in this report, we

distinguish six compounds that contribute to the total deposition:

$$D_{\text{N tot}} = \begin{aligned}&D_{\text{NH}_4 \text{ wet}} + D_{\text{NH}_3 \text{ primary dry}} + D_{\text{NH}_4 \text{ secondary dry}} + \\ &D_{\text{NO}_3 \text{ wet}} + D_{\text{NO}_x \text{ primary dry}} + D_{\text{NO}_3 \text{ secondary dry}}\end{aligned}$$

Eq. 1

For each compound, the model calculations are calibrated against measurements. In this way, the best estimate on the levels of nitrogen deposition on the Netherlands is obtained. For the calculations of the wet deposition, we calibrate the model against the observations of the wet deposition. In the case of dry deposition, insufficient measurement data is available for direct calibration. Moreover, there are no real-time measurements of the deposition velocity. Therefore, the relation between the modelled and measured air concentration of the compounds is used to calibrate the dry deposition.
In Chapter 3 and 4, we will calculate the uncertainty of both the uncalibrated and the calibrated values per compound and the overall uncertainty.

2.3 Reading Guide

In Chapter 3, we will present the results on the uncertainty estimates in the various deposition compounds. Subsequently, in Chapter 4, we will describe the overall uncertainty in the total nitrogen deposition. In Chapter 5, we will present the effect on uncertainty in the nitrogen deposition due 6to the feedback mechanism of the deposition processes on the concentration. Then in Chapter 6 we will show the comparison between the deposition maps on 1 x 1 km^2 (GCN/GDN) and ha scales (DN). We will finish off with the conclusion and recommendations in Chapter 7.

3   Uncertainty in nitrogen deposition estimates per compound

Authors: Koen Siteur, Joost Wesseling, Ronald Hoogerbrugge, Cor Jacobs

In this chapter, we estimate the uncertainties of the six compounds of the nitrogen deposition by comparing OPS model outputs to measurements over the 2005-2021 period. We evaluate the residual uncertainty. So we define the uncertainty as the residuals after calibration of the model output against measurements and that are assumed to be random.

3.1   Measurements

The aim of this chapter is to estimate the uncertainty of the modelled deposition fluxes by comparing the model results to measurements. However, deposition measurements are not available for each and every compound. This means that we partly rely on concentration measurements. The measurements used in this study are listed in Table 1. All the measurements are annual averages.
The dataset consists of measurements used in the production of GCN/GDN maps, combined with the data collected by the relatively recent and expanding network of COTAG systems that measure the dry deposition of NH_3 (Rutledge-Jonker et al., 2023).

Table 1 also lists the uncertainty estimates for each of the measurement methods, which were derived in previous studies. The listed estimates relate to the uncertainty of the annual average of the measured quantity. NO_2 measurements by passive samplers are performed in duplicates to reduce measurement uncertainty. For NH_3, at least one site per nature area has triplicate measurements. To account for duplicates and triplicates, the measurement uncertainty of the passive samplers of NO_2 and NH_3 is divided by the square root of the number of passive samplers per site.

For most of the compounds, an approximately equal number of measurements is available for each of the years included in this study. Two exceptions are NH_3 and NO_2 concentrations, for which the number of sites has been increasing in recent years. For NO_2, the number of measurement sites has doubled in 2019, to approximately ninety sites, by including measurements of Palmes diffusion tubes performed in the 'Samen Meten' programme and the MAN network (Siteur et al., 2021). For NH_3, the number of sites in the MAN network has been increasing steadily since 2005 (man.rivm.nl). As a result, the uncertainty estimates that are derived in this chapter are slightly biased towards recent years.

Table 1 Measurements included in this study. n is total number of measurements included in this study, and the number of measurements performed in 2021 has been added between brackets. The uncertainty column provides an equation of the uncertainty of the measurement (s^2) because, in most cases, the uncertainty depends on the flux (F) or on the concentration (C).

Quantity	Unit	Method/device	Period	n	Uncertainty	Reference
Dry deposition NH₃	mol/ha/y	COTAG	2012-2020	18 (3)	$s^2 = (0.1F)^2$	(Rutledge-Jonker et al., 2023)
Concentration NH₃	µg/m³	Gradko tubes	2005-2021	3123 (278)	$s^2 = 0.30^2 + (0.06C)^2$	(Noordijk et al., 2020)
Concentration NH₄⁺	µg/m³	Low Volume Sampler Leckel Leckel	2005-2008* 2009-2012 2013-2021**	18 16 36 (4)	$s^2 = (0.080C)^2$ $s^2 = (0.080C)^2$ $s^2 = (0.101C)^2$	Stefess, 2022, pers. com.
Wet deposition NHₓ	mol/ha/y	Wet only samplers	2005-2021	135 (6)	$s^2 = (0.031F)^2$	Stefess, 2022, pers. com.
Concentration NO₂	µg/m³	Chemiluminescence Palmes tubes	2005-2021 2017-2021	651 (41) 142 (51)	$s^2 = 0.993^2 + (0.0412C)^2$ $s^2 = (0.121C)^2$	Stefess, 2022, pers. com. (Nguyen and Wesseling, 2016)
Concentration NO₃⁻	µg/m³	Low Volume Sampler Leckel Leckel	2005-2008* 2009-2012 2013-2021**	18 16 36 (4)	$s^2 = (0.052C)^2$ $s^2 = (0.052C)^2$ $s^2 = (0.070C)^2$	Stefess, 2022. pers. com.
Wet deposition NOᵧ	mol/ha/y	Wet only samplers	2005-2021	135 (6)	$s^2 = (0.031F)^2$	Stefess, 2022, pers. com.

*For the Low Volume Sampler used until 2008, no uncertainty estimates are available. The used uncertainty estimate is probably an underestimation.
**For the 2013-2021 period, NH₄⁺ and NO₃⁻ concentrations were measured every other day, increasing the uncertainty in the annual average concentrations.

3.2 Model calculations

We performed model runs of OPS-LT version 5.1.1.0 to obtain modelled annual average concentrations and deposition fluxes at the measurement sites over the 2005-2021 period. These runs on receptor points provide the concentrations and deposition fluxes at the exact coordinates of the measurement sites. The model input consists of annual NH_3 and NO_x emissions at a 1 x 1 km^2 resolution, with a spatial distribution of each GCN/GDN emission sector set to the 2020 value. The sums of the Dutch emissions were scaled per sector and per year, following the emission data of the Emission Registration (ER; www.emissieregistratie.nl). Emission sums of foreign sources were scaled using emission data of the Centre on Emission Inventories and Projections (CEIP; www.ceip.at). The meteorological statistics that we used to run OPS were calculated for each year using METPRO with meteo data from the Royal Netherlands Meteorological Institute (KNMI; www.knmi.nl) as input. Land use and roughness maps were derived from LGN2020 (www.lgn.nl).

The resolution of the land use and roughness maps determines the resolution of the dry deposition calculations. As GDN maps are currently produced at a resolution of 1 x 1 km^2, the analysis in this chapter is based on 1 x 1 km^2-resolution land use and roughness maps. We realise that this resolution may not match the footprint of the COTAG dry deposition measurements, making a comparison with measurements less reliable for estimating the uncertainty. To study the sensitivity of this choice, we also perform model runs at resolutions of 0.25 x 0.25, 0.5 x 0.5, 2.5 x 2.5 and 5 x 5 km^2.

3.2.1 Post-processing of OPS outputs

OPS produces outputs of concentrations and deposition fluxes for each compound. OPS also computes annual average dry deposition velocities, which, however, are not included in the model outputs. As the dry deposition velocity is required for uncertainty estimation of the dry deposition fluxes (see Section 3.5.1), a post-processing step is required. The dry deposition velocity is obtained by dividing the annual, modelled deposition flux by the modelled annual concentration:

$$V_{d,X} = \frac{F_{d,X}}{C_X}$$

Eq. 2

where C is the concentration of compound X, F_d is the dry deposition flux of that compound and V_d is the dry deposition velocity. Note that OPS takes into account that the vegetation can (re-)emit NH_3 to the atmosphere, by using a compensation point for the vegetation. Hence, for NH_3, Eq. 2 yields the effective annual averaged deposition velocity. OPS calculates and returns the concentrations of all the measured compounds listed in Table 1, except for NO_2. Within OPS, the NO_2 concentrations used to compute the NO_2 deposition flux are derived from the NO_x concentration with the following empirical relationship (Sauter et al., 2023):

$$C_{NO_2} = \beta_1 \ln(C_{NO_x}) + \beta_2 \quad \text{for } C_{NO_x} > \exp\left(1 - \frac{\beta_2}{\beta_1}\right)$$
$$C_{NO_2} = \beta_1 \exp\left(\frac{\beta_2}{\beta_1} - 1\right) C_{NO_x} \text{ for } C_{NO_x} < \exp\left(1 - \frac{\beta_2}{\beta_1}\right)$$

Eq. 3

where $\beta_1 = 8.6$ and $\beta_2 = -12.4$ (concentrations in ppb). As this relationship is used within OPS, we also use it in the computation of the NO_2 concentration from the NO_x concentration.

Finally, in the model output, the dry deposition fluxes are grouped into the deposition of primary and secondary compounds.

For the reduced compounds, the primary compound is NH_3, and the secondary compound is NH_4^+.

For the oxidised compounds in the model, the primary compounds are $NO_x = NO + NO_2 + HNO_2$, and the secondary compounds are $NO_3^- + HNO_3$.

In this study, we derive relative uncertainties in concentrations and ultimately deposition fluxes of NO_2 and NO_3, and we assume that these are representative of the uncertainties of the primary and secondary compounds, respectively.

3.3 Removing systematic model bias

The biases of the model are corrected by calibrating the modelled deposition fluxes against measurements. We use the calibration techniques as applied in constructing the GDN maps. That is, the wet deposition fluxes are calibrated against measured deposition fluxes (Hoogerbrugge et al., 2022) and the dry deposition of NH_3 is calibrated against NH_3 concentration measurements of the MAN network (Wichink Kruit et al., 2020). In Table 2, these calibration variables are marked in green.

The dry deposition fluxes of NH_4^+, NO_3^-, and NO_2, are currently not calibrated in the GDN procedure. To estimate the bias in the deposition fluxes of these compounds, the modelled concentrations are calibrated against measured concentrations using the methods currently applied to calculate the official GCN concentration maps. In Table 2, these calibration variables are marked in blue.

Biases in the dry deposition velocities of NH_3, NH_4^+, NO_2 and NO_3^- could not be estimated. In Table 2, these dry deposition velocities are marked in orange.

*Table 2 Calibration methods to estimate biases in the deposition fluxes. Column 3 and 4 indicates if the variables are calibrated: N means No and Y means Yes. Column 3 (**T**) for the analysis in **T**his study and 4 (**G**) in the **G**DN procedure.*

Flux	Variable	T	G	Method/Reference
$F_{d,NH_3} = V_{d,NH_3} \cdot C_{NH_3}$	V_{d,NH_3}	N	N	
	C_{NH_3}	Y	Y	Wichink Kruit et al., 2020
$F_{d,NO_x} = V_{d,NO_x} \cdot (C_{NO} + C_{NO_2} + C_{HNO_2})$	V_{d,NO_x}	N	N	
	C_{NO}	N	N	
	C_{NO_2}	Y	N	Siteur et al., 2021
	C_{HNO_2}	N	N	
$F_{d,NH_4^+} = V_{d,NH_4^+} \cdot C_{NH_4}$	V_{d,NH_4^+}	N	N	
	C_{NH_4}	Y	N	Linear regression through origin
$F_{d,HNO_3 +NO_3^-} = V_{d,HNO_3 +NO_3^-} \cdot (C_{NO_3} + C_{HNO_3})$	$V_{d,HNO_3 +NO_3^-}$	N	N	
	C_{NO_3}	Y	N	Linear regression through origin
	C_{HNO_3}	N	N	
F_{w,NH_x}		Y	Y	Linear regression through origin
F_{w,NO_y}		Y	Y	Linear regression through origin

3.4 Uncertainty in the model

The combined uncertainty in the model and measurements is obtained by:

$$s_{\mathrm{OPS}}^2 = \frac{\sum_{i=1}^n (X_{i,\mathrm{obs}} - X_{i,\mathrm{OPS}})^2}{n}$$

Eq. 4

where $X_{i,\mathrm{obs}}$ is one of the measured quantities in Table 1, and $X_{i,\mathrm{OPS}}$ is the same quantity as modelled by OPS, both at measurement site i. The number of measurements is represented by n.
Similarly, the uncertainty in the calibrated model output is obtained using:

$$s_{\mathrm{cal}}^2 = \frac{\sum_{i=1}^n (X_{i,\mathrm{obs}} - X_{i,\mathrm{cal}})^2}{n}$$

Eq. 5

where $X_{i,\mathrm{cal}}$ is the calibrated OPS output at measurement site i. In Eq. 5, the modelled quantity X at location i is calibrated against all the measurements except the measurement at location i. This is referred to as leave-one-out cross-validation. This validation enables a fair comparison between calibrated model and measurement, because the measurements used for calibration are not used for validation (Siteur et al., 2021).

The uncertainty obtained through Eq. 5 is composed of model and measurement uncertainty. Random uncertainties in measurements have been estimated in previous studies and are listed in Table 1. By subtracting the random measurement uncertainty, s_{obs}, from the uncertainty estimated by means of Eq. 5, the uncertainty that can be attributed to the model is obtained:

$$s_{\mathrm{mod}}^2 = s_{\mathrm{cal}}^2 - s_{\mathrm{obs}}^2$$

Eq. 6

3.5 Uncertainties in dry deposition

Measurements of dry deposition fluxes are available for NH_3 only, which means that a direct uncertainty estimate of the modelled dry deposition flux can only be made for NH_3, using the procedure described in the previous section. For the dry deposition fluxes of the other compounds, no uncertainty estimate can be made directly. For these compounds, we will approximate the uncertainty in the deposition flux by combining our uncertainty estimate of the concentration C with an approximation of the uncertainty in the dry deposition velocity V_d, as we will describe in this section.

3.5.1 Decomposition of the uncertainty in dry deposition fluxes
Dry deposition fluxes can be calculated with the product of the deposition velocity and the concentration:

$$F_{\mathrm{d}} = V_{\mathrm{d}} \cdot C$$

Eq. 7

Using a Taylor expansion, the uncertainty in F_d can be approximated by:

$$s_{F_d}^2 = \left|\frac{\partial F_d}{\partial V_d}\right|^2 s_{V_d}^2 + \left|\frac{\partial F_d}{\partial C}\right|^2 s_C^2 + 2\frac{\partial F_d}{\partial V_d}\frac{\partial F_d}{\partial C}s_{V_d C}^2 + \cdots$$
$$= F_d^2\left[\frac{s_{V_d}^2}{V_d^2} + \frac{s_C^2}{C^2} + 2\cdot\frac{s_{V_d}}{V_d}\cdot\frac{s_C}{C}\cdot s_{V_d C}^2 + \cdots\right]$$

Eq. 8

where $s_{V_d C}^2 = \rho(V_d, C)s_{V_d}s_C$, with ρ being the correlation coefficient, s_C is the uncertainty in the concentration estimated using Eq. 5, and s_{V_d} denotes the uncertainty in the deposition velocity. The "..." denotes higher-order terms.

In Appendix B, we will show that, on the local scales considered here, the contribution to the covariance term is negligible. Assuming, V_d and C are indeed independent variables, the exact uncertainty in F_d can be written as (see Appendix B.1 and Goodman, 1960)

$$s_{F_d}^2 = F_d^2\left[\frac{s_{V_d}^2}{V_d^2} + \frac{s_C^2}{C^2} + \frac{s_{V_d}^2}{V_d^2}\frac{s_C^2}{C^2}\right]$$

Eq. 9

which is the relationship that is used in the present analysis to estimate the uncertainty in the dry deposition of NH_4^+, NO_3^-, and NO_2. Note that the uncertainty in F_d is proportional to F_d, and that the relative uncertainty in F_d is composed of the relative uncertainties in V_d and C.

3.5.2   *Estimation of uncertainty in dry deposition velocities of NH_4^+, NO_3^-, and NO_2*

The uncertainty in F_d can be computed for NH_4^+, NO_3^-, and NO_2 using Eq. 9, with the relative uncertainty in C and an approximation of the relative uncertainty in V_d. For the present analysis, we will assume that the relative uncertainty in V_d can be approximated by the relative uncertainty in V_d for NH_3. This is achieved by computing the uncertainty in the effective dry deposition velocity of NH_3 using dry deposition measurements, and subtracting uncertainty resulting from uncertainties in the estimation of the compensation point, as described below.

The dry deposition flux of NH_3 is calculated with the product of the effective deposition velocity and the NH_3 concentration,

$$F_d = V_{d,eff} \cdot C$$

Eq. 10

where the effective deposition velocity accounts for deposition and (re-)emission. The effective deposition velocity is determined by the compensation concentration, which in turn is a function of the atmospheric background concentration C:

$$V_{d,eff} = f(C)V_d$$

Eq. 11

Using these two relationships, we can derive a relative uncertainty in V_d.

The uncertainty in the effective deposition velocity is calculated with:

$$\frac{s_{V_{d,eff}}^2}{V_{d,eff}^2} = \left[\frac{s_{F_d}^2}{F_d^2} - \frac{s_C^2}{C^2}\right]\left[1 + \frac{s_C^2}{C^2}\right]^{-1}$$

Eq. 12

This relationship can be obtained by rewriting the equation for exact variance (Goodman, 1960). Here, $s^2_{F_d}$ is estimated using COTAG measurements, while s^2_C is estimated using the concentration measurements from the MAN network.

Following the same reasoning, the uncertainty in the dry deposition velocity, $s^2_{V_d}$ can be obtained with:

$$\frac{s^2_{V_d}}{V^2_d} = \left[\frac{s^2_{V_{d,eff}}}{V^2_{d,eff}} - \frac{s^2_{f(C)}}{f(C)^2}\right]\left[1 + \frac{s^2_{f(C)}}{f(C)^2}\right]^{-1} \qquad\qquad Eq.\ 13$$

This is the uncertainty that is adopted for the dry deposition velocities of NH_4^+, NO_3^-, and NO_2.

To get an estimate for the uncertainty resulting from the compensation concentration, we need to define function $f(C)$. Both in the OPS model and in observations over peatland (Cape et al., 2008), we find that for relevant ranges of C, $f(C)$ can be approximated by:

$$f(C) = \exp(-aC) \qquad\qquad Eq.\ 14$$

We estimate the exponent to be $a \approx 0.16 \frac{m^3}{\mu g}$, which is based on observations by Cape et al. (2008) over peatland, across a concentration range of 1 to 10 µg/m³.

Given the exponential function, the relative uncertainty in $f(C)$ becomes:

$$\frac{s^2_{f(C)}}{f(C)^2} = a^2 s^2_C \qquad\qquad Eq.\ 15$$

which can be substituted in Eq. 13 to obtain the uncertainty in the deposition velocity. Note that s_C is the absolute uncertainty in the atmospheric background concentration. In OPS, this atmospheric background concentration is obtained by iteratively running the model until a constant concentration is reached. No spatial calibration is performed in this iteration. Therefore, s_C is the uncertainty in the uncalibrated OPS result, which we obtain using the MAN NH_3 concentration measurements.

3.6   Results

To illustrate the performance of the OPS model, Figure 2 and Figure 3 show the modelled and observed values of the measured quantities over the whole observation period (2005-2021), both before and after calibration. The calibration, which was performed for each separate year using all observations except for the observation under consideration (leave-one-out cross-validation), generally moves the modelled results closer to the 1:1 line, without removing the scatter. This indicates that the calibration removes much of the bias, without affecting the random uncertainty. A notable exception is the NH_3 concentration, for which the calibration removes a significant amount of the scatter. This is because part of the scatter in NH_3 concentrations is caused by an east-west gradient in the residuals, which is removed using a spatially explicit calibration method (Wichink Kruit et al., 2020). The average bias in the NH_3 calculations is small.
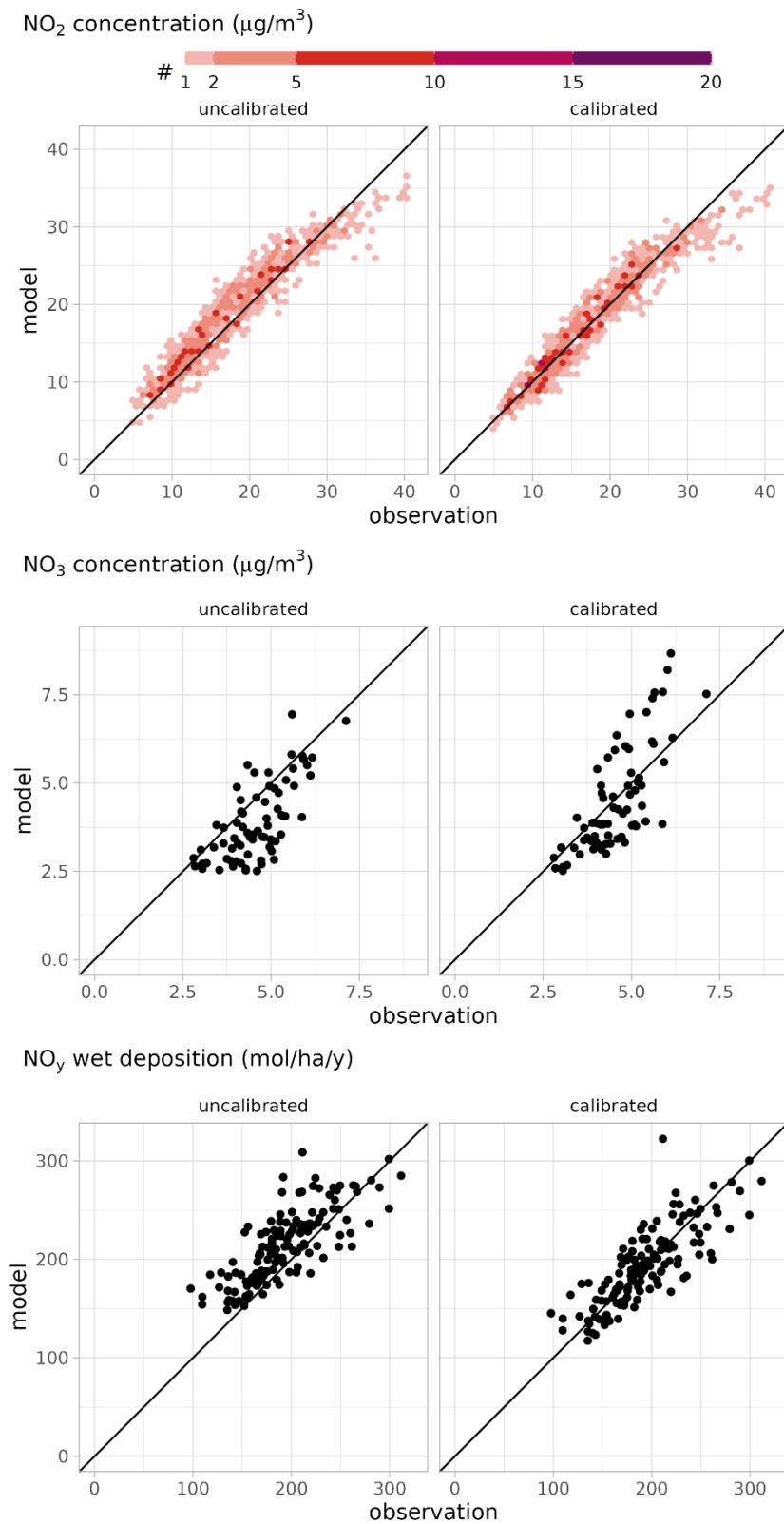
Figure 2 Modelled and observed concentrations and wet deposition fluxes of oxidised compounds at the observation sites, before and after calibration.

NH$_3$ concentration (μg/m^3)
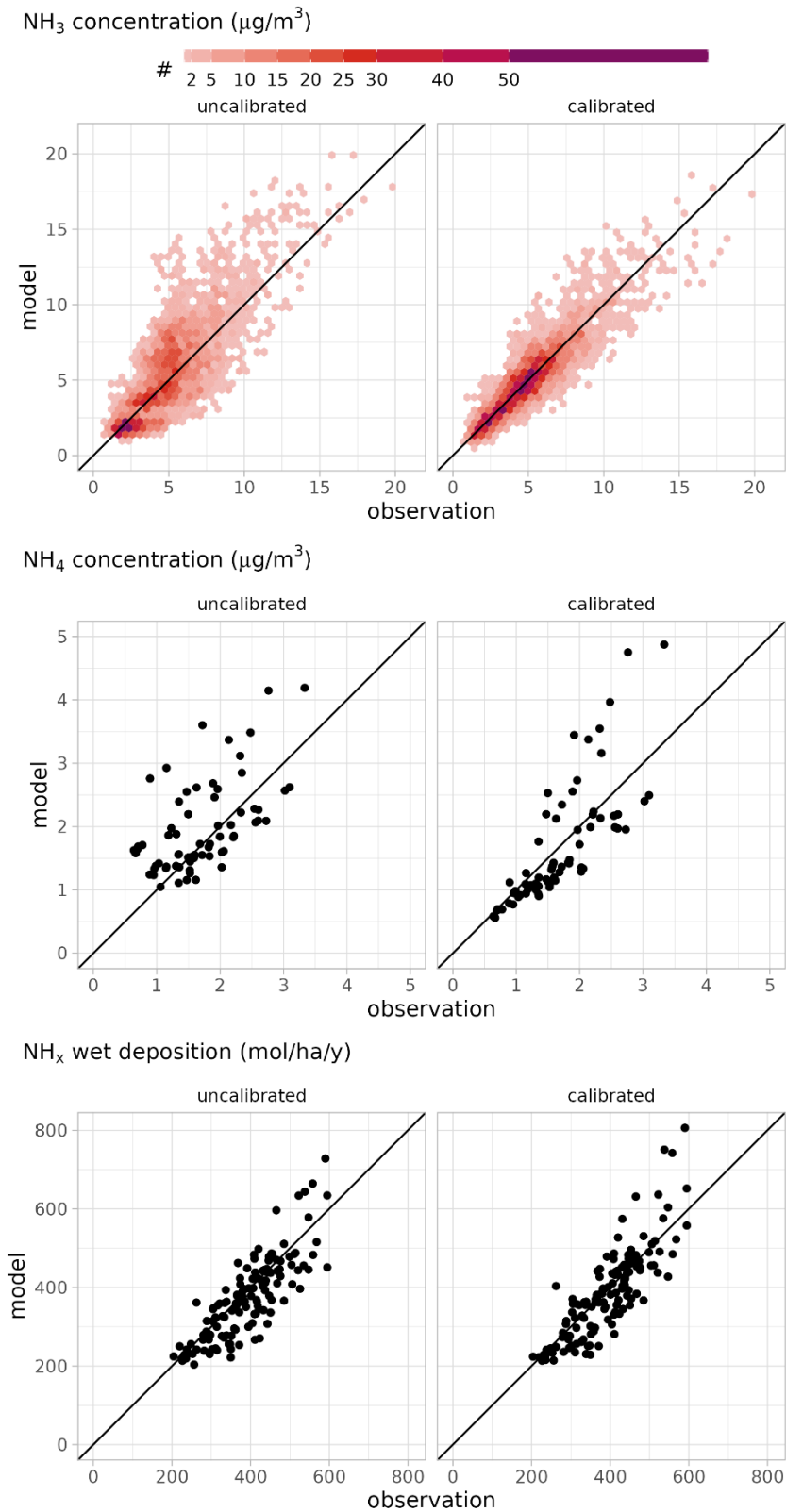
Figure 3 Modelled and observed concentrations and wet deposition fluxes of reduced compounds at the observation sites, before and after calibration.

NH$_3$ dry deposition (mol/ha/y)
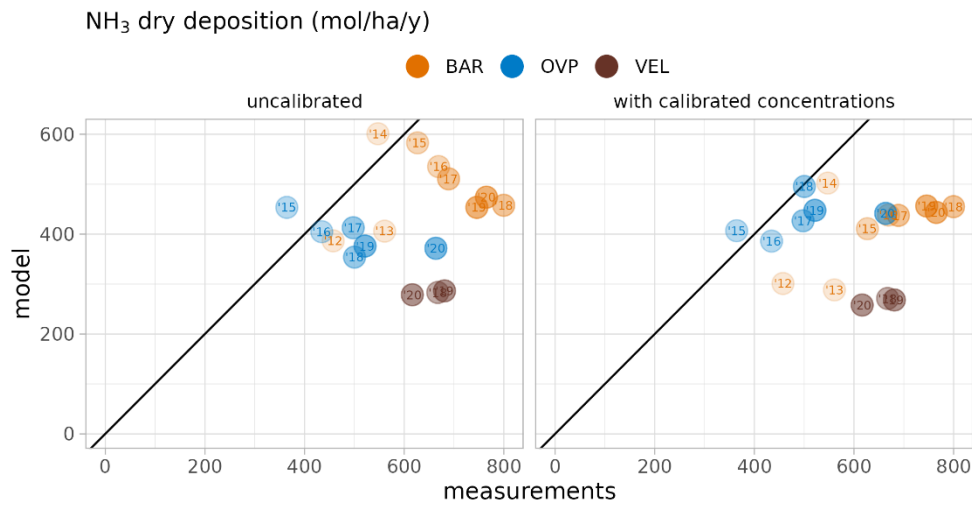
Figure 4 Modelled and observed NH$_3$ dry deposition fluxes (BAR: Bargerveen, OVP: Oostelijke Vechtplassen, VEL: Hoge Veluwe). In the right-hand figure, concentrations are calibrated, using the MAN observations, following the current GCN/GDN procedure. Calibration of the resulting deposition flux is not yet possible (see text).

Figure 4 shows measured and modelled dry deposition fluxes of NH$_3$ at the COTAG locations.

Table 3 summarises the model performance for each of the measured quantities, both before and after calibration. The uncalibrated model performs relatively well on NO$_2$ concentrations and wet deposition fluxes, as indicated by the low relative standard deviations. The uncertainties in modelled NH$_3$ concentrations and the concentrations of the secondary compounds are relatively high. However, the calibration improves the model performance on these concentrations considerably.

Table 3 Model performance before and after calibration.
Subscripts obs, OPS and cal refer to statistics of observations, uncalibrated results and calibrated results, respectively. s_{mod} is the model uncertainty, i.e. the uncertainty that remains after subtracting measurement uncertainty. The operator ⟨ ⟩ means the average over all results at the observation sites.

compound	quantity	unit	$\langle X_{obs} \rangle$	s_{obs}	$\langle X_{OPS} \rangle$	s_{OPS}	$\langle X_{cal} \rangle$	s_{cal}	s_{mod}
			observed		uncalibrated		Calibrated		Calibrated without s_{obs}
NH$_3$	C	µg/m^3	5.2	0.4	5.7	2.1	5.2	1.2	1.1
NO$_2$	C	µg/m^3	18.1	1.2	19.0	2.4	18.1	1.9	1.4
NH$_4^+$	C	µg/m^3	1.7	0.2	2.0	0.7	1.7	0.6	0.6
NO$_3^-$	C	µg/m^3	4.6	0.3	3.9	1.0	4.5	1.0	1.0
NH$_x$	F_w	mol/ha/y	391	12	373	61	384	64	62
NO$_y$	F_w	mol/ha/y	194	6	215	34	193	25	24
NH$_3$	F_d	mol/ha/y	604	62	428	228	403	249	241

Table 4 Relative uncertainties per deposition flux.

compound	quantity	$\frac{s_{C,cal}}{\langle C_{cal}\rangle}$	$\frac{s_{V_d}}{\langle V_d\rangle}$	$\frac{s_{F,cal}}{\langle F_{cal}\rangle}$	$\frac{s_{C,mod}}{\langle C_{mod}\rangle}$	$\frac{s_{V_d,mod}}{\langle V_{d,mod}\rangle}$	$\frac{s_{F,mod}}{\langle F_{cal}\rangle}$
			Calibrated			*Calibrated without s_{obs}*	
NH_3	F_d	23%	56%*	62%	21%	55%*	60%
NO_2	F_d	11%	46%	47%	8%	44%	45%
NH_4^+	F_d	36%	46%	60%	35%	44%	58%
NO_3^-	F_d	22%	46%	52%	21%	44%	50%
NH_x	F_w	-	-	17%	-	-	16%
NO_y	F_w	-	-	13%	-	-	13%

*For NH_3, the uncertainties in the dry deposition velocity represent uncertainties in the effective deposition velocity.

Relative uncertainties were computed by dividing the uncertainties listed in Table 3 by the respective means. These relative uncertainties were then used to calculate the relative uncertainties of the six deposition fluxes using Eq. 9, as shown in Table 4.
Table 3 and Table 4 show that the relative uncertainties in the dry deposition fluxes are large, compared to those in the wet deposition fluxes. This can be attributed to the relatively large uncertainty in the dry deposition velocities. Subtracting the measurement uncertainty has little effect, which means that most of the uncertainty is caused by the model, particularly the calculation of the deposition velocity.

3.7 Interpretation of difference between modelled and measured dry deposition fluxes

The uncertainty estimates of the dry deposition fluxes are based on a small number of observations at the three COTAG sites only. As the difference between observations and the model is relatively large at these sites (see Figure 4), our uncertainty estimates for the dry deposition fluxes are relatively high. Figure 4 suggests that the model mostly underestimates the dry deposition fluxes at the COTAG sites. To investigate the cause of this apparent bias, we used NH_3 concentrations measured at the same sites (at ~5m above the surface) to compute the effective dry deposition velocities. We compare these with the modelled effective dry deposition velocities. From Figure 5, we conclude that the difference between measured and modelled deposition fluxes can be explained by an underestimation of the dry deposition velocities at the COTAG sites. As we only use this limited dataset, it is impossible to assess if this bias is a systematic model bias that also applies to other areas in the Netherlands. Therefore, we have compared the modelled and measured deposition velocities with measurements reported in the literature and with observations with a high resolution deposition flux equipment (GRAHAM) at Solleveld (Vendel et al., 2023), as described in Appendix E.1. On the basis of these comparisons, we cannot confirm that OPS systematically underestimates the dry deposition velocity. Therefore, no bias correction is applied to the modelled dry deposition velocities in this study. A more detailed analysis of the differences between the calculated and measured dry deposition fluxes will be carried out. The improvement on the knowledge on deposition velocities is an important objective in the Dutch research programme 'Nationaal Kennisprogramma Stikstof' (NKS).

NH₃ dry deposition velocity (cm/s)   NH₃ concentration (µg/m³)
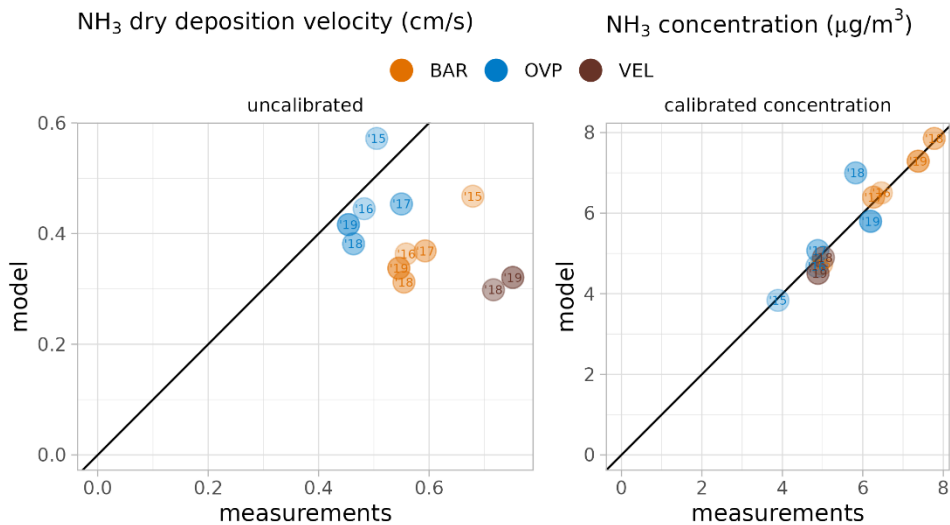
Figure 5 Modelled and measured NH₃ effective dry deposition velocities (left), and concentrations (right) at the COTAG sites (BAR: Bargerveen, OVP: Oostelijke Vechtplassen, VEL: Hoge Veluwe). The modelled deposition velocities are obtained by dividing modelled deposition fluxes by modelled concentrations at a height of ~5m. The observed deposition fluxes are obtained by dividing measured deposition fluxes (COTAG) with measured concentrations (MAN) at a height of ~5m.

3.8   Conclusion & Discussion

In this chapter, we have derived estimates of the uncertainties in six modelled deposition fluxes. The dry deposition fluxes have the largest relative uncertainty, mainly due to uncertainties in the dry deposition velocities. Both modelled and observed deposition velocities for ammonia fall well within the range of values reported in the international literature. Measurement uncertainty contributes little to the total uncertainty, implying that the differences between modelled and measured fluxes and concentrations are mainly caused by model uncertainties, particularly uncertainties in the deposition velocities. Given the small number of sites for which dry deposition measurements are available, it is hard to get reliable uncertainty estimates of the dry deposition fluxes. This can be solved in future studies by expanding the number of COTAG sites, and/or by deriving uncertainty estimates of the dry deposition velocities using uncertainties in underlying variables, such as the friction velocities, land use and roughness lengths. Finally, for a fair comparison between model and measurement, the resolution of the roughness and land use maps in the model should match the footprint of the COTAGs. In present analysis, we have opted for a resolution of $1 \times 1 \ km^2$, as this is the resolution currently used in the production of GDN maps. A more detailed analysis of the differences between the calculated and measured dry deposition fluxes at the COTAG-sites needs to be made.

4   Uncertainty in total nitrogen deposition

Authors: Koen Siteur, Joost Wesseling, Ronald Hoogerbrugge

In Chapter 3, we derived the relative uncertainties in each of the six modelled deposition fluxes. However, the uncertainty of the six individual fluxes does not yet inform us about the uncertainty in the total nitrogen deposition. In addition, the derived uncertainties represent the performance of calibrated model fluxes. In GDN and DN maps, not all fluxes are currently calibrated, and the bias should be accounted for in our uncertainty estimate. In addition, the uncertainty of the uncalibrated model result is of interest, as it informs us about the performance of the OPS model.

In this chapter, we establish a way to compute the uncertainty in the total nitrogen deposition, given a combination of the six deposition fluxes. We then compute the random uncertainty and bias for each GCN/GDN grid cell. Finally, we determine the average uncertainty for the total nitrogen deposition on Natura 2000 habitats and approximate the uncertainty in the national average total nitrogen deposition.

4.1   Uncertainty in total nitrogen deposition

Since the six deposition fluxes are linked through chemical and physical processes, both in the model and in the real world, they cannot be viewed as independent random variables.

The variance in the sum of dependent random variables is calculated with the sum of (co-)variances. Hence, the uncertainty in the total nitrogen deposition is:

$$s_{Ftot}^2 = \sum_{i=1}^{6} \mathrm{Var}(F_i) + 2 \sum_{j=1}^{5} \sum_{i=j+1}^{6} \mathrm{Cov}(F_i, F_j) \qquad \text{Eq. 16}$$

The first term in Eq. 16 is the sum of the squared random uncertainties of each of the six deposition fluxes, $\sum_{i=1}^{6} s_{Fi}^2$, as derived in Chapter 3. The second term results from covariance between uncertainties. The covariances in the second term can be written as:

$$\mathrm{Cov}(F_i, F_j) = s_{F_i} s_{F_j} \rho(F_i, F_j) \qquad \text{Eq. 17}$$

Where ρ is the correlation coefficient between flux pairs. In Appendix C.2, we use a result from Bohrnstedt and Goldberger (1969) to establish that ρ is solely determined by the relative uncertainties in C, V_d and F_d, as derived in Chapter 3, and by the correlation between the concentrations and the dry deposition velocities. Relative uncertainties being constant, this implies that ρ is constant, i.e. it is independent of the model result to which we wish to apply Eq. 16. In Appendix C.3, we will compute the correlation matrices for V_d and C using residuals at the measurement sites, supplemented with model results. These correlation matrices are combined to obtain the correlation matrix for F, as presented in Table 5.

Table 5 Correlation matrix for the six deposition fluxes. This matrix was derived using the model uncertainties (s_{mod}) from Chapter 3. The correlation matrix based on s_{cal} is very similar (differences are of a magnitude of ≈0.01) and is shown in Appendix C.3.

ρ	$F_{d,\mathrm{NH_3}}$	$F_{d,\mathrm{NO_x}}$	$F_{d,\mathrm{NH_4^+}}$	$F_{d,\mathrm{HNO_3+NO_3^-}}$	$F_{w,\mathrm{NH_x}}$	$F_{w,\mathrm{NO_y}}$
$F_{d,\mathrm{NH_3}}$	1.00	0.74	0.58	0.66	-0.03	-0.10
$F_{d,\mathrm{NO_x}}$		1.00	0.55	0.57	-0.01	-0.05
$F_{d,\mathrm{NH_4^+}}$			1.00	0.76	0.34	0.24
$F_{d,\mathrm{HNO_3+NO_3^-}}$				1.00	0.30	0.22
$F_{w,\mathrm{NH_x}}$					1.00	0.67
$F_{w,\mathrm{NO_y}}$						1.00

Next, we can compute the absolute uncertainty for each deposition flux s_{F_i} for each GDN grid cell for each year. We do this by multiplying the relative uncertainties derived in Chapter 3 by the (calibrated) modelled fluxes. This, in combination with Table 5, is then used to calculate the uncertainty in the total deposition flux, averaged over all years. This procedure yields Figure 6, a map in which the uncertainty in total nitrogen deposition is averaged over the 2005-2021 period.
Note that the analysis described above assumes that uncertainties in C and V_d are proportional to the modelled C and V_d. This assumption will be evaluated in Appendix A by comparing the assumed proportional variance model with binned absolute uncertainty estimates. From this comparison we conclude that for the current analysis, the proportional model can be applied.
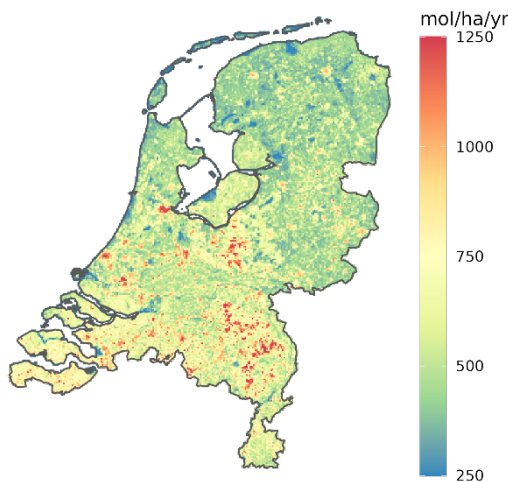
mean random model unc. 2005-2021

Figure 6 Random model uncertainty (s_{mod}) in total nitrogen deposition, averaged over the 2005-2021 period.

4.2   Total uncertainty in total nitrogen deposition

The map derived in the previous section reflects the uncertainty after removing the known model biases from the model result. This remaining uncertainty we interpret as random uncertainty, and it contains both the unbiased uncertainties in the model and uncertainties resulting from the bias correction. To obtain an estimate of the total model uncertainty, we again add the known model biases to the obtained uncertainty estimates.

4.2.1   *Sum of model biases*

The bias for each flux i is determined by subtracting the calibrated model result from the uncalibrated model result for each grid cell:

$$\Delta_i = F_{\text{OPS},i} - F_{\text{cal},i} \qquad\qquad Eq.\ 18$$

The sum of the biases becomes the total model bias:

$$\Delta = \sum_{i=1}^{6} \Delta_i \qquad\qquad Eq.\ 19$$

Figure 7 shows the average total model bias over the 2005-2021 period, for the OPS model (Δ_{OPS}) and for the GDN maps (Δ_{GDN}). The calibration of the GDN maps, and specifically the NH$_3$ concentration map, reduces the known bias by a factor of ~50. However, the known bias in the GDN maps is not zero, as not all measured variables are currently used in the calibration of GDN maps (see Chapter 3, Table 2). The major spatial signature of the estimated bias in the OPS model is strongly reduced by the calibration.
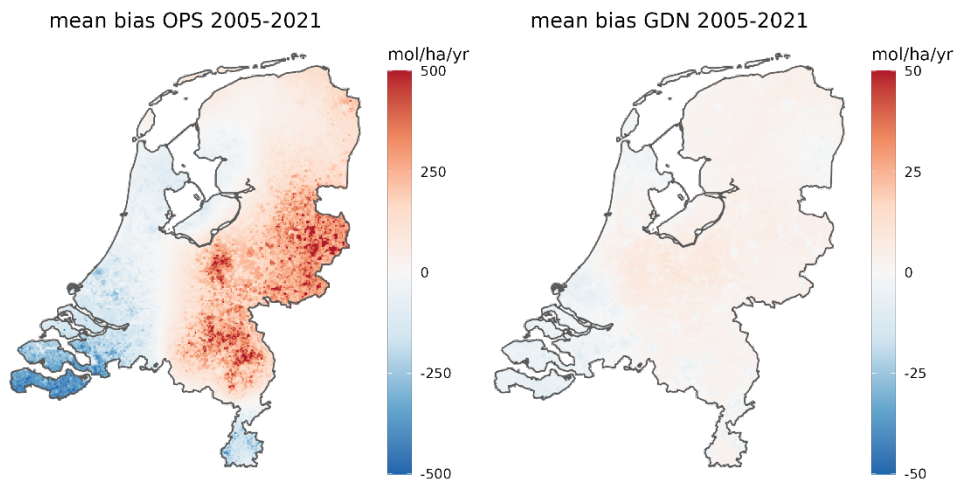
Figure 7 Known bias in total nitrogen deposition of the OPS model and of the partially calibrated GDN map. These maps are obtained by subtracting the calibrated maps from uncalibrated maps (Eq. 18). Note the factor-ten difference in the range of the colour bar.

The estimation of the bias is itself subject to uncertainty. Bias corrections that are based on a large number of observations yield a low uncertainty in the estimation of the bias, and vice versa. This uncertainty is accounted for by cross-validation, which means that it is

part of the uncertainties derived in Chapter 3. As we currently are unable to assess a bias in the deposition velocities, Figure 7 should be interpreted with care. The distribution of known biases suggests an underestimation in the west of the Netherlands and an overestimation in the east, implying that model processes or model inputs are less well captured in these regions.

4.2.2   *Estimation of total uncertainty in total nitrogen deposition*
Now that we have established the random uncertainty and bias for each GDN grid cell, we will estimate the total uncertainty by assuming that the local random uncertainty and the local uncertainty due to uncorrected bias are mutually independent. The total uncertainty of the uncalibrated OPS output, can be estimated as:

$$s_{F_{tot},\text{OPS}} = \sqrt{s_{F_{tot},OPS}^2 + \Delta_{\text{OPS}}^2}$$ *Eq. 20*

The total uncertainty in the GDN maps is becomes:

$$s_{F_{tot},\text{GDN}} = \sqrt{s_{F_{tot},GDN}^2 + \Delta_{\text{GDN}}^2}$$ *Eq. 21*

Figure 8 presents the resulting maps. Note that, since the estimated known bias is smaller than the estimated random uncertainty, it contributes little to the total uncertainty.
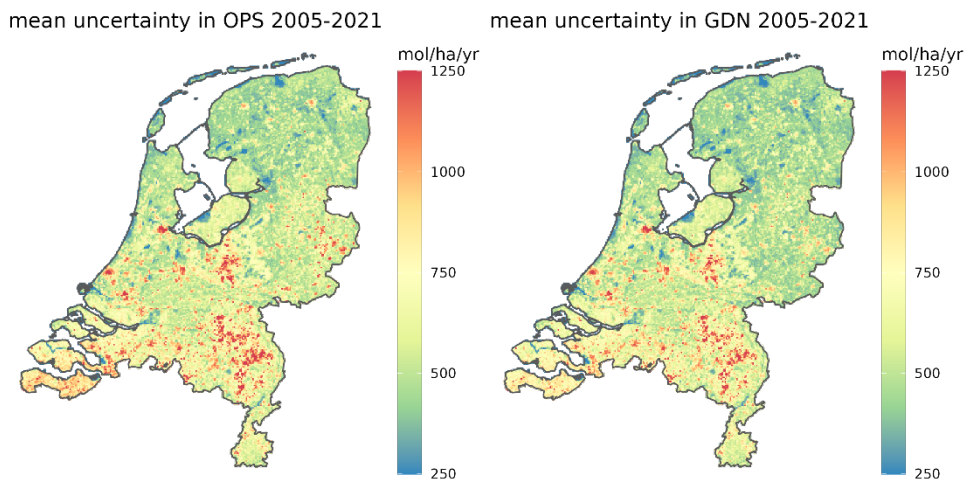
Figure 8 Sum of the random model uncertainty and the bias (Δ) for OPS and GDN.

4.3   Average uncertainty in nitrogen deposition on Natura 2000 habitats

The maps in the previous sections show estimates of the uncertainties for each 1×1 km^2 GDN grid cell. Since we are interested in the uncertainty of the total nitrogen deposition on sensitive Natura 2000 habitats, we computed the average uncertainty, weighted by the fractional cover of sensitive Natura 2000 habitats (Figure 9). A Natura 2000 habitat is considered sensitive if its critical nitrogen

deposition load is less than 2400 mol/ha/y (Dobben and Hinsberg, 2008).

cover of relevant N2000 habitats
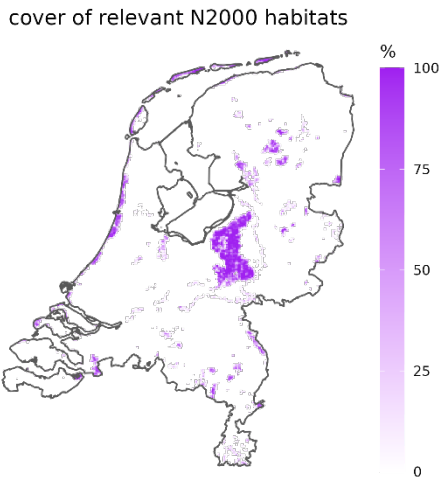
Figure 9 Fractional cover of relevant Natura 2000 habitat for all 1 × 1 km² GDN grid cells.

Table 6 shows the average model uncertainty in total nitrogen deposition on sensitive Natura 2000 habitats. Note that the absolute uncertainties in the uncalibrated OPS model are greater than the absolute uncertainties on the GDN maps, whereas the relative uncertainties are approximately equal. This is caused by the fact that the overestimation by OPS results in a greater denominator in the computation of the relative uncertainty.

Table 6 Average absolute and relative model uncertainties in total nitrogen deposition on Natura 2000 habitats.

	F_{tot} mol/h/yr	$\sqrt{s_{mod}^2 + \Delta^2}$ mol/h/yr	$\frac{\sqrt{s_{mod}^2 + \Delta^2}}{F_{tot}}$ %	$\sqrt{s_{cal}^2 + \Delta^2}$ mol/h/yr	$\frac{\sqrt{s_{cal}^2 + \Delta^2}}{F_{tot}}$ %
		Calibrated; excluding s_{obs}		*Calibrated; including s_{obs}*	
Calibrated ($\Delta = 0$)	1562	491	31%	507	32%
OPS	1663	519	31%	534	32%
GDN	1565	491	31%	508	32%

4.4   Uncertainty of the national average (total) nitrogen deposition

So far, we have described how the random uncertainties in (total) nitrogen deposition fluxes on a local scale are obtained. In some applications (e.g. https://www.clo.nl/en/indicators/en0189-nitrogen-deposition), GDN maps are used to compute the national average (total) nitrogen deposition. In the computation of national averages, the uncertainties resulting from the calibration will dominate. These uncertainties can be derived from approximating the calibration process by a simple subtraction of the mean difference between model and measurement from the national average model result:

$$\langle X_{cal} \rangle = \langle X_{mod} - \langle X_{mod} - X_{obs} \rangle_{Nobs} \rangle_{Ngrid} \qquad \text{Eq. 22}$$

where $\langle X_{obs} - X_{mod} \rangle_{Nobs}$ is a correction computed by averaging the difference between model and measurement across all N_{obs} measurement sites, and $\langle \quad \rangle_{Ngrid}$ averages the calibrated result across all N_{grid} GDN grid cells. Note that for this simplification of calibration, the correction is constant for all N grid cells.

We can rewrite Eq. 22 as:

$$\langle X_{cal} \rangle = \langle X_{mod} \rangle_{Ngrid} + \langle X_{obs} \rangle_{Nobs} - \langle X_{mod} \rangle_{Nobs} \qquad \text{Eq. 23}$$

In general, when taking the mean of N draws of random variable X, the variance in that mean is (see Appendix D):

$$s^2_{\langle X \rangle} = \left(\rho + \frac{1-\rho}{N} \right) \langle s^2_X \rangle \langle X \rangle \qquad \text{Eq. 24}$$

where ρ is the average correlation between the draws, $\langle s^2_X \rangle$ is the uncertainty in X, and $s^2_{\langle X \rangle}$ is the uncertainty in the mean of X.

Assuming that $\langle X_{mod} \rangle_{Ngrid}$, $\langle X_{obs} \rangle_{Nobs}$ and $\langle X_{mod} \rangle_{Nobs}$ are independent, we can write the uncertainty in $\langle X_{cal} \rangle$ as:

$$\begin{aligned} s^2_{\langle X_{cal} \rangle} \\ = \left(\rho_{Xobs} + \frac{1-\rho_{Xobs}}{N_{grid}} \right) \langle s^2_{Xobs} \rangle_{Ngrid} + \left(\rho_{Xobs} + \frac{1-\rho_{Xobs}}{N_{obs}} \right) \langle s^2_{Xobs} \rangle_{Nobs} \\ + \left(\rho_{Xmod} + \frac{1-\rho_{Xmod}}{N_{obs}} \right) \langle s^2_{Xmod} \rangle_{Nobs} \end{aligned} \qquad \text{Eq. 25}$$

The number of GDN grid cells is very large, while the average correlation coefficient between uncertainties in these grid cells within the Netherlands is probably low ($N_{grid} \gg 1 - \rho_{Xobs}$), which means that the first term is negligible. For the observations, it is safe to assume that their uncertainties are independent ($\rho_{Xobs} = 0$). For the model uncertainties, we assume that the observation sites are sufficiently far apart to ensure independence ($\rho_{Xmod} = 0$). The uncertainty in the national average now reads:

$$s^2_{\langle X_{cal} \rangle} = \frac{\langle s^2_{Xobs} \rangle + \langle s^2_{Xmod} \rangle}{N_{obs}} = \frac{\langle s^2_{Xcal} \rangle}{N_{obs}} \qquad \text{Eq. 26}$$

where s^2_{Xcal} is the uncertainty in the model plus the uncertainty in the measurement, as derived for all measured quantities in Chapter 3. For N_{obs} we take the number of measurement sites against which the calibration is performed.

Over the 2005-2021 period, the average number of MAN sites that were used to calibrate the modelled NH₃ concentrations against amounted to 184. However, the MAN network itself is calibrated against an average of 4.6 sites in the LML network. Therefore, we use $N_{obs} = 4.6$ for NH₃ concentrations. The average number of sites that is used to calibrate the wet deposition fluxes against is $N_{obs} = 7.9$. The concentrations of NH₄ and NO₃ are calibrated using an average of 4.1 sites, and the NO₂ concentrations are calibrated against 38.3 sites

(excluding the passive samplers). By applying Eq. 26 to the uncertainties derived in Chapter 3, we obtain the uncertainties in the averaged calibrated concentrations and wet deposition fluxes listed in Table 7.

In order to translate the uncertainty in the national average concentrations to uncertainties in the national average dry deposition fluxes, we need to account for the fact that on larger spatial scales, uncertainties in concentrations and dry deposition velocities can no longer be assumed to be independent, due to mass conservation. For example, an overestimation in V_d, will results in lower atmospheric concentrations and consequently lower dry and wet deposition fluxes. In Chapter 5, we show that a relative change in V_d results in a reduced relative change in the dry deposition fluxes of NH_x and NO_y. This reduced sensitivity is expressed by sensitivity factor f. A change of $x\%$ in the dry deposition velocity yields a change in the dry deposition of $f \cdot x\%$. For NH_x, the sensitivity factor is approximately 0.38-0.45 and for NO_y, it is approximately 0.63-0.75.

To account for the reduced sensitivity, we multiply the uncertainties in V_d by these sensitivity factors. Although changes in the dry deposition velocities also affect the wet deposition fluxes and concentrations, we do not incorporate these dependencies in our uncertainty analysis. This is because both wet deposition fluxes and concentrations are calibrated with measurements and are thus unaffected by biases in V_d.
In addition to the reduced sensitivity of the modelled deposition to changes in the dry deposition velocity, we need to account for the fact that dry deposition fluxes are currently only partially calibrated. That is, we only correct for biases in the concentrations, while a possible bias in the dry deposition velocity is not removed from the model result. To account for the resulting possible bias in the national average dry deposition flux, we add the uncertainty in the emission totals as derived by Wever et al. (2023). For NH_3, the relative uncertainty in the emission total is 14% (1 sigma), and for NO_x the relative uncertainty is 9%. Multiplying these relative uncertainties by both domestic and foreign contributions to the dry deposition fluxes yields uncertainties of 83 mol/ha/yr for NH_3 and 32 mol/ha/yr for NO_x.

Table 7 presents the resulting uncertainties of the national averages. The uncertainty in the national average total nitrogen deposition is 201 mol/ha/yr, or 13%. Using the upper and lower bounds of the sensitivity factors of V_d yields slightly lower and higher uncertainties, respectively. Hence, we conclude that the uncertainty in the national average is probably between 10% and 15%.

Table 7 Composition of uncertainties in the national average total nitrogen deposition. Dry and wet deposition fluxes are denoted as F_d and F_w, and emission fluxes as F_Q. Sensitivity factor f is set to 0.415 for NH_x and to 0.69 for NO_y, which are the mid points of the factors derived in Chapter 5.

	F_{cal} mol/ha/yr	F_{OPS} mol/ha/yr	estimated bias mol/ha/yr	RSD C %	f*(RSD V_d) %	RSD F %	SD F mol/ha/ yr
F_{d,NH_3}	575	657	+82	11%	23%	26%	147
F_{d,NO_x}	227	239	+11	2%	39%	39%	88
F_{d,NH_4^+}	29	36	+7	18%	23%	30%	9
$F_{d,HNO_3 +NO_3^-}$	120	106	-15	11%	39%	40%	49
F_{w,NH_x}	415	406	-8			6%	24
F_{w,NO_y}	196	219	+24			5%	9
F_{Q,NH_3}						14%	83
F_{Q,NO_x}						9%	32
sum	**1562**	**1663**	**147(+3)***			**13%**	**201**

*For GDN the average known bias in the national average total nitrogen deposition over the period 2005-2021 is +3 mol/ha/yr.

4.5 Conclusions

In this chapter, we computed the uncertainty in the total nitrogen deposition by summing the uncertainties in the individual fluxes derived in Chapter 3, while accounting for correlations between the uncertainties of these fluxes. The uncertainty in the total nitrogen deposition depends on the relative contributions made by the six fluxes at a given location, but the average uncertainty in the total deposition on sensitive Natura 2000 habitats is approximately 900-1100 mol/ha/yr (2σ), or approximately 60-70%. This uncertainty is dominated by uncertainties in the dry deposition velocities. As a result, removing biases through calibration or subtracting measurement uncertainties has minor effects on the uncertainty estimate.

In addition, we have derived an uncertainty in the national average total nitrogen deposition of 20-30% (2σ) for the calibrated GDN maps. This uncertainty is dominated by uncertainties resulting from calibration, and by uncertainties due unknown biases in the dry deposition fluxes. The uncertainty in the national average total nitrogen deposition is lower than the local uncertainty within Natura 2000 habitats. This is caused by negative atmospheric feedbacks, which we will describe in the next chapter, and by a reduction of the uncertainty due to averaging.

5 Impact of atmospheric feedback on sensitivity of nitrogen deposition to deposition velocity

Authors: Cor Jacobs, Ronald Hoogerbrugge

5.1 Introduction

5.1.1 Background

Uncertainties in model parameters may only have limited effects on model estimates for deposition on larger scales. This is because the atmospheric mass balance implies a negative feedback cycle. For example, consider a simulation in which the modelled deposition velocity, V_d, is too low. In that case, the initial (local) estimate of the N deposition will also be too low. Too little nitrogen will be removed from the atmosphere, causing too high N concentrations on large spatial scales. However, the higher concentrations enhance the deposition again, compensating the initial effect.

Van Jaarsveld (2004) studied the impact of such surface-atmosphere interactions on the deposition of NH_x, using OPS-Pro 4.1. He reduced V_d of 'grassland' (pasture) by—roughly – 20%. This land use class represents almost 40% of the total surface area of the Netherlands. Thus, a significant influence of surface-atmosphere feedback was anticipated. Van Jaarsveld (2004) evaluated deposition at six locations: three locations in an area dominated by 'grassland' and three in an area dominated by cropland. His simulations confirmed that the reduction of V_d over 'grassland' resulted in larger atmospheric concentrations. In turn, this led to an increase of dry deposition: the effect of the V_d change was smaller than anticipated without any change in concentration. The increased atmospheric concentration also enhanced the wet deposition. At the 'grassland' sites, these effects of the surface-atmosphere feedback compensated the initial reduction of the dry deposition by the change in V_d to a large degree.

Interestingly, the reduced V_d of 'grassland' also resulted in a larger and opposite effect at the cropland locations. This also attributed to the afore-mentioned feedback mechanism. At the cropland locations, hardly any change in V_d occurred, whereas increased atmospheric concentrations resulted in enhanced total deposition. This finding by Van Jaarsveld (2004) reveals another possible implication of surface atmosphere interactions for uncertainties in N deposition estimates on larger scales.

In regions with under- or overestimated deposition, negative surface-atmosphere feedback can reduce the impact on total deposition estimates, but it cannot completely undo it. In addition, due to atmospheric transport, N concentrations – and therefore deposition – may be too high or too low in areas with initially correct. This effect must be opposite to the effect in the 'source area' of the error. As a consequence, averaging over large areas that include both effects implies compensation between negative and positive impacts, and hence a reduction in the total error.

5.1.2   *Goal*
Here, we assess the effect of the mass balance on error propagation across scales. The study by Van Jaarsveld (2004) is extended by examining the sensitivity of the deposition of NH_x (NH_3 + NH_4^+) and NO_y (NO + NO_2 + NO_3^{2-} + HNO_3^-) to V_d on scales where land-atmosphere feedback may be significant. We consider effects on atmospheric concentration and related impacts on both dry and wet deposition and their sum (total deposition) at 362 receptor points in the Netherlands. The receptor points represent locations in the MAN and LML observational networks.

5.2   Method

5.2.1   *Model simulations: general*
Calculations were performed with OPS-LT version L-5010 for the year 2019. As primary compounds, both NH_3 and NO_2 were considered. Emissions for the year 2019 used here include both domestic and foreign sources of these compounds. Spatially averaged meteorological conditions in 2019 for the Netherlands were used to drive the model.

5.2.2   *Variation of V_d*
Deposition velocity V_d for 'grassland' was varied by increasing or decreasing surface resistance, R_c. R_c and V_d are related by:

$$V_d = \frac{1}{R_a + R_b + R_c}$$ *Eq. 27*

where R_a is the aerodynamic resistance, determined by turbulent transport in the lower atmosphere, and R_b is the quasi-laminar boundary layer resistance, determined by the depth and conditions of the thin layer of air neighbouring the surface elements within a canopy (leaves, soil, water).

OPS uses the DEPAC module (DEPosition of Acidifying Compounds, see Sauter et al., 2020; Zanten et al., 2010) to compute R_c. Here, R_c results from a weighted contribution by several component resistances: the canopy-integrated stomatal resistance and the external leaf resistance, the soil resistance and the in-canopy resistance. Van Jaarsveld (2004) changed the in-canopy resistance, but in practice, this approach only results in cases with reduced V_d. Here, we chose to allow both negative and positive V_d changes by forcing R_c from DEPAC to lower or higher values.

In order to vary R_c, and hence V_d, the value of R_c computed by DEPAC at each timestep was systematically multiplied by a change factor, f, to force a difference in V_d with the reference run in which $f = 1$ by definition. For the sensitivity runs, R_c was varied between 20% and 500% of the value computed by DEPAC (f = 0.2, 0.5, 0.8, 1.25, 2.0 and 5.0). Thus, including the reference run, seven runs were performed for both NH_3 and NO_2.

5.2.3   *Land use-dependent variation of V_d at receptor points*
A given relative (fractional) change in R_c will result in different relative changes of V_d. This depends on both the chemical species under consideration and the land use characteristics near the receptor point that is being evaluated. The dependence on land use is obtained because OPS uses a so-called tiling approach to compute V_d and the fluxes at receptor points. In this approach, V_d is first computed for the nine land use classes implemented in DEPAC (see Table 8). Next, a weighted average is computed, using the land use fraction of each class at the receptor point as the weighing factor. As a result, even upon a fixed change of V_d of 'grassland' only, the tiling approach results in different effects on the average V_d at each location. This depends on the composition of the land use around the receptor point.

Since we apply a V_d change to 'grassland', the resulting V_d change 'observed' at a specific receptor point will mainly depend on the 'grassland' fraction surrounding that location. However, Eq. 27 shows that the relative (fractional) response of V_d to a change in R_c also depends on the values of R_a and R_b. Since these resistances also depend on the surface characteristics, the sensitivity is further modulated by the land use surrounding the receptor points. Thus, the tiling approach allows us to effectively sample many different landscape types in our numerical experiment.

Table 8 Fractional cover of the nine DEPAC land use classes in the Netherlands (Sauter et al., 2020), in the receptor footprints and the number of footprints where the specific class is dominant

Land use class	Fractional cover (%) in the Netherlands	Fractional cover (%) in receptor footprints	Number of receptor where dominant
Grassland	37.1	31.7	117
Arable land	24.3	7.5	30
Permanent crops (orchards)	1.2	0.7	4
Coniferous forest	4.2	3.7	10
Deciduous forest	6.2	7.6	17
Water	13.2	8.4	21
Built-up area	11.1	4.3	11
Heather and other nature	2.4	34.4	147
Bare soil	0.3	1.9	5

Table 8 lists the mean characteristics of the landscapes surrounding the receptor locations in terms of land use classes distinguished by DEPAC. The land use throughout the Netherlands is presented for comparison. The land use characteristics near the receptors are determined from the land use map applied in the OPS simulations. The map has a resolution of 250 × 250 m². In turn, this map is based on LGN7 (Hazeu et al., 2014). The nine DEPAC land use classes in the actual OPS map are derived from 39 different land use types distinguished in LGN7, determined at a resolution of 25 × 25 m² (Sauter et al., 2020). We assume that land cover in the OPS map square containing a receptor point roughly represents the main characteristics within the flux

footprint[3] of that receptor. Hence, we will refer to this map area as 'footprint'.

Most of the receptor points are part of the MAN network. The dominant land use at a large fraction of the locations is 'Heather and other nature'. Some overrepresentation of this land use class in the receptor sample is justified, because it corresponds to the areas with habitats sensitive to excessive nitrogen deposition. Cropland appears to be particularly underrepresented. Especially when average effects on the national level need to be evaluated, a correction for representativeness needs to be made.

5.2.4   *Analysis of results*
At the receptor points, we analyse the annual average of V_d, the atmospheric concentration at a height of 3.5 m, and dry and wet deposition fluxes as well as their sums (total deposition). The present version of OPS provides the sum of the deposition of primary and secondary compounds in the output. Therefore, V_d is evaluated using the dry deposition of NH_x and NO_y and the concentration of primary plus secondary compounds. Thus, because the deposition and concentrations are lumped, V_d should be understood as an effective deposition velocity of NH_x and NO_y, respectively. In the case of NH_x, V_d also includes a contribution by the NH_3 compensation concentration at the surface. As we stated before, in the present setup, the impact of changes in R_c on V_d and dry deposition will primarily depend on the fraction of 'grassland' area surrounding the receptor point. However, the composition of the land use beyond the footprint affects the results through the atmospheric feedback, via its impact on both dry and wet deposition.

5.3   **Results and discussion**

5.3.1   *Deposition velocity V_d*
First, we examine the effect of a change in R_c (and hence in V_d) of 'grassland' on the average V_d perceived at the receptor points, which have different fractions of 'grassland' in their footprint (Figure 10). This is the starting point of the analysis. The different colours of the symbols correspond to the different relative changes in R_c used to drive the V_d change over 'grassland' (20%,…,500%); the reference case is represented by the black line (100%). As expected, reduced R_c results in increased V_d and vice versa.
The change in V_d of homogeneous 'grassland', due to the R_c change imposed on the numerical experiment, can be estimated from the results for receptor points with 100% 'grassland' in their footprint. For NH_x, the average change in V_d varies between approximately -20% and +12% for an increase or decrease of R_c, respectively, with a factor of 5. In the case of NO_y, the corresponding changes are much larger, approximately between -35% and +100%. Based on (16), the smaller response for NH_x is expected because of its smaller R_c relative to R_a and R_b. When R_c is small, V_d is dominated by $R_a + R_b$. This implies a smaller (relative) sensitivity to R_c.

---

[3] When measuring concentrations or fluxes, such as deposition, at a given position, the result contains contributions from a wider surface area surrounding this position, depending on the measurement height and meteorological conditions. This area is called the 'footprint'.

The V_d ratio at the receptor points varies roughly linearly with the 'grassland' fraction in the footprint of the receptor. As explained before, this is to be expected because of the tiling approach in OPS, based on weighted contributions to V_d per land cover type. Deviations from this linear behaviour are caused by differences in the average $R_a + R_b$, also related to land use in the footprints of the individual receptors, by differing concentrations of secondary compounds and, in the case of NH$_x$, by differences in the NH$_3$ compensation point. The latter quantity depends on the atmospheric concentration and hence on the large-scale spatial distribution of sources and sinks. Hence, even for a footprint of 100% 'grassland', some variation in V_d change is obtained.
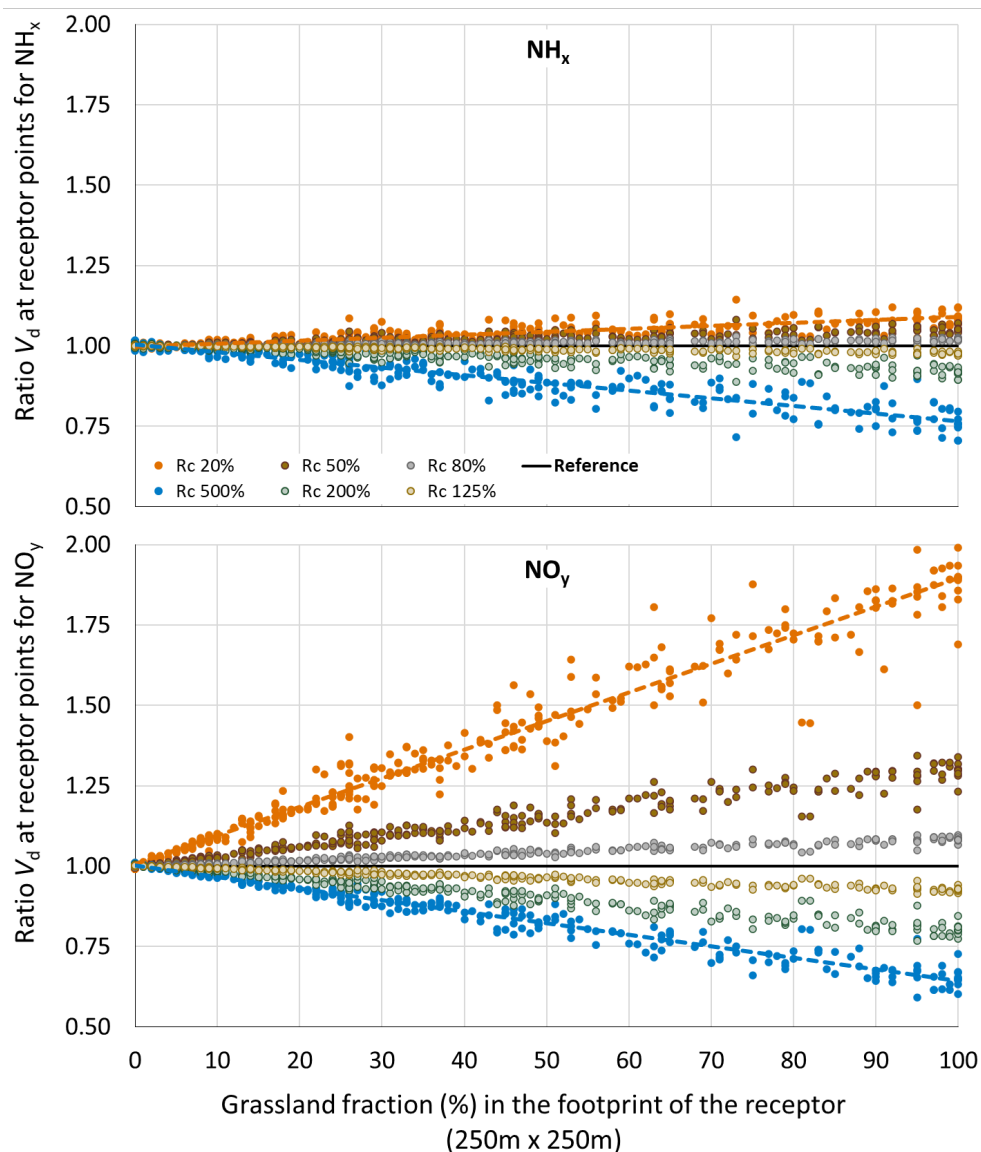

Figure 10 Change in V_d at the receptor points (expressed as the V_d ratio in the reference case) as a function of the 'grassland' fraction in the footprint of the receptors. Upper panel: NH$_x$; lower panel: NO$_y$. The purpose of the regression lines through the results for R_c at 20% and 500% is only to facilitate orientation and comparison.
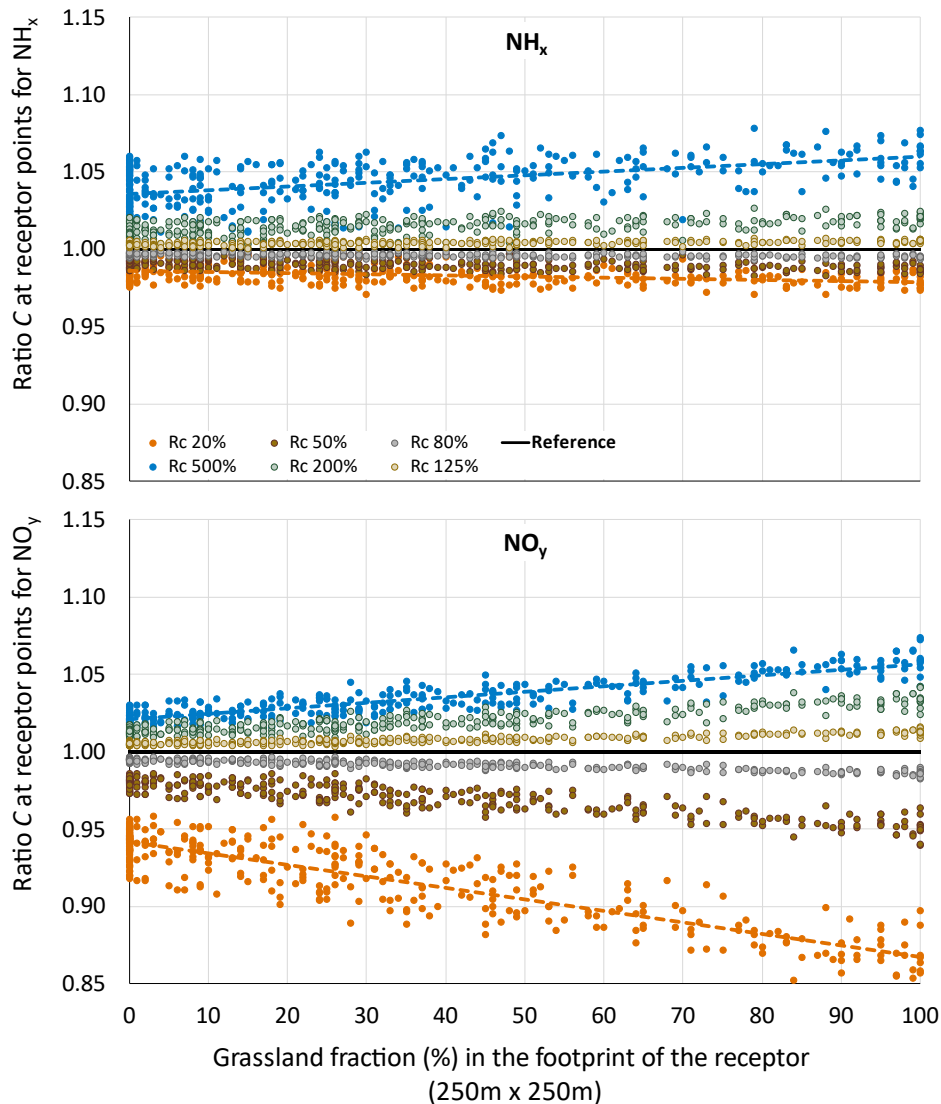
Figure 11 Change in atmospheric concentration, C, at the receptor points at a height of 3.5m (expressed as the ratio with the concentration in the reference case) as a function of the 'grassland' fraction in the footprint of the receptors. Upper panel: NH$_x$; lower panel: NO$_y$.

5.3.2   *Atmospheric concentration*
Mass balance considerations imply that the large-scale change in V_d must result in corresponding atmospheric concentration changes of opposite sign (see Section 5.1). This effect is shown in Figure 11, which depicts the relative change in the atmospheric concentration, *C*, of primary plus secondary N compounds at the receptor points, at a height of 3.5 m. Owing to atmospheric transport and dispersion, the changes are not restricted to 'grassland' areas. For NH$_x$, the concentration changes typically range between -3% and +5%, with a hardly noticeable dependence on 'grassland' fraction. For NO$_y$, the changes are somewhat larger on average, corresponding to the larger changes in V_d, and they do depend on 'grassland' fraction. NO$_y$ concentration changes range between -14% and +7% at 100% 'grassland' locations and between -8% and +2% at locations without 'grassland'.

Figure 12 Change in dry deposition, D_{dry}, at the receptor points as a function of the 'grassland' fraction in the footprint of the receptors. D_{dry} is expressed as the ratio with the dry deposition in the reference case. Upper panel: NH_x; lower panel: NO_y

5.3.3 Deposition

The next step in the feedback loop are atmospheric concentration differences affecting responses of N deposition, both dry (Figure 12) and wet (Figure 13). At first sight, the relative changes in dry deposition at the individual receptor points appear to be similar to the relative changes in V_d (Figure 10). Indeed, local dry deposition is mainly driven by local V_d. However, on closer inspection, the dry deposition ratios turn out to be smaller than the V_d ratios. This is caused by the surface-atmosphere feedback on the larger scales, resulting in the higher concentrations.
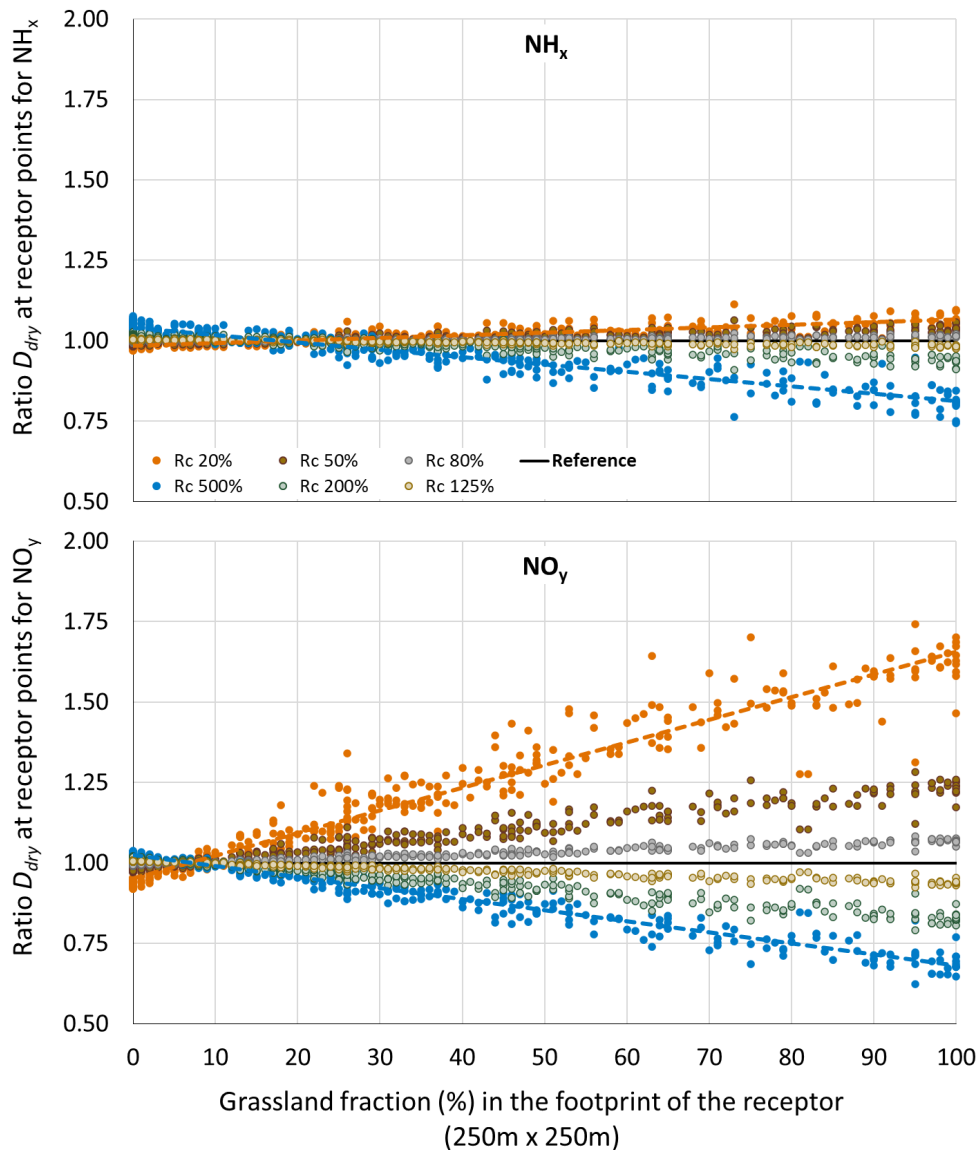
Figure 13 Change in wet deposition, D_{wet}, at the receptor points as a function of the 'grassland' fraction in the footprint of the receptors. D_{wet} is expressed as the relationship with the wet deposition in the reference case. Upper panel: NH_x; lower panel: NO_y.

The changes in wet deposition are almost independent of 'grassland' fraction, both for NH_x and NO_y. This is consistent with the idea that these changes are mainly related large-scale, average concentration changes.

Finally, the net impact on the total deposition will depend on the contribution by the component deposition fluxes. Atmospheric feedback on both dry and wet deposition reduces the relative sensitivity, depending on the share of dry and wet deposition in the total deposition.
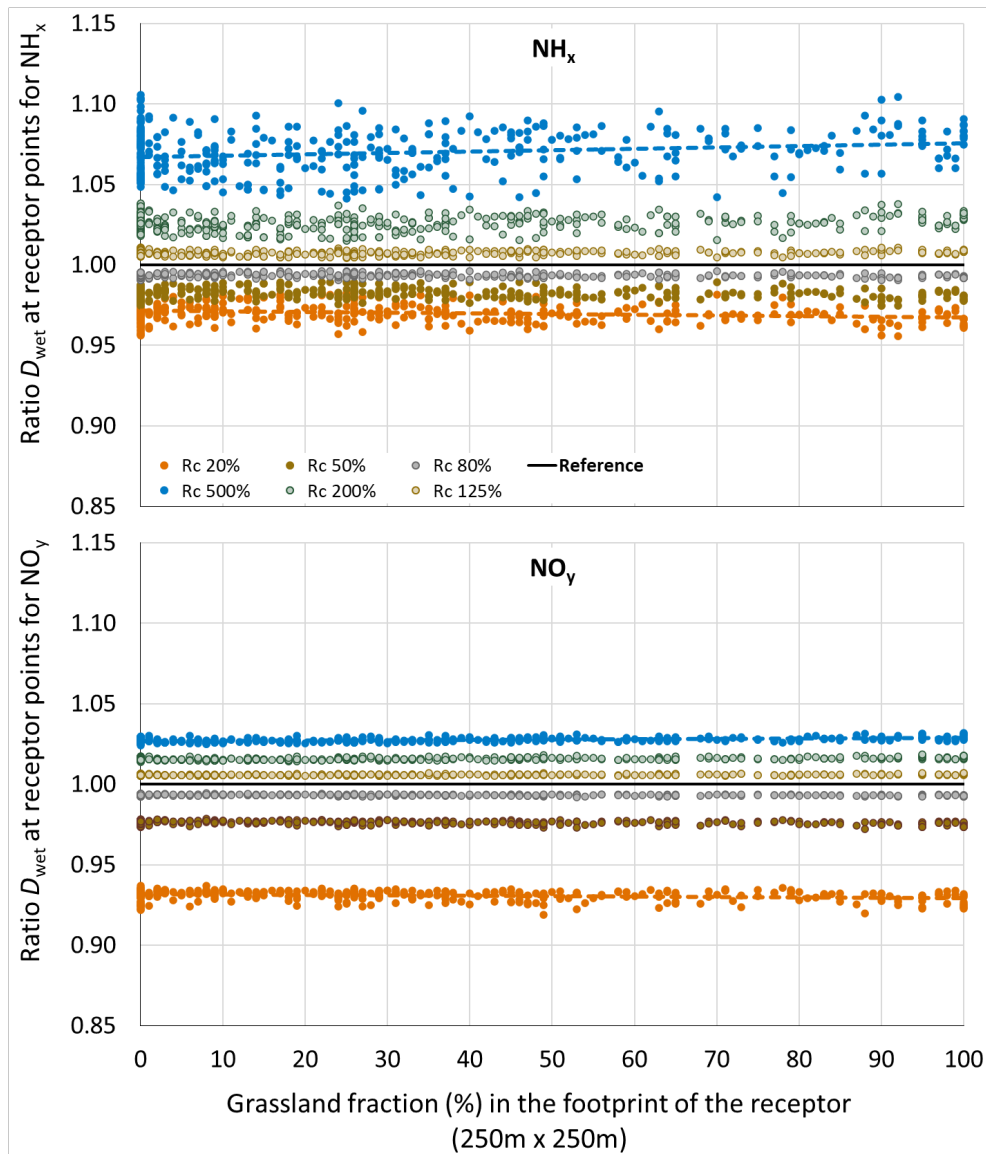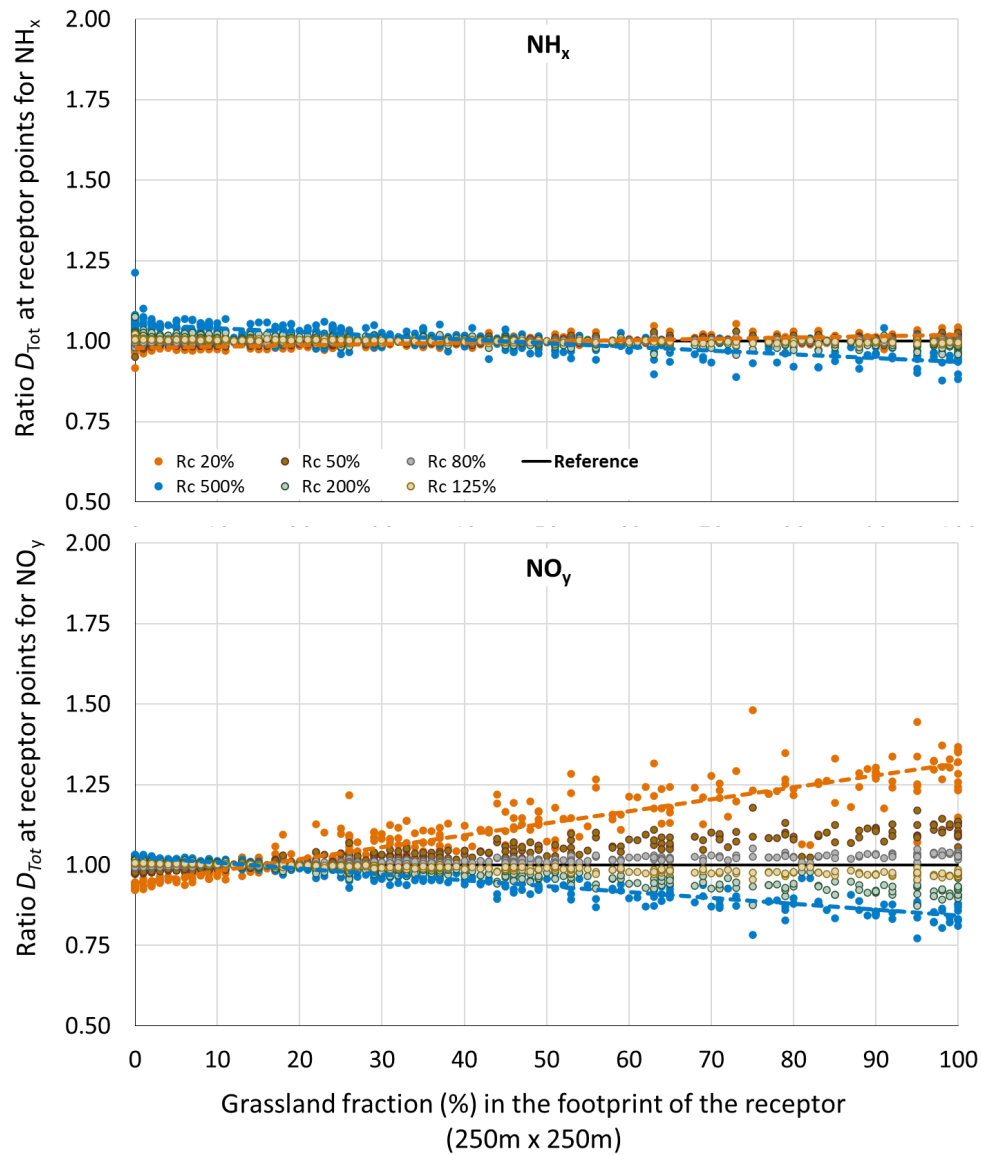
Figure 14 Change in total deposition, $D_{dry+wet}$, at the receptor points as a function of the 'grassland' fraction in the footprint of the receptors. $D_{dry+wet}$ is expressed as the relationship with the total deposition in the reference case. Upper panel: NH_x; lower panel: NO_y.

Figure 14 depicts the change in total deposition on the set of receptor points considered here. The figure shows that the relative change in total deposition is much smaller than the change in deposition velocity V_d and dry deposition (Figure 14 versus Figure 10 for V_d and versus Figure 12 for F_d).

The results presented in Figure 14 confirm that total N deposition estimates are comparatively robust, both for NH_x and for NO_y. This is because the sensitivity of N deposition to (large-scale) V_d is limited and strongly reduced by atmospheric feedback via the concentrations. Note that the outcome regarding concentrations is often constrained by observations.

5.3.4 Carry-over effects

Our results confirm the conclusion by Van Jaarsveld (2004) that a given fractional change in V_d of 'grassland' results in a much smaller fractional change in dry deposition and in total deposition over 'grassland'. Our study also supports the conclusion by Van Jaarsveld (2004) that a large-scale change in V_d of 'grassland' may result in opposite changes in total deposition over other land use classes, without a V_d change. In the case of NH_x, we obtain positive changes in total deposition for a negative change in V_d over 'grassland' at receptor points where 'grassland' fractions are smaller than ~40%. In the case of NO_y, the same applies to for receptor points with less than ~15% 'grassland' in their footprint. However, according to our results, N deposition responses over non-'grassland' areas are not necessarily stronger than responses over (nearly) 100% 'grassland' areas. On average, the relative decrease of total deposition at (nearly) 100% 'grassland' sites is almost equal to the relative increase over non-'grassland' sites. Furthermore, in the case of NO_y the carry-over effect appears to be much smaller for 'non-grassland' sites, instead of larger or nearly equal.

5.3.5 Aggregation to larger spatial scales

To conclude, we further explore the consequences of the surface-atmosphere feedbacks on large scales in the context of spatial averaging. In this context, the carry-over effect described above may help to further increase the robustness of N deposition estimates on ever larger scales.

To this end, we directly examine the sensitivity of dry, wet and total deposition to V_d. This is done in three steps (Figure 15):

1. *No averaging*

   The relative change in dry, wet and total deposition is plotted versus the relative change in V_d at each individual receptor point (circles). We do this for the two most extreme changes in R_c (set at 20% and 500%, respectively, of its original value) and hence V_d over 'grassland' (cf. Figure 10). Recall that the local change in V_d depends on the characteristics of the flux footprint of a specific receptor point. Also recall that V_d should be understood as an effective V_d. Thus, effects of primary and secondary components are combined, along with effects of the compensation point in the case of NH_y. This explains why the sign of the V_d change ratios at receptor points with low 'grassland' fractions in their footprint may be opposite to the sign of the V_d change of 'grassland'. Regarding total deposition (lower panels) at individual receptor points, we find the relative change to be – only—about one third of the relative V_d change for the larger V_d changes. For example, a 30% V_d change at the receptor points induces a change of only about 10% in total average deposition. For intermediate changes in V_d of 5-15%, there may be hardly any effect on the total deposition. In addition, there are clusters of data that represent hardly any local change in V_d. They represent receptors with hardly any 'grassland' in their footprint. At these points, there may still be a significant change in the total deposition, in a direction opposite to the change in 'grassland' V_d. Next, it is explained how changes in both dry and wet deposition contribute to this negative feedback behaviour.

Relative changes in dry deposition (upper panels) are, roughly, 10-25% lower than the relative changes in V_d at the receptor points, depending on the species considered. While they are obviously strongly related to the ones in V_d, they are clearly lower, because of mass balance considerations, resulting in compensating changes in the atmospheric concentration. However, especially in the case of NH$_x$ (left panels) there is a cluster of locations with a near-zero change in local V_d, but, at the same time, with a significant change in the dry deposition, consistent with the carry-over effect discussed earlier.

The relative changes in wet deposition (middle panels) are nearly constant across the entire range of V_d changes shown here. This is to be expected, since wet deposition is driven on larger scales, not by local V_d at the receptor points. The sign of the changes is opposite to the one from the change in V_d, consistent with the mass balance considerations related to surface-atmosphere feedback.

2. *Averaging over receptor points with a given dominant DEPAC land use class (diamonds, see also* Table 8*).*
In all cases, the scatter of the individual points can, to some extent, be considered as a kind of random 'noise'. This is mainly due to the differences in land use characteristics in the flux footprint at a specific receptor point. Hence, when averaging over a larger number of receptor points, the related uncertainty is reduced. This is illustrated in the present step. The averages tend to cluster more towards the ratio 1 for dry as well as for total deposition. Note that the average for locations with 'grassland' as dominant land use in their footprint is somewhat outside the cluster of averages for other dominant land use classes. This is to be expected since the V_d 'forcing' has been applied to 'grassland' in the first place.

3. *Estimated response of national mean, created by averaging results over all receptor points, weighed with fractional occurrence in the Netherlands of the dominant land use in their footprint (pluses, see also Table 6).*
Deviations from the ratio 1 are reduced further. For NH$_x$ in particular (left), negative deviations are compensated by positive ones at near-zero V_d change. As a result, the overall mean total deposition hardly changes (i.e. by less than 0.1%). The overall relative mean change in dry deposition is only about half the one in V_d. For example, in this case, a 6-7% decrease in mean V_d results in a 2-3% decrease in dry deposition. In the case of NO$_y$ (right), the compensation of negative ratios by positive ones is lower, but still significant. For example, a 28% increase in mean V_d changes the overall mean dry deposition by about 18% and the total deposition by about 8%.
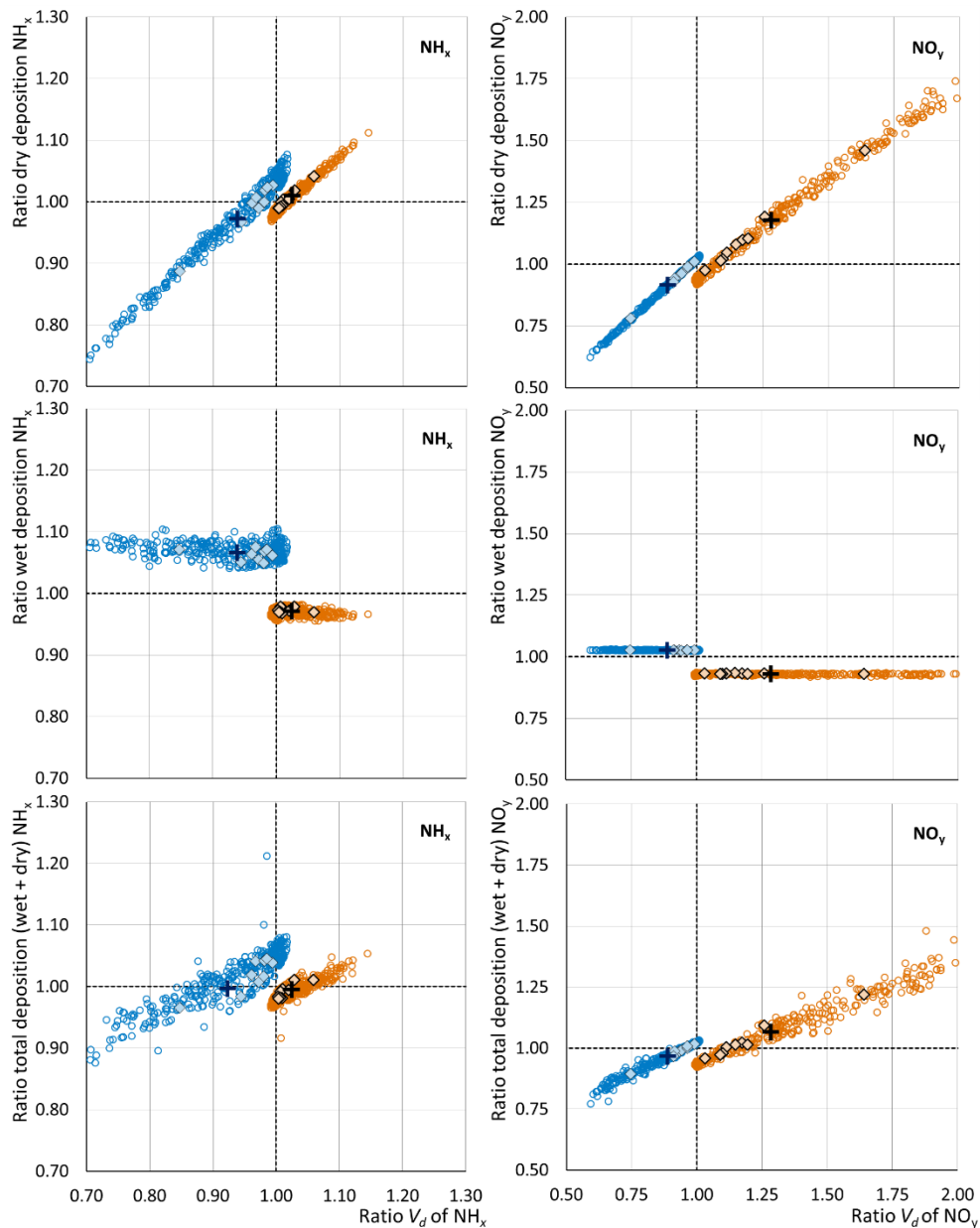
Figure 15 Effect of a change in V_d (x-axis) on dry deposition (upper), wet deposition (middle) and total deposition (lower) for NH$_x$ (left) and NO$_y$ (right). Recall that changes are given as weighed, relative changes of V_d and the deposition considering land use composition in the footprint of a receptor point. The relative changes are expressed as the ratio of the value after a change in R_c of pasture 'grassland' with a factor of five to the value obtained in the reference case without a change in 'grassland' R_c. Open circles (o): at individual receptor points; diamonds (): averaged over clusters of receptors with a specific dominant land use; pluses (+): overall mean. Orange: R_c for 'grassland' is 20% of base value; Blue: R_c for 'grassland' is 500% of base value. Note the differences in axis scales between left (NH$_x$) and right (NO$_y$). The ratio of the relative change in the average F_d over the relative change in the average V_d (indicated by the + marks in the upper panels) was used to obtain the sensitivity factors applied in Section 4.4 to derive the uncertainty in the national average total nitrogen deposition.

5.4 Conclusions

Total N deposition calculations by dispersion models such as OPS appear to be comparatively robust on large spatial scales. In the sensitivity study presented here, large-scale systematic changes in deposition velocity over 'grassland' (~40% of the Dutch land area) are found to to have hardly any impact on total N deposition estimates on the national scale. This has two main reasons.

First, mass balance considerations dictate negative feedback between the surface and the atmosphere: more removal by deposition implies lower atmospheric concentrations, and vice versa. These changes modulate both wet and dry deposition, such that they compensate the initial change. As a result, in our sensitivity studies, the relative change in total N deposition at specific receptor points was found to be – typically—only about one third of the relative V_d change.

Second, owing to atmospheric transport, atmospheric concentration is affected beyond 'grassland' areas as well. Thus, N deposition over non-'grassland' areas will also change. The sign of the change in such areas tends to be opposite to the one over 'grassland'. This reduces the effect of the initial change on the average on a national scale, since negative and positive deviations in N deposition tend to compensate each other. Calibration of the model outcomes against measurements can become confounded by the atmospheric feedbacks. However, on a national scale, this confounding effect will be limited since the average calibration effect is very small.

6 Spatial variability of nitrogen deposition: comparing of GCN/GDN and DN

Authors: Sebastiaan Hazelhorst, Wouter Marra

6.1 Introduction

In this chapter, we compare nitrogen depositions and ammonia concentrations at two different spatial resolutions. The goal of this comparison is to gain insight into the effect of spatial resolution of emissions and grid size on calculated concentrations and depositions. For this comparison, we use data from DN 2021 and GCN/GDN 2021 of ammonia concentrations (unpublished for DN) and total nitrogen deposition. DN contains nitrogen depositions calculated at a high-resolution (1-hectare) hexagonal grid covering Dutch Natura 2000 areas. GCN/GDN contains depositions and concentrations on a 1×1 km^2 grid covering the whole of the Netherlands.

DN and GCN/GDN use the same model (OPS) and emission data to calculate nitrogen depositions. The difference between the two sets is the resolution of the input and the output. For the calculation of GDN-GCN, gridded emissions at a resolution of 1×1 km^2 are used. DN makes use of more detailed information concerning the locations of emission sources, where available. Examples of more detailed emission sources are the locations of roads and the emissions from farms and agricultural fields.

The higher resolution of the DN maps is used in combination with high-resolution data on designated nitrogen-sensitive habitats and breeding and resting sites for rare and threatened species.

6.2 Methods

For the comparison between DN 2021 and GCN/GDN 2021, we used several datasets. First, we compared modelled NH$_3$ concentrations with observations from MAN. For this comparison, we used calculations with emission files that were also used for DN 2021 and GCN/GDN 2021. These emission files are elaborated in more detail below. The receptor file used for the calculations contained the exact coordinates of the measuring sites, including height. These calculations were performed for the year 2018, using emissions from the Dutch Emissieregistratie (Wever et al., 2020), and meteorological conditions for that year. Note that the modelled concentrations of NH$_3$ used here are not bias-corrected (not calibrated against the measurements), as the case with depositions in DN or GCN/GDN, and therefore directly indicate the performance of the model.

Furthermore, we also used NH$_3$ concentrations and total nitrogen depositions from DN 2021 and GCN-GDN 2021 for the projection year 2030.[4] These datasets are obtained using projected emissions. To this end, data from the Dutch Emissieregistratie is combined with projections of emissions in the Netherlands from the KEV-2020 (Klimaat en Energie

---

[4] A comparison between AERIUS and GCN/GDN for an actual year was not possible. The reason is that all calculations for DN are based on long-term average meteorology (2005-2014) and are bias-corrected on the basis of five years of differences between model and observations.

Verkenning; Climate and Energy Outlook). For other European countries, emissions from the MACC III emission inventory[5] are combined with projections of the NAPCP scenario from the EU's second Clean Air Outlook (IIASA, 2021)[6].

The calculations for the projection year are performed using average weather conditions from the 2005-2014 period. The results were bias-corrected on the basis of five years of differences between model results and measurements from the 2014-2018 period. More details on the construction of the DN and the GCN/GDN deposition maps can be found in the AERIUS manual (https://www.aerius.nl/nl/handboeken) and the GCN/GDN report (Hoogerbrugge et al., 2022), respectively. In the analyses, we only used data on so-called relevant hexagons. Relevant hexagons are, in short, hexagons containing nitrogen-sensitive habitats and breeding and resting sites for rare and threatened species.

In order to link DN data with GCN/GDN data, a geographic overlay was made between the hexagonal grid structure of DN and the square grid of GCN/GDN. For every GCN/GDN grid cell, the mean total nitrogen deposition of DN hexagons within each grid cell is calculated.

Thus, we compare the DN values with those of GCN/GDN in the same grid cell. The analysis only includes GDN grid cells containing more than 90 relevant hexagons (>90% coverage). GCN/GDN grid cells with fewer than ninety relevant hexagons will generally not give a fair comparison, as these hexagons are often located on one side of a GCN/GDN grid cell only. Therefore, such clusters of hexagons cannot be considered representative for the GCN/GDN grid cell they are located in. This analysis essentially shows the difference between calculating the deposition at a coarse resolution and calculating the deposition at a high resolution and averaging those values for a larger area.

In addition to a comparison of averages, we directly compared total nitrogen depositions and ammonia concentrations between individual relevant hexagons and the corresponding GCN/GDN grid cells. This provides an assessment of the sub-grid spatial variability of depositions and concentrations within GCN/GDN grid cells. This variability is mainly related to the effect of local emission sources and small-scale (100 m) variations in terrain properties on the outcome. The differences between the two resolutions are further illustrated with an example for the Natura 2000 area Meijendal & Berkheide, located in the province of Zuid-Holland.

6.3 Results

6.3.1 *Comparing of modelled NH$_3$ concentrations with observations*
Modelled concentrations calculated in DN 2021 and GCN/GDN 2021 are each lower than the observations (Figure 16). With a linear regression coefficient of 0.91, the GCN/GDN setup performs slightly better than DN, which has a coefficient of 0.85.

Differences between these two setups can be explained by the locations of emissions. As GCN/GDN uses emissions aggregated on a scale of 1×1 km^2 and DN a more detailed emissions on a hectare scale, the location of the measuring site within a GCN/GDN grid cell plays a key role here (Figure 17).

---

[5] https://cordis.europa.eu/project/id/633080/reporting
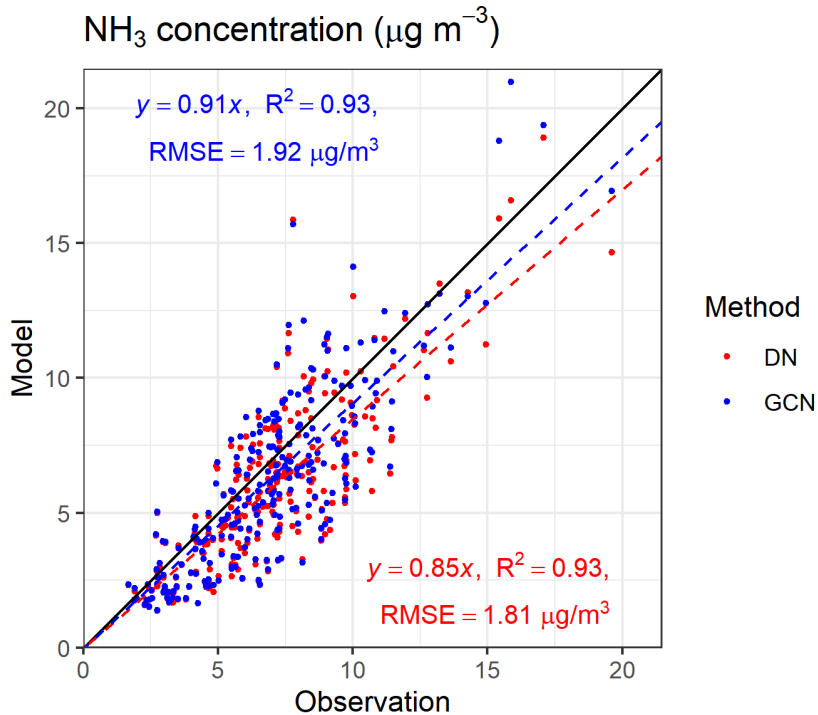[6] https://ec.europa.eu/environment/air/clean_air/outlook.htm

Figure 16 Modelled (y-axis) and measured (x-axis) NH₃ concentrations for the year 2018. In red, concentrations modelled by DN 2021. In blue, concentrations are from GCN/GDN 2021. Observations are yearly averages from MAN and LML. Modelled data are not bias-corrected. The trendlines are based on linear interpolation with the formula $y = a \cdot x$. The standard deviations of a in the formula are equal to 0.015 for DN and 0.016 for GCN.

When, for instance, the measuring site is relatively close (within approximately a couple of hundred meters) to an emission location, the concentration modelled by DN is higher than the one modelled with GCN. This is because the same amount of emission is spread over a large surface in GCN, whereas in DN, the NH₃ is emitted at a specific location. In contrast, as the distance between emission location and measurement site increases, the modelled concentration from GCN/GDN becomes relatively higher than in DN, since the modelled concentration from GCN/GDN remains roughly the same, while in DN, it decreases significantly with distance.

The dominant wind direction in relation to the location of the local sources and receptor also plays a role in explaining the differences between DN and GCN/GDN. At measurement sites that are located on a large distance from sources, i.e. in a grid cell without large emission sources, modelled concentrations of DN and GCN/GDN are more comparable. For the calibrations of both maps, measurement sites that are located directly next to large sources are excluded.
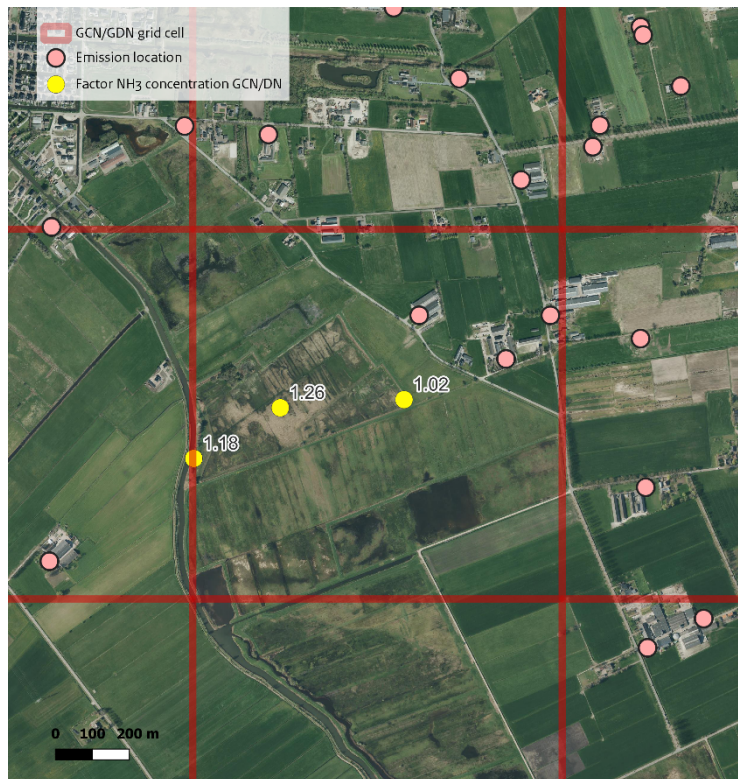
Figure 17 Example of the effect of more detailed emission locations on the ratio between GCN/GDN and DN modelled concentrations on measuring sites (in yellow the location of Binnenveld is shown here). In red, the outlines of the 1 × 1 km² GCN/GDN grid cells are shown. Emissions for GCN/GDN are spread equally over these grid cells. The pink circles are the emission sources used in the DN setup.

6.3.2   *Comparing of DN hexagonal grid and GDN square grid.*
Deposition data of 2030 from DN compares very well with GDN (regression coefficient of 1.003 and R^2 of 0.9996, Figure 19). A root mean square error of 25 mol N/ha/yr is relatively small compared to an average deposition of approximately 1220 mol/ha/yr. The largest differences are found at locations with transitions in terrain properties (Figure 19). For example, on the island Terschelling, the effect of large differences in surface roughness due to the land-sea transition is clearly visible in the average deposition.

Although the average total nitrogen deposition of DN hexagons in a 1 × 1 km² grid cell are often within 5% (Figure 19), local variations in deposition are larger (Figure 20). As a result of local terrain properties and emission sources, more detailed patterns in deposition become visible. For example, the local forest area close to the beach area Wassenaarse Slag has a higher deposition in DN than in GDN. This is a result of the larger local roughness length in the more detailed calculations in DN.

Figure 18 Comparison of total N deposition between GDN 2021 and DN 2021 for the year 2030 for grid cells containing more than ninety relevant hexagons. The trendline is based on linear interpolation with the formula $y = a \cdot x$. The standard deviation of a in the formula is equal to 0.00061.

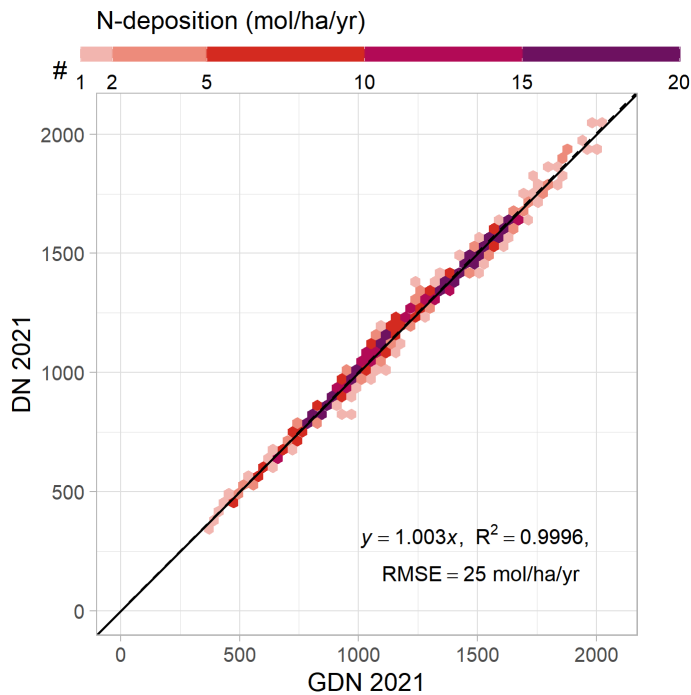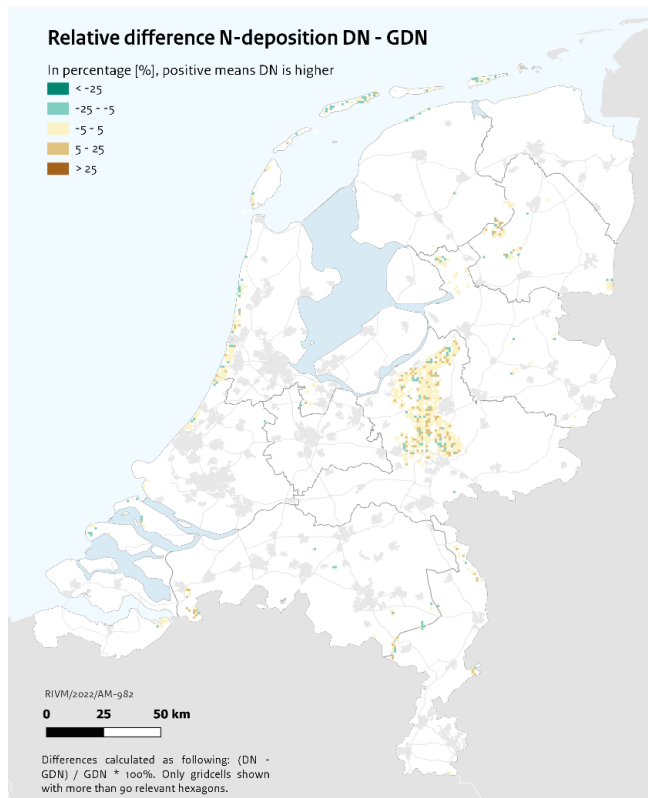*Figure 19 Relative difference in N deposition between GDN 2021 and DN 2021 for the year 2030, for grid cells containing more than ninety relevant hexagons.*
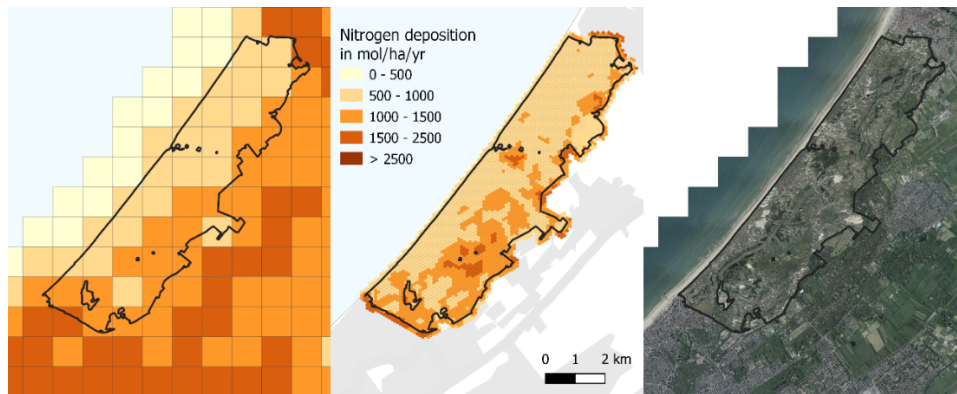
Figure 20 Total nitrogen deposition in 2030 on the square grid of 1 × 1 km² of GDN (left) and on the DN hexagonal grid of 1 hectare (middle) for the coastal Natura 2000 area Meijendel & Berkheide. An aerial picture is shown in the right picture as a reference. Although the average differences between both grids are small, more detailed patterns in deposition due to local terrain properties and emission sources become visible in the DN deposition map.
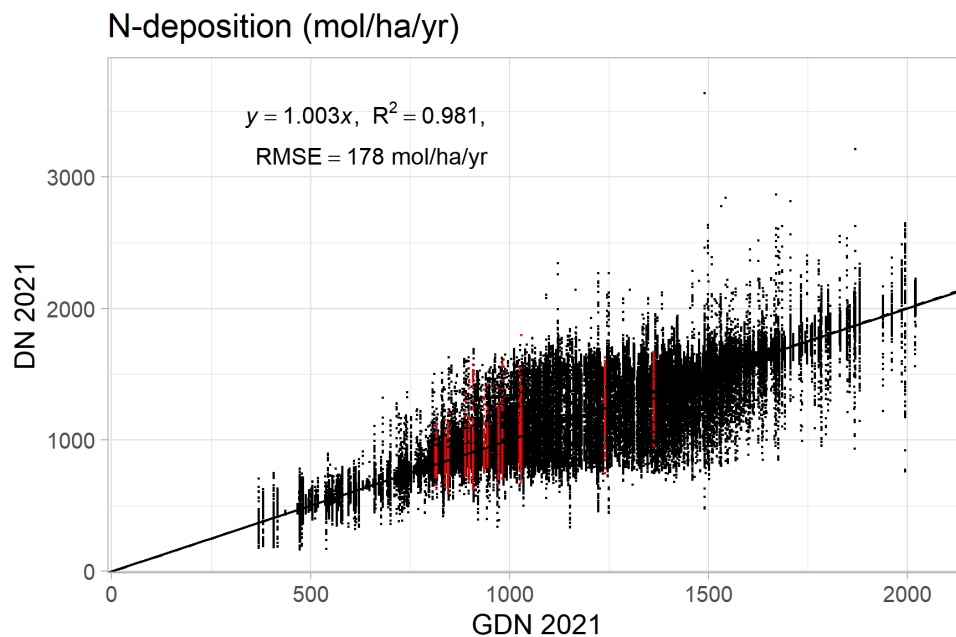
Figure 21 Total nitrogen deposition in 2030 calculated on DN hexagons of 1 hectare (y-axis) compared to the deposition of the corresponding GDN grid cell of 1 × 1 km2 (x-axis). The locations in the Natura2000 area 'Meijendel & Berkheide' are highlighted in red. The data is filtered on relevant hexagons and grid cells containing more than ninety hexagons. The trendline is based on linear interpolation with the formula $y = a \cdot x$. The standard deviation of a in the formula is equal to 0.00043.

When comparing depositions on 1-hectare hexagons directly to the GDN grid cell it is located in, the local variability within a 1 × 1 km² grid cell can be quantified (Figure 21). A root mean square error of 178 mol N/ha/yr corresponds to an average variability in nitrogen deposition of 14.6% when compared to the average deposition (~ 1220 mol/ha/yr on the selection of GDN grid cells). Furthermore, the RMSE of 178 mol/ha/yr indicates that local variation in deposition can be

quite large. This is especially important for small Natura 2000 areas, as local variations can have a large effect on the average deposition of such a small area. The variability is attributed to a combination of more detailed emission locations and local terrain properties.

NH$_3$ concentration (μg/m^3)
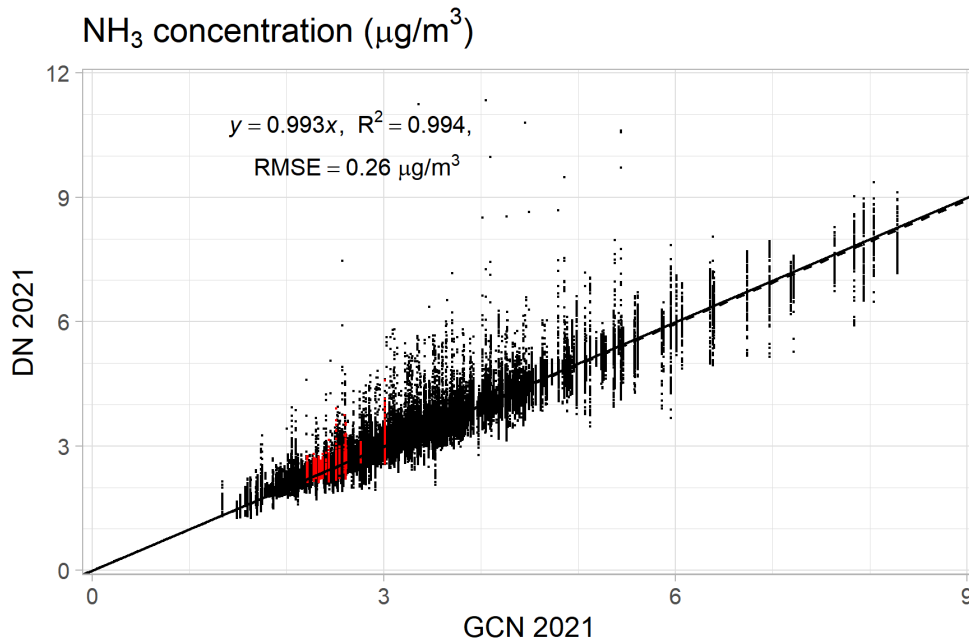
Figure 22 NH$_3$ concentration in 2030 calculated on DN hexagons of 1 hectare (y-axis) compared to the NH$_3$ concentration of the corresponding GCN/GDN grid cell of 1 × 1 km^2 (x-axis). The locations in the Natura2000 area Meijendal & Berkheide are highlighted in red. The data is filtered on relevant hexagons and grid cells containing more than ninety hexagons. The trendline is based on linear interpolation with the formula $y = a \cdot x$. The standard deviation of a in the formula is equal to 0.00025.

For a large part, the variability in total nitrogen deposition in Figure 21 is caused by variations in deposition velocity due to varying terrain properties. However, part of the variability is a result of differences in emissions. In order to separate the effect of terrain properties and that of emissions, we also looked at concentrations on different grid levels (Figure 22). A root mean square error of 0.26 ug m^{-3} NH$_3$ indicates an average variability in NH$_3$ concentration of 8.3% when compared to the average concentration (~ 3.12 ug m^{-3} NH$_3$ on the selection of GDN grid cells). This means that the variation in the deposition in a GDN grid is largely caused by the variation in the terrain properties: two thirds of the variation in the deposition in a GCN/GDN grid cell is explained by the variation in the deposition calculation that considers more detailed terrain properties.

6.4   Conclusions

In general, GDN and DN have no systematic difference for either the calculated NH_3 concentrations or the nitrogen deposition. Variations in the 1×1 km^2 scale of the GDN grid can be significant. An RMSE between 1 ha hexagons within the 1×1 km^2 grid average of nearly 10% is observed for NH_3 concentrations, and of approximately 15% for nitrogen deposition. The major part of this variation originates from terrain properties.

7   General discussion and conclusion

This status report combines several approaches to studying the uncertainty in the determination of the nitrogen deposition in the Netherlands. Compared to the uncertainty analyses of calculated concentrations, the analysis of deposition is much more complicated. Firstly, because several paths of deposition exist of which six compounds are considered in this report. Secondly, because the parameter of interest, nitrogen deposition, is not measured directly for three of the compounds. For these, the uncertainty in deposition is determined by combining an uncertainty in the concentration estimate with an uncertainty in the deposition velocity.

In combining the uncertainties of the various compounds, another complexity arises because some estimates should be made on the correlation between the compounds. Since the compounds are calculated using the same model, OPS 5.1.0.1, the assumption that uncertainties are uncorrelated is not realistic. For example, the important equation for the deposition resistance has similar R_a for all airborne compounds. A proxy of the correlation in uncertainties in deposition velocities has been estimated using the correlation between the spatial distribution of the compounds. If we use this estimate, the uncertainty estimate increases from 23 to 32%. Obtaining better knowledge of this correlation is therefore recommended.

The dry depositions of NH_3, NO_2, NO_3^-/NH_4^+, have high relative uncertainties due to a large uncertainty in the deposition velocity. The most important component is dry deposition of NH_3. For NH_3, a large set of concentration measurements is available, combined with a smaller set of deposition measurements. The standard deviation of the differences between the measured and modelled deposition is quite large. The result indicates a systematic difference between the modelled and measured depositions. However, we assess the information as being insufficient for the determination of the bias and subsequent calibration. This assessment of insufficient coherent information was based on several observations:
- additional measurements in the Netherlands, for shorter periods, show opposite differences;
- measurement values from international studies show a wide range of results, even after selection of similar land use classes and correction for concentration differences.

A more detailed analysis of the differences between the calculated and measured dry deposition at the COTAG sites will be carried out. Without the possibility for a bias correction, a large uncertainty in NH_3 deposition and deposition velocity is estimated, resulting in an overall uncertainty estimate of 60-70% (2σ) on a local scale.
In the estimate of the uncertainty of the total N deposition, the contribution of the NH_3 dry deposition is dominating. Fortunately, more deposition measurement locations have been planned. Both the concentration measurements and the deposition measurements are concentrated in Natura 2000 areas. This implies that the uncertainty

estimates are representative for locations like the Natura 2000 areas. Uncertainties for other locations, such as agricultural areas, built up areas and transition locations, might be different.

In this report, six compounds are considered. In the OPS model, some compounds actually contain several sub-compounds, which may behave quite differently. For example, deposition of secondary oxidised nitrogen is considered to consist of the relatively slow deposition of ammonium nitrate particles and the quick deposition of HNO_3. It is recommended to adjust OPS to distinguish between these compounds.

The above considerations all reflect the small-scale uncertainty estimates and their correlations. In Chapter 5, atmospheric feedbacks are studied that may affect uncertainty on large scales. This is achieved by introducing variations ('deviations') in the deposition velocity over 'grassland'. In general, the variation in the deposition velocity over 'grasslands' results in a negative feedback. This can be explained as follows: decreasing the deposition velocity will decrease the deposition, which will result in increased concentration. The higher concentration then leads to a higher deposition and thus partly compensates the initial effect. As a result, the decrease of deposition at 'grassland' locations is less than might be expected on the basis of the change in the deposition velocity.

At locations with no or very small amounts of 'grasslands', only an increase in concentration will be observed, leading to somewhat increased deposition. As a result, the average deposition over larger areas (consisting of 'grassland' as well as other land cover) will be even less sensitive to a change in the deposition velocity than expected by the local effects.

Finally, a compensation through the wet deposition is calculated as well. The feedback part of the study shows that the impact of the uncertainty in the deposition velocity on the total national nitrogen deposition is considerably smaller than the estimate on the local scale. On the basis of this feedback study, the uncertainty in the total national nitrogen deposition is estimated at 20-30%.

8   References

Bohrnstedt, G.W. and Goldberger, A.S., 1969. On the exact covariance of products of random variables. Journal of the American Statistical Association, 64(328): 1439-1442, https://doi.org/10.2307/2286081.

Cape, J.N. et al., 2008. Estimate of annual NH_3 dry deposition to a fumigated ombrotrophic bog using concentration-dependent deposition velocities. Atmospheric Environment, 42(27): 6637-6646, https://doi.org/10.1016/j.atmosenv.2008.04.027.

Dobben, H.v. and Hinsberg, A.v., 2008. Overzicht van kritische depositiewaarden voor stikstof, toegepast op habitattypen en Natura 2000-gebieden Alterra, Wageningen, https://edepot.wur.nl/45419.

EMEP, 2022. Transboundary particulate matter, photo-oxidants, acidification and eutrophication components. , Joint MSC-W & CCC & CEIP &CIAM Report. EMEP Status Report 1/2022, https://emep.int/publ/reports/2022/EMEP_Status_Report_1_2022.pdf.

Flechard, C.R. et al., 2011. Dry deposition of reactive nitrogen to European ecosystems: a comparison of inferential models across the NitroEurope network. Atmospheric Chemistry and Physics, 11(6): 2703-2728, https://doi.org/10.5194/acp-11-2703-2011.

Goodman, L.A., 1960. On the exact variance of products. Journal of the American Statistical Association, 55(292): 708-713, https://doi.org/10.2307/2281592.

Hazeu, G.W., Schuiling, C., Dorland, G.J., Roerink, G.J., Naeff, H.S.D. and Smidt, R.A., 2014. Landelijk Grondgebruiksbestand Nederland versie 7 (LGN7); Vervaardiging, nauwkeurigheid en gebruik, Alterra Wageningen UR (University & Research centre), Wageningen.

Hoogerbrugge, R. et al., 2022. Grootschalige concentratie- en depositiekaarten Nederland. Rapportage 2022, https://doi.org/10.21945/RIVM-2022-0059.

Hordijk, L. et al., 2020. Meer meten, robuuster rekenen - Eindrapport van het Adviescollege Meten en Berekenen Stikstof, https://www.rijksoverheid.nl/documenten/rapporten/2020/06/15/meer-meten-robuuster-rekenen.

Marra, W., Hazelhorst, S., Brandt, K., Kruit, R.W. and Schram, J., 2022. Monitor stikstofdepositie in Natura 2000-gebieden 2022. Uitgangssituatie voor de Wet Stikstofreductie en Natuurverbetering, Rijksinstituut voor Volksgezondheid en Milieu, Bilthoven, https://doi.org/10.21945/RIVM-2022-0120.

Nguyen, P. and Wesseling, J., 2016. Metingen van stikstofdioxideconcentraties (NO_2) met Palmes buisjes - Periode 2012-2015, Rijksinstituut voor Volksgezondheid en Milieu, Bilthoven, https://www.rivm.nl/bibliotheek/rapporten/2016-0089.pdf.

Noordijk, H., Braam, M., Rutledge-Jonker, S., Hoogerbrugge, R., Stolk, A.P. and van Pul, W.A.J., 2020. Performance of the MAN ammonia monitoring network in the Netherlands. Atmospheric Environment, 228: 117400, https://doi.org/10.1016/j.atmosenv.2020.117400.

Rutledge-Jonker, S. et al., 2023. Ammonia deposition measured with Conditional Time-Averaged Gradient (COTAG) systems in the Netherlands National Institute for Public Health and the Environment (RIVM), Bilthoven, https://doi.org/10.21945/RIVM-2022-0202.

Sauter, F., Sterk, M., Swaluw, E.v.d., Kruit, R.W., Vries, W.d. and Pul, A.v., 2020. The OPS-model; Description of OPS 5.0.0.0, National Institute for Public Health and the Environment (RIVM), Bilthoven, https://www.rivm.nl/documenten/uitgebreide-modelbeschrijving-van-ops-versie-5000.

Sauter, F., Sterk, M., Swaluw, E.v.d., Kruit, R.W., Vries, W.d. and Pul, A.v., 2023. The OPS-model; Description of OPS 5.1.1.0, National Institute for Public Health and the Environment (RIVM), Bilthoven, https://www.rivm.nl/documenten/uitgebreide-modelbeschrijving-van-ops-versie-5110.

Schrader, F. and Brümmer, C., 2014. Land use specific ammonia deposition velocities: a review of recent studies (2004-2013). Water Air Soil Pollut, 225(10): 2114, https://doi.org/10.1007/s11270-014-2114-7.

Siteur, K., Volten, H., Vendel, K., Bongers, P. and Hoogerbrugge, R., 2021. Nauwkeurige NO_2-concentratiekaarten dankzij vrijwilligers. Tijdschrift Lucht 17(3): 12-16.

Sutton, M.A., Dragosits, U., Geels, C., Gyldenkærne, S., Misselbrook, T.H. and Bussink, W., 2015. Review on the scientific underpinning of calculation of ammonia emission and deposition in the Netherlands, https://www.tweedekamer.nl/kamerstukken/detail?id=2015D32494&did=2015D32494.

van Jaarsveld, J.A., 2004. The Operational Priority Substances model. Description and validation of OPS-Pro 4.1, Rijksinstituut voor Volksgezondheid en Milieu, Bilthoven, https://www.rivm.nl/bibliotheek/rapporten/500045001.pdf.

Velders, G.J.M., Aben, J.M.M., Jaarsveld, J.A.v., Pul, W.A.J.v., Vries, W.J.d. and Zanten, M.C.v., 2010. Grootschalige stikstofdepositie in Nederland. Herkomst en ontwikkeling in de tijd, Planbureau voor de Leefomgeving (PBL), Den Haag/Bilthoven, https://www.rivm.nl/bibliotheek/rapporten/500088007.pdf.

Vendel, K.J.A. et al., 2023. Dry deposition of ammonia in a coastal dune area: Measurements and modeling. Atmospheric Environment, https://doi.org/10.1016/j.atmosenv.2023.119596: 119596, https://doi.org/10.1016/j.atmosenv.2023.119596.

Walker, J.T. et al., 2019. Aspects of uncertainty in total reactive nitrogen deposition estimates for North American critical load applications. Science of The Total Environment, 690: 1005-1018, https://doi.org/10.1016/j.scitotenv.2019.06.337.

Wever, D. et al., 2020. Informative Inventory Report 2020 : Emissions of transboundary air pollutants in the Netherlands 1990-2018, Rijkinstituut voor Volksgezondheid en Milieu, Bilthoven, https://doi.org/10.21945/RIVM-2020-0032.

Wever, D. et al., 2023. Informative Inventory Report 2023. Emissions of transboundary air pollutants in the Netherlands 1990–2021, Rijkinstituut voor Volksgezondheid en Milieu, Bilthoven, https://doi.org/10.21945/RIVM-2023-0057.

Wichink Kruit, R. et al., 2021. Op weg naar een optimale meetstrategie voor stikstof, Rijksinstituut voor Volksgezondheid en Milieu, Bilthoven, https://doi.org/10.21945/RIVM-2021-0118.

Wichink Kruit, R., Braam, M., Hoogerbrugge, R. and Pul, A.v., 2020. Implementation of a data fusion approach to assess the concentration and dry deposition of ammonia in the Netherlands, Rijksinstituut voor Volksgezondheid en Milieu, Bilthoven, https://doi.org/10.21945/RIVM-2020-0076.

Wintjen, P., Schrader, F., Schaap, M., Beudert, B. and Brümmer, C., 2022a. Forest–atmosphere exchange of reactive nitrogen in a remote region – Part I: Measuring temporal dynamics. Biogeosciences, 19(2): 389-413, https://doi.org/10.5194/bg-19-389-2022.

Zanten, M.C.v., Sauter, F.J., Kruit, R.J.W., Jaarsveld, J.A.v. and Pul, W.A.J.v., 2010. Description of the DEPAC module. Dry deposition modelling with DEPAC_GCN2010, Rijksinstituut voor Volksgezondheid en Milieu, Bilthoven, https://www.rivm.nl/bibliotheek/rapporten/680180001.pdf.

Appendix A Proportional random uncertainty and alternative models

In our analysis, we estimate the uncertainty in the concentrations and deposition fluxes at locations other than the observation sites by assuming proportional uncertainty:

$$s_X^2(X) = \text{RSD}^2 X^2 \qquad\qquad \textit{Eq. A1}$$

where X is a measured quantity, s_X is the model uncertainty of that quantity, and RSD is the relative uncertainty. We approximate parameter RSD by $\text{RSD} = \frac{s_X}{\langle x \rangle}$. In the literature (Thunis, 2013; Pernigotti 2013), the uncertainty is often split into a part that is constant and a part that is proportional to X:

$$s_X^2(X) = s_0^2 + \text{RSD}^2 X^2 \qquad\qquad \textit{Eq. A2}$$

In this appendix, we study the validity of Eq. A1, as used in the present analysis.
By subdividing variable X into twenty equally-sized bins, with a minimum of five observations per bin, and plotting both the Eq. A1 and the uncertainties per bin, we obtain Figure A1. From visual inspection, the proportional model used in our study seems to perform well for relevant ranges of concentrations and wet deposition fluxes.
Besides a visual comparison, we computed the Akaike Information Criterion (AIC) for both models Eq. A1 and Eq. A2. The model with the lowest AIC gives the most likely relation between s_X and X. For this analysis, we estimate the parameters of Eq. A2 through linear regression.
We find that the proportional model (Eq. A1) gives a lower AIC for all compounds except NH_3. For NH_3, the AIC of the more advanced model of Eq. A2 is lower. For simplicity and reproducibility, we use Eq. A1 in this report for all compounds.
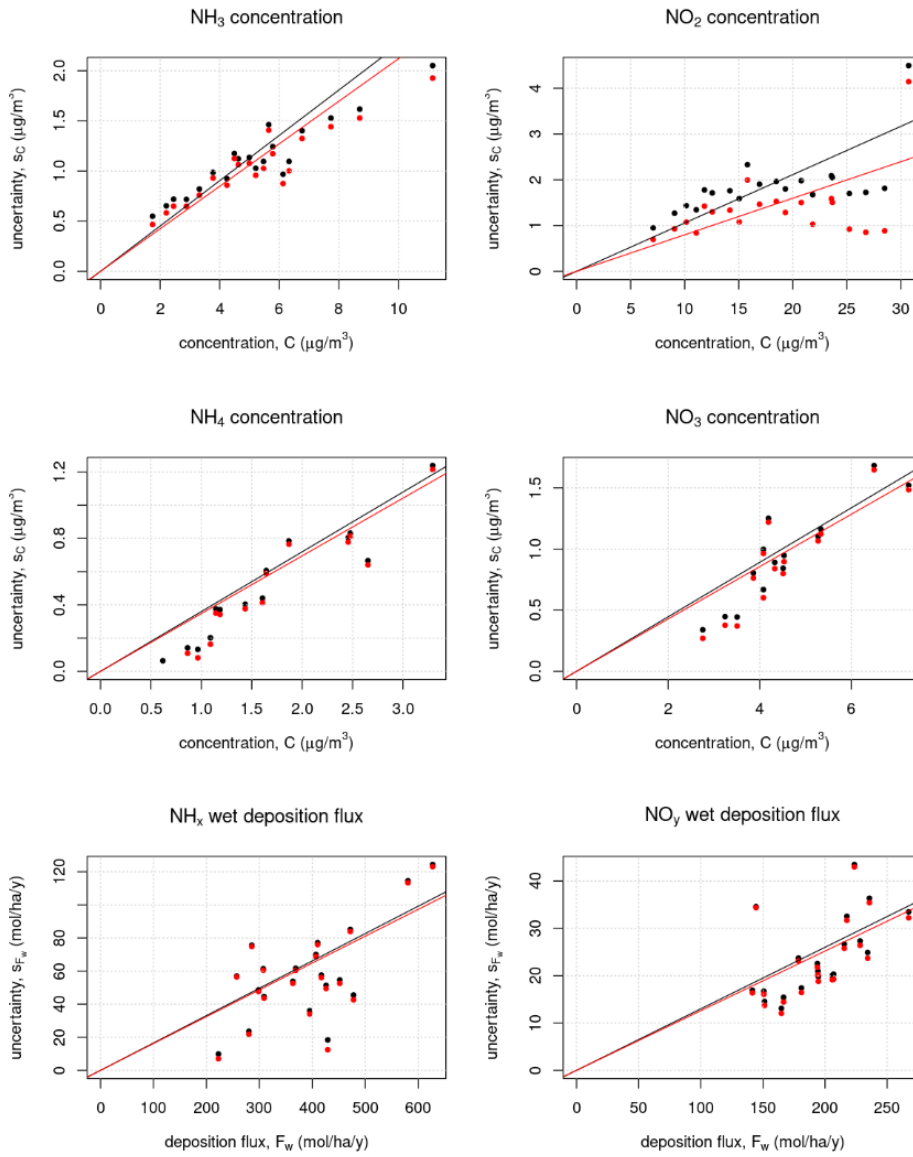
Figure A1 Binned uncertainties (points) and the proportional model of Eq. A1 (lines). In black: model uncertainty + measurement uncertainty (s_{cal}) In red: only model uncertainty (s_{mod}).

Appendix B Independence between deposition velocities and concentrations

In Chapters 3 and 4, we assume independence between the residuals in deposition velocities and concentrations. To test this assumption, deposition velocities have been computed using NH₃ concentration measurements at ~5m above the surface at the COTAG sites. The concentration measurements are part of the MAN network and were performed independently from measurements by the COTAGs. We found no correlation between residuals of the calibrated model concentrations and the residuals of the modelled deposition velocities ($\rho = -0.006$). This is illustrated by Figure A2.
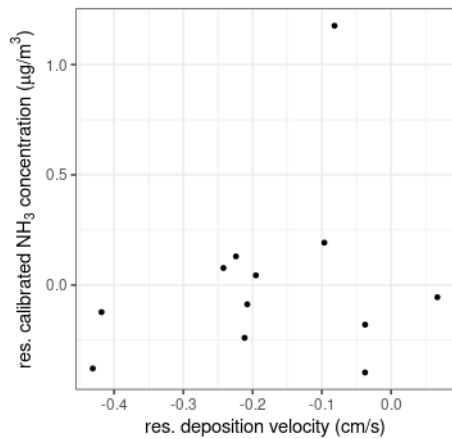
Figure A2 Residuals in the effective dry deposition velocity and calibrated NH₃ concentration at the COTAG sites.

Note that although the covariance between residuals in C and V_d may be negligible on a local scale (i.e. the footprint of the COTAG), this may not hold true on larger spatial scales. On larger scales, atmospheric feedbacks between deposition and concentration, involving depletion due to deposition, become important. This is studied in detail in Chapter 5.

Appendix C Uncertainties in dry deposition fluxes and correlations between fluxes

C.1 Variance of the product of two independent random variables

In many cases, we need to estimate the variance of combinations of variables, where we know the variances of these underlying variables. For the sum of variables, the resulting variance can be determined in a simple way. Determining the products of two independent random variables is more complex, but an exact solution is available. If two variables x and y are independent, the variance of their product is (Goodman, 1960):

$$\text{Var}(xy) = E(x)^2\text{Var}(y) + E(y)^2\text{Var}(x) + \text{Var}(x)\text{Var}(y) \qquad \textit{Eq. A3}$$

substituting V_d, C and F_d $(= V_d \cdot C)$ the uncertainty in F_d can be written as:

$$s_{F_d}^2 = C^2 s_{V_d}^2 + V_d^2 s_C^2 + s_{V_d}^2 s_C^2 \qquad \textit{Eq. A4}$$

or as in the main text:

$$s_{F_d}^2 = F_d^2 \left[\frac{s_{V_d}^2}{V_d^2} + \frac{s_C^2}{C^2} + \frac{s_{V_d}^2}{V_d^2}\frac{s_C^2}{C^2} \right] \qquad \textit{Eq. A5}$$

C.2 Exact Covariance of Products of Random Variables

In 1969, Bohrnstedt and Goldberger published an analysis of the covariance of products of random variables. Assuming multivariate normality, they showed that:

$$
\begin{aligned}
&\text{Cov}(xy, uv) \\
&= E(x)E(u)\text{Cov}(y,v) + E(x)E(v)\text{Cov}(y,u) + E(y)E(u)\text{Cov}(x,v) \\
&+ E(y)E(v)\text{Cov}(x,u) + \text{Cov}(x,u)\text{Cov}(y,v) + \text{Cov}(x,v)\text{Cov}(y,u)
\end{aligned}
\qquad \textit{Eq. A6}
$$

Where x, y, u and v are random variables.
This result can be used to determine the covariance between two dry deposition fluxes from the underlying deposition velocities and concentrations. Substituting C, V_d and F_d and rewriting yields:

$$
\text{Cov}(F_{d,i}, F_{d,j}) = F_{d,i}F_{d,j}\left(\frac{\text{Cov}(C_i,C_j)}{C_iC_j} + \frac{\text{Cov}(C_i,V_{d,j})}{C_iV_{d,j}} + \frac{\text{Cov}(V_{d,i},C_j)}{V_{d,i}C_j} + \right.
$$
$$
\left. \frac{\text{Cov}(V_{d,i},V_{d,j})}{V_{d,i}V_{d,j}} + \frac{\text{Cov}(C_i,C_j)\text{Cov}(V_{d,i},V_{d,j}) + \text{Cov}(V_{d,i},C_j)\text{Cov}(C_i,V_{d,j})}{F_{d,i}F_{d,j}} \right)
\qquad \textit{Eq. A7}
$$

Assuming C and V_d can be treated as independent, this simplifies to:

$$
\begin{aligned}
&\text{Cov}(F_{d,i}, F_{d,j}) \\
&= F_{d,i}F_{d,j}\left(\frac{\text{Cov}(C_i,C_j)}{C_iC_j} + \frac{\text{Cov}(V_{d,i},V_{d,j})}{V_{d,i}V_{d,j}} + \frac{\text{Cov}(C_i,C_j)\text{Cov}(V_{d,i},V_{d,j})}{F_{d,i}F_{d,j}} \right)
\end{aligned}
\qquad \textit{Eq. A8}
$$

or in terms of correlation:

$$\rho(F_{d,i}, F_{d,j}) = \frac{F_{d,i}}{s_{F_{d,i}}} \frac{F_{d,j}}{s_{F_{d,i}}}$$
$$\left(\rho(C_i, C_j) \frac{s_{C_i}}{C_i} \frac{s_{C_j}}{C_j} + \rho(V_{d,i}, V_{d,j}) \frac{s_{V_{d,i}}}{V_{d,i}} \frac{s_{V_{d,j}}}{V_{d,j}} \right.$$
$$\left. + \rho(C_i, C_j) \frac{s_{C_i} s_{C_j}}{C_i C_j} \rho(V_{d,i}, V_{d,j}) \frac{s_{V_{d,i}}}{V_{d,i}} \frac{s_{V_{d,j}}}{V_{d,j}} \right)$$

Eq. A9

Note that the correlation coefficient between two dry deposition fluxes is solely determined by the relative uncertainties in C, V_d and F_d, as derived in Chapter 3, and by the correlations between the concentrations and the dry deposition velocities. These correlation coefficients are determined in Appendix C.3.

From the result of Bohrnstedt and Goldberger (1969), the correlation between a wet and a dry deposition flux can also be derived:

$$\rho(F_{w,i}, F_{d,j}) = \frac{F_{w,i}}{s_{F_{w,i}}} \left(\rho(F_{w,i}, C_j) \frac{s_{C_j}}{C_j} + \rho(F_{w,i}, V_{d,j}) \frac{s_{V_{d,j}}}{V_{d,j}} \right)$$

Eq. A10

Assuming dry deposition velocities and dry deposition fluxes to be independent yields:

$$\rho(F_{w,i}, F_{d,j}) = \frac{F_{w,j}}{s_{F_{w,i}}} \rho(F_{w,i}, C_j) \frac{s_{C_j}}{C_j}$$

Eq. A11

C.3 Correlation between residuals in concentrations, dry deposition velocities and wet deposition fluxes

Correlations between residuals (modelled minus observed value) can be derived for pairs of measured quantities, using sites where both are measured over the same period. Table A1 shows the number of such overlapping observations for the 2005-2021 period.
Note that the number of overlapping observations is generally much smaller than the number of observations for each individual compound (diagonal in Table A1).
The correlations between residuals of measured variables are presented in Table A2.

Table A1 Number of observation pairs that can be used to compute the correlation coefficient between residuals of the measured quantities.

n	$C_{\mathrm{NH_3}}$	$C_{\mathrm{NO_2}}$	$C_{\mathrm{NH_4^+}}$	$C_{\mathrm{NO_3^-}}$	$F_{w,\mathrm{NH_x}}$	$F_{w,\mathrm{NO_y}}$
$C_{\mathrm{NH_3}}$	3123	155	43	43	39	39
$C_{\mathrm{NO_2}}$		793	67	67	71	71
$C_{\mathrm{NH_4^+}}$			70	70	52	52
$C_{\mathrm{NO_3^-}}$				70	52	52
$F_{w,\mathrm{NH_x}}$					135	135
$F_{w,\mathrm{NO_y}}$						135

Table A2 Correlation coefficients of the residuals, for each combination of the measured variables

ρ	$C_{\mathrm{NH_3}}$	$C_{\mathrm{NO_2}}$	$C_{\mathrm{NH_4^+}}$	$C_{\mathrm{NO_3^-}}$	$F_{w,\mathrm{NH_x}}$	$F_{w,\mathrm{NO_y}}$
$C_{\mathrm{NH_3}}$	1.00	0.17	0.38	-0.12	-0.08	-0.27
$C_{\mathrm{NO_2}}$		1.00	0.03	-0.17	-0.07	-0.30
$C_{\mathrm{NH_4^+}}$			1.00	0.77	0.56	0.40
$C_{\mathrm{NO_3^-}}$				1.00	0.69	0.51
$F_{w,\mathrm{NH_x}}$					1.00	0.67
$F_{w,\mathrm{NO_y}}$						1.00

For the approach outlined in Appendix C.2, correlation coefficients between the residuals of dry deposition velocities are required. As the dry deposition velocities are currently not measured, they cannot be computed. There is much overlap in the model variables that determine the dry deposition velocity, and therefore the errors in the model are probably highly correlated. Here, we approximate the required correlation coefficients by computing the correlation of modelled deposition velocities on 1 x 1 km^2 GDN grid cells over the 2005-2021 period, weighted by the fraction of relevant Natura 2000 habitats. This results in Table A3.

Table A3 Correlation coefficients of the residuals, for each combination of the dry deposition velocities

ρ	$V_{d,\mathrm{NH_3}}$	$V_{d,\mathrm{NO_2}}$	$V_{d,\mathrm{NH_4^+}}$	$V_{d,\mathrm{NO_3^-}}$
$V_{d,\mathrm{NH_3}}$	1.00	0.81	0.71	0.85
$V_{d,\mathrm{NO_2}}$		1.00	0.74	0.67
$V_{d,\mathrm{NH_4^+}}$			1.00	0.79
$V_{d,\mathrm{NO_3^-}}$				1.00

Combining both tables, using the equations derived in Appendix C.2, yields two correlation tables. One that is based on the combined model and observation uncertainty (s_{cal}, Table A4) and one that is solely based

on the model uncertainty (e.g. after subtracting the observation uncertainty, s_{mod}, Table A5). Note that the correlation coefficients in both tables are roughly equal.

Table A4 Correlation coefficients of the residuals, for each combination of deposition fluxes. The computation of this table is described in Appendix C.2, using relative uncertainties in F_d, F_w, V_d and C, before removing the measurement uncertainty (s_{cal}).

ρ	F_{d,NH_3}	F_{d,NO_x}	F_{d,NH_4^+}	$F_{d,HNO_3 +NO_3^-}$	F_{w,NH_x}	F_{w,NO_y}
F_{d,NH_3}	1.00	0.73	0.58	0.66	-0.03	-0.10
F_{d,NO_x}		1.00	0.54	0.55	-0.02	-0.07
F_{d,NH_4^+}			1.00	0.76	0.34	0.24
$F_{d,HNO_3 +NO_3^-}$				1.00	0.30	0.22
F_{w,NH_x}					1.00	0.67
F_{w,NO_y}						1.00

Table A5 Correlation coefficients of the residuals, for each combination of the deposition fluxes. The computation of this table is described in Appendix C.2, using relative uncertainties in F_d, F_w, V_d and C, after removing the measurement uncertainty (s_{mod}).

ρ	F_{d,NH_3}	F_{d,NO_x}	F_{d,NH_4^+}	$F_{d,HNO_3 +NO_3^-}$	F_{w,NH_x}	F_{w,NO_y}
F_{d,NH_3}	1.00	0.74	0.58	0.66	-0.03	-0.10
F_{d,NO_x}		1.00	0.55	0.57	-0.01	-0.05
F_{d,NH_4^+}			1.00	0.76	0.34	0.24
$F_{d,HNO_3 +NO_3^-}$				1.00	0.30	0.22
F_{w,NH_x}					1.00	0.67
F_{w,NO_y}						1.00

Appendix D The average of multiple draws of a random variable

The average of N draws of a random variable is:

$$\langle X \rangle_N = \frac{1}{N}\sum_{i=1}^{N} X_i \qquad\qquad Eq.\ A12$$

We are interested in the variance of the average of N random variables, which can be written as:

$$\mathrm{Var}(\langle X \rangle_N) = \frac{1}{N^2}\mathrm{Var}\left(\sum_{i=1}^{N} X_i\right) = \frac{1}{N^2}\sum_{i=1}^{N}\sum_{j=1}^{N}\mathrm{Cov}(X_i, X_j) \qquad\qquad Eq.\ A13$$

Where $\mathrm{Cov}()$ is the covariance between two draws of X. The number of terms on the diagonal of the covariance matrix is N. The total contribution by these terms to the variance in the average is $N \cdot \mathrm{Var}(X)$. The number of cross terms is $N^2 - N$. The total contribution by the cross terms is $(N^2 - N)\rho\mathrm{Var}(X)$, where ρ is the average correlation between draws of X. Hence, the variance in the average of N random variables is:

$$\mathrm{Var}(\langle X \rangle_N) = \frac{1}{N^2}\sum_{i=1}^{N}\sum_{j=1}^{N}\mathrm{Cov}(X_i, X_j)$$
$$= \frac{1}{N^2}\left(N \cdot \mathrm{Var}(X) + (N^2 - N)\rho\mathrm{Var}(X)\right) = \left(\rho + \frac{1-\rho}{N}\right)\mathrm{Var}(X) \qquad\qquad Eq.\ A14$$

Appendix E

E.1   Assessing V$_d$ of NH$_3$ in an international context

Figure A3 shows a comparison between V_d values obtained from the international scientific literature for vegetation surfaces ((semi)natural, agricultural, forest) (Schrader and Brümmer, 2014; henceforth SB14), from Dutch measurement sites and from OPS runs for the Dutch sites. From the SB14 review, only data derived from estimates in all four seasons per year is shown. Most of the V_d data in their set was obtained with the so-called inferential method. This is considered a modelling approach, and therefore, data from this method is distinguished from data based on micrometeorological measurements (open versus closed symbols). Little information on V_d from more direct observations is available, particularly for 'forest'.

It is clear that within the land use classes considered here, the spread in V_d values listed by SB14 is considerable. Note that some of the variability will be caused by the fact that differences in measurement height and climatic conditions cannot be accounted for. Nonetheless, in the 'agriculture and seminatural' class, the variability for the subset of measured data (filled symbols) remains similar to the one including the inferential method. For 'forest', only three comparatively high V_d values remain when only considering measurements.

Observations from the Dutch sites show less spread. This may be due to the fact that climatic conditions and heights for the evaluation of V_d are similar, with the exception of the Solleveld site. Regarding OPS results, we conclude that the range in V_d from the simulations agrees reasonably well within the range of both Dutch and international observations. Again, the Solleveld results may be an exception, since OPS has overestimated V_d for that site. Possible causes are discussed in Vendel et al. (2023). So far, no direct comparison can be made between OPS and measurements at forest sites. Details on the data from SB14 and from Vendel et al. (2023) can be found in Appendix E.2.
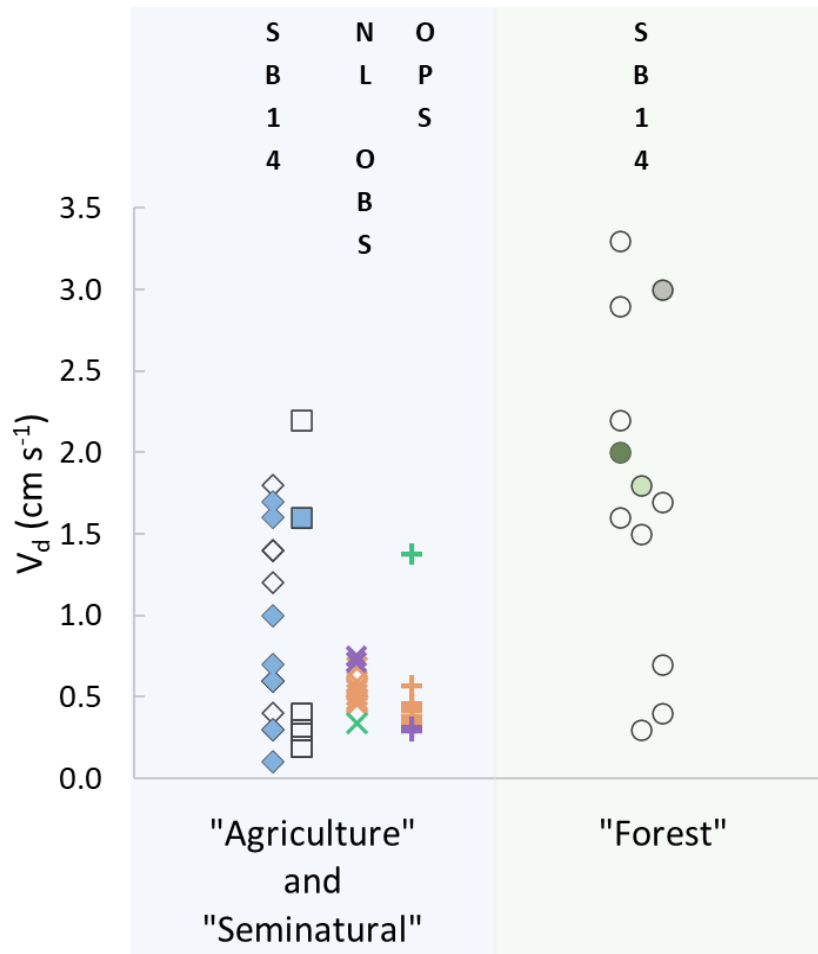
Figure A3 Comparison of measured V_d values from the international review by Schrader and Brümmer (2014; SB14) with Dutch measurements at COTAG sites (Rutledge-Jonker et al., 2023) and the Solleveld site (Vendel et al., 2023) (labelled together as NL OBS) and with corresponding OPS computations for the Dutch sites (OPS). These data sources have been highlighted in the top of the figure, above the corresponding V_d data clusters. Diamonds: SB14 seminatural; squares: SB14 agricultural; circles: SB14 forest (from left to right: coniferous, deciduous, mixed). Open symbols refer to V_d values derived from the inferential method, which is essentially a modelling approach; coloured symbols refer to V_d values derived from micrometeorological measurements. X: Dutch measurements (orange: Bargerveen and Oostelijke Vechtplassen (n=10); green: Solleveld (n=1); purple: Hoge Veluwe (n=2)); +: output from OPS with colour coding as for measurements. See Appendix E.2 for further details.

E.2 Interpretation and processing of data in Schrader & Brümmer (2014) and Vendel et al. (2023)

To further assess the uncertainty of deposition velocity, V_d values for NH₃ collected by SB14 were used. In their review, these authors extracted V_d data published in the scientific literature in the 2004-2013 period. In total, they collected 61 V_d values from 42. In 59 cases, the V_d value could be assigned to one of the seven land use classes they distinguished. The land use classes are presented in Table A6, along with the number of V_d values reported in each class. Individual V_d data and metadata from the review has been made available as

Supplementary Information to the paper, partly to encourage additional analyses.

Table A6 Land use classes distinguished by Schrader and Brümmer (2014) and number of observations in each class upon filtering.

Land use	All (n=59)	$w_s = 4$ (n=44)	$w_s = 4$ & measured (n=16)
Agricultural	18	10	1
Coniferous forest	6	5	1
Deciduous forest	4	3	1
Mixed forest	4	4	1
Seminatural	19	15	7
Urban	5	5	3
Water	3	2	2

The V_d data listed in SB14 is meant to be used as annual averages. However, in practice, some V_d values are based on a limited number of observations throughout the year. To this end, SB14 also provide quality flags indicative of the data coverage within a year, with two weight indicators (w):

- The w_s indicator weighs the number of seasons that were sampled: (1-4).
  Subscript s refers to 'season'.
- The w_c indicator refers to the measurement duration within the sampled season.
  From 1 for '1 day to 3 weeks per season' to 4 for 'nine weeks or more per season'.
  Subscript c refers to 'data coverage'.

Since our purpose is a comparison of annual V_d, we decided to exclude data with $w_s < 4$. This choice implies that V_d should have been obtained from observations in all seasons of the year. It can be argued that, as long as each season has been sampled, the exact duration of the measurement periods in each of the seasons is less important. Thus, w_c was not used to further filter the data.

In our own analysis, we also decided to consider the method on which the V_d was based. First, data from earlier reviews was excluded because it may contain unwanted and unknown overlaps among the data considered. Second, much of the remaining V_d data in SB14 is based on the so-called inferential method (INF). Measurements—e.g. concentrations, standard meteorological conditions and sometimes also turbulence observations—are used to drive a V_d model. In fact, this makes the INF method a modelling approach. Nevertheless, reports on V_d derived from INF have been accepted in the peer-reviewed scientific literature as defensible assessments of V_d (e.g. Flechard et al., 2011). Therefore, we decided not to exclude this data beforehand. Instead, we distinguish it from V_d measurements that are based solely on micrometeorological measurements, such as eddy covariance measurements and gradient techniques.

A limited literature search was performed to assess whether new annual V_d measurements have been published since SB14. This was performed by means of a Google Scholar search of peer-reviewed scientific publications in English that cite SB14. The idea is that new V_d values will probably be compared with the numbers collected by SB14.

The search resulted in thirty publications (Table A7; last update: 12 April 2023). Most of these papers cite SB14 in a more general sense, for example to underpin or illustrate the statement that V_d is uncertain. Other papers choose a V_d value partly or entirely based on SB14 in order to use this value to estimate the deposition from their own measured or computed concentrations. Papers citing SB14 and publishing new V_d values on the basis of measurements are rare. Amongst these, one paper (Wintjen et al., 2022a) would meet the criterion $w_s = 4$, but this paper reported lumped V_d values for total nitrogen, so that V_d of NH3 ammonia could not be separated out anymore. All in all, no data was added to the SB14 data.

Several shortcomings in the SB14 review can be identified. Major ones are the lack of climatic information (wind speed), more specific information on terrain properties (e.g. aerodynamic roughness) and information on the height for which V_d was calculated. For the time being, we assume that this contributes to the scatter in the V_d numbers from SB14.

In summary, it was decided to use from SB14:
   1. all land-use specific V_d data, for which $w_s = 4$;
   2. A subset of 1), in which V_d was obtained from micrometeorological observations.

Figure A3 in Appendix E.1 compares data from SB14 for predominantly vegetated land use (i.e., excluding the land use classes 'urban' and 'water') with observations from the COTAG sites (Rutledge-Jonker et al., 2023) and with measurements of V_d near Solleveld (Vendel et al., 2023). Results from OPS simulations for the Dutch measurement sites are compared with the observations for the following years: Bargerveen (COTAG) 2015-2019; Oostelijke Vechtplassen (COTAG) 2015-2019; Hoge Veluwe (COTAG) 2018-2019; Solleveld (GRAHAM) 2014/2015. Note that in the latter case, data from 2014 and 2015 was combined into one full year. In OPS, all measurement sites are classified as 'other nature' and as such they are compared with the 'seminatural' from SB14. So far, no recent Dutch NH3 observations for any of the forest types distinguished in SB14 are available. The receptor height in OPS was set to 5m, which matches the upper measurement level of the COTAG sites. However, at Solleveld, V_d has been evaluated at the height of ~1m (Vendel et al., 2023). Thus, it should be kept in mind that V_d from OPS would become somewhat larger when placing the receptor point on this lower level (since the aerodynamic resistance becomes smaller).

Papers citing Schrader and Brümmer (2014) published in the English peer-reviewed scientific literature [obtained with Google Scholar; last update 12-4-2023]

Adon, M., Galy-Lacaux, C., Serça, D., Guedant, P., Vongkhamsao, A., Rode, W., . . . Guérin, F. (2018). First assessment of inorganic nitrogen deposition budget following the impoundment of a subtropical hydroelectric reservoir (Nam Theun 2, Lao PDR). *Journal of Geophysical Research: Atmospheres, 123*, 12,413-412,428.

Ahrends, B., Schmitz, A., Prescher, A.-K., Wehberg, J., Geupel, M., Andreae, H., & Meesenburg, H. (2020). Comparison of methods for the estimation of total inorganic nitrogen deposition to forests in Germany. *Frontiers in Forests and Global Change, 3*, 103.

Aksoyoglu, S., & Prévôt, A. S. (2018). Modelling nitrogen deposition: dry deposition velocities on various land-use types in Switzerland. *International Journal of Environment and Pollution, 64*, 230-245.

Baker, J., Battye, W. H., Robarge, W., Arya, S. P., & Aneja, V. P. (2020). Modeling and measurements of ammonia from poultry operations: Their emissions, transport, and deposition in the Chesapeake Bay. *Science of The Total Environment, 706*, 135290.

Battye, W. H., Bray, C. D., Aneja, V. P., Tong, D., Lee, P., & Tang, Y. (2019). Evaluating ammonia (NH3) predictions in the NOAA NAQFC for Eastern North Carolina using ground level and satellite measurements. *Journal of Geophysical Research: Atmospheres, 124*, 8242-8259.

Braun, S., Ahrends, B., Alonso, R., Augustin, S., García-Gómez, H., Hůnová, I., . . . Thimonier, A. (2022). Nitrogen deposition in forests: Statistical modeling of total deposition from throughfall loads. *Frontiers in Forests and Global Change, 5*.

Geupel, M., Heldstab, J., Schäppi, B., Reutimann, J., Bach, M., Häußermann, U., . . . Breuer, L. (2021). A national nitrogen target for Germany. *Sustainability, 13*, 1121.

Guo, H., Liu, J., Froyd, K. D., Roberts, J. M., Veres, P. R., Hayes, P. L., . . . Weber, R. J. (2017). Fine particle pH and gas–particle phase partitioning of inorganic species in Pasadena, California, during the 2010 CalNex campaign. *Atmospheric Chemistry and Physics, 17*, 5703-5719.

Guo, H., Otjes, R., Schlag, P., Kiendler-Scharr, A., Nenes, A., & Weber, R. J. (2018). Effectiveness of ammonia reduction on control of fine particle nitrate. *Atmospheric Chemistry and Physics, 18*, 12241-12256.

Guo, H., Sullivan, A. P., Campuzano-Jost, P., Schroder, J. C., Lopez-Hilfiker, F. D., Dibb, J. E., . . . Nenes, A. (2016). Fine particle pH and the partitioning of nitric acid during winter in the northeastern United States. *Journal of Geophysical Research: Atmospheres, 121*, 10,355-310,376.

Guo, X., Pan, D., Daly, R. W., Chen, X., Walker, J. T., Tao, L., . . . Zondlo, M. A. (2022). Spatial heterogeneity of ammonia fluxes in a deciduous forest and adjacent grassland. *Agricultural and Forest Meteorology, 326*, 109128.

Häni, C., Flechard, C., Neftel, A., Sintermann, J., & Kupper, T. (2018). Accounting for field-scale dry deposition in backward Lagrangian stochastic dispersion modelling of NH3 emissions. *Atmosphere, 9*, 146.

Hůnová, I., Kurfürst, P., Vlček, O., Stráník, V., Stoklasova, P., Schovankova, J., & Srbová, D. (2016). Towards a better spatial quantification of nitrogen deposition: A case study for Czech forests. *Environmental Pollution, 213*, 1028-1041.

Jia, Y., Yu, G., Gao, Y., He, N., Wang, Q., Jiao, C., & Zuo, Y. (2016). Global inorganic nitrogen dry deposition inferred from ground-and space-based measurements. *Scientific Reports, 6*, 1-11.

Johnson, J., Cummins, T., & Aherne, J. (2016). Critical loads and nitrogen availability under deposition and harvest scenarios for conifer forests in Ireland. *Science of The Total Environment, 541*, 319-328.

Khan, M. A. H., Lowe, D., Derwent, R., Foulds, A., Chhantyal-Pun, R., McFiggans, G., . . . Shallcross, D. (2020). Global and regional model simulations of atmospheric ammonia. *Atmospheric Research, 234*, 104702.

Kosonen, Z., Schnyder, E., Hiltbrunner, E., Thimonier, A., Schmitt, M., Seitler, E., & Thöni, L. (2019). Current atmospheric nitrogen deposition still exceeds critical loads for sensitive, semi-natural ecosystems in Switzerland. *Atmospheric Environment, 211*, 214-225.

Kubota, T., Kuroda, H., Watanabe, M., Takahashi, A., Nakazato, R., Tarui, M., . . . Ouchi, T. (2020). Role of advection in atmospheric ammonia: A case study at a Japanese lake basin influenced by agricultural ammonia sources. *Atmospheric Environment, 243*, 117856.

Lassman, W., Collett Jr, J. L., Ham, J. M., Yalin, A. P., Shonkwiler, K. B., & Pierce, J. R. (2020). Exploring new methods of estimating deposition using atmospheric concentration measurements: a modeling case study of ammonia downwind of a feedlot. *Agricultural and Forest Meteorology, 290*, 107989.

Thimonier, A., Kosonen, Z., Braun, S., Rihm, B., Schleppi, P., Schmitt, M., . . . Thöni, L. (2019). Total deposition of nitrogen in Swiss forests: Comparison of assessment methods and evaluation of changes over two decades. *Atmospheric Environment, 198*, 335-350.

Tiwari, A., Kumar, P., Baldauf, R., Zhang, K. M., Pilla, F., Di Sabatino, S., . . . Pulvirenti, B. (2019). Considerations for evaluating green infrastructure impacts in microscale and macroscale air pollution dispersion models. *Science of The Total Environment, 672*, 410-426.

Van Der Graaf, S., Dammers, E., Segers, A., Kranenburg, R., Schaap, M., Shephard, M. W., & Erisman, J. W. (2022). Data assimilation of CrIS NH 3 satellite observations for improving spatiotemporal NH 3 distributions in LOTOS-EUROS. *Atmospheric Chemistry and Physics, 22*, 951-972.

Van Der Graaf, S. C., Dammers, E., Schaap, M., & Erisman, J. W. (2018). How are NH 3 dry deposition estimates affected by combining the LOTOS-EUROS model with IASI-NH 3 satellite observations? *Atmospheric Chemistry and Physics, 18*, 13173-13196.

Van Der Graaf, S. C., Kranenburg, R., Segers, A. J., Schaap, M., & Erisman, J. W. (2020). Satellite-derived leaf area index and roughness length information for surface–atmosphere exchange modelling: a case study for reactive nitrogen deposition in north-western Europe using LOTOS-EUROS v2. 0. *Geoscientific Model Development, 13*, 2451-2474.

Walker, J. T., Beachley, G., Zhang, L., Benedict, K. B., Sive, B. C., & Schwede, D. B. (2020). A review of measurements of air-surface exchange of reactive nitrogen in natural ecosystems across North America. *Science of The Total Environment, 698*, 133975.

Weber, R. J., Guo, H., Russell, A. G., & Nenes, A. (2016). High aerosol acidity despite declining atmospheric sulfate concentrations over the past 15 years. *Nature Geoscience, 9*, 282-285.

Wintjen, P., Schrader, F., Schaap, M., Beudert, B., & Brümmer, C. (2022a). Forest–atmosphere exchange of reactive nitrogen in a remote region–Part I: Measuring temporal dynamics. *Biogeosciences, 19*, 389-413.

Wintjen, P., Schrader, F., Schaap, M., Beudert, B., Kranenburg, R., & Brümmer, C. (2022b). Forest–atmosphere exchange of reactive nitrogen in a remote region–Part II: Modeling annual budgets. *Biogeosciences, 19*, 5287-5311.

Yi, W., Shen, J., Liu, G., Wang, J., Yu, L., Li, Y., . . . Wu, J. (2021). High NH3 deposition in the environs of a commercial fattening pig farm in central south China. *Environmental Research Letters, 16*, 125007.

Zöll, U., Brümmer, C., Schrader, F., Ammann, C., Ibrom, A., Flechard, C. R., . . . Kutsch, W. L. (2016). Surface–atmosphere exchange of ammonia over peatland using QCL-based eddy-covariance measurements and inferential modeling. *Atmospheric Chemistry and Physics, 16*, 11283-11299.

Committed to
health and sustainability